UNIVERSITA' DEGLI STUDI DI MILANO

Facoltà di Scienze Matematiche, Fisiche e Naturali

DOCTORATE SCHOOL IN CHEMICAL SCIENCE - XXIII CYCLE

CHIM/06 Organic Chemistry

TYROSINE KINASES AS TARGET FOR THE SYNTHESIS OF ANTI-ANGIOGENIC AND ANTI-CANCER COMPOUNDS

PhD thesis of

Francesco COLOMBO

Matr. R07834

Tutor: Prof. Daniele Passarella

Coordinator: Prof. Silvia Ardizzone

Academic year 2009/2010

Alla mia Famiglia

“Considerate la vostra semenza:
Fatti non foste a viver come bruti,
ma per seguir virtute e canoscenza”.

(Dante Alighieri, Divina commedia Canto XXVI)

Index

Abbreviations

Abl	Abelson tyrosine kinase
aFGF	Acidic fibroblast growth factor
ATP	Adenosine triphosphate
bFGF	Basic fibroblast growth factor
BOP-Cl	Bis(2-oxo-3-oxazolidinyl)phosphinic chloride
BT-474	Human breast tumor cell line
CML	Chronic myeloid leukemia
CPT	Camptothecin
CTCL	Cutaneous T-cell lymphoma
CuAAC	Copper(I) catalyzed alkyne-azide cycloaddition
DCC	*N,N*'-Dicyclohexylcarbodiimide
DFT	Density functional theory
DIBAL	Diisobutylaluminum hydride
DIC	*N,N*'-Diisopropylcarbodiimide
DIPEA	*N*,*N*-Diisopropylethylamine
DMAP	4-(Dimethylamino)pyridine
DMC	2-Chloro-1,3-dimethylimidazolinium chloride
DMP	Dess-Martin periodinane
DMF	*N,N*-Dimethylformamide
DMSO	Dimethylsulfoxide
DNA	Deoxyribonucleic acid
ECs	Endothelial cells
EDC	*N*-(3-Dimethylaminopropyl)-N'-ethylcarbodiimide
EGF	Epidermal growth factor
EGFR	Epidermal growth factors receptor
ERG	Electron releasing group
EWG	Electron withdrawing group
FBS	Fetal bovine serum
FDA	Food and drug administartion
FGF	Fibroblast growth factor
GTL-16	Human gastric carcinoma cell line
HATU	*O*-(7-Azabenzotriazol-1-yl)-*N,N,N',N'*tetramethyluroniumhexafluorophosphate

HepG2	Human hepatocellular liver carcinoma
HGF	Hepatocyte growth factor
HOBt	1-hydroxybenzotriazole
MCF7	Human breast cancer cell line
MDA-MB231	Human breast cancer cells
MDCK	Madin darby canine kidney cell line
MDR	Multidrug resistance
MeOH	Methanol
Met	Hepatocyte growth factor receptor or scatter factor receptor
MHz	Mega Hertz
MMPs	Matrix metalloproteinases
MW	Microwave
NCI	National cancer institute
NMR	Nuclear magnetic resonance
NOEs	Nuclear overhauser effects
NP	Natural product
NRTK	Non receptor tyrosine kinase
NSCLC	Non-Small cell lung carcinoma
PDGF	Platelet derived growth factor
PDGFR	Platelet derived growth factor receptor
PTK	Protein tyrosine kinase
RNA	Ribonucleic acid
RTK	Receptor tyrosine kinase
SF	Scatter factor
SPR	Surface plasmon resonance
TEA	Triethylamine
T-cells	Thimus cells
TCR	Thimus cell antigen receptor
THF	Tetrahydrofuran
TK	Tyrosine kinase
TKI	Tyrosine kinase inhibitor
TLC	Thin-layer chromatography
TSP-1	Thrombospondin-1
VEGF	Vascular endothelial growth factor
VEGFR	Vascular endothelial growth factor receptor

Chapter I: Introduction

1.1 Cancer

Cancer is one of the most studied diseases in the world. Its mortality rates are second only to cardiovascular diseases. After a quarter century of rapid advances, cancer research has generated a rich and a complex body of knowledge, revealing that cancer is a disease involving dynamic changes in the genome.[1] Cancer can be defined as a disease caused by a series of cumulative genetic changes that occur in a normal cell. These genetic mutations cause cellular transformations and evolutions, which can lead to an uncontrolled growth of abnormal cells.[2] Moreover, these mutated cells can invade nearby tissues and spread to distant sites using bloodstream and lymphatic system. Actually we can define two different kind of tumors classified by their aggressiveness: the benigns, which featured by only local growth, and the maligns, in which the most important characteristics are the invasiveness and the potential occurrence of metastasis.[3]

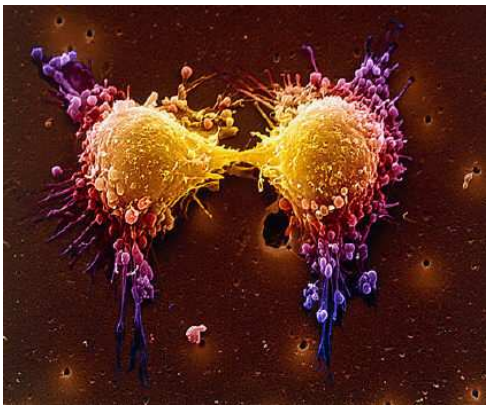

Figure 1: *Cancer Cells.*

1.2 Anticancer drugs

Most of the antitumoral drugs which used nowadays for cancer treatment are referred as cytotoxic agents because of their ability to kill directly the cancer cells. They are usually used in combination with other treatments like radiotherapy or surgery to increase the efficiency but they show their cytotoxic activity also in healthy cells. The selectivity and the efficiency of these drugs on tumoral cells are usually due to the faster growth compared to normal cells.[4]

---

[1] D. Hanahan, R.A. Weinberg, The hallmarks of cancer, *Cell* **2000**, *100*, 57-70.

[2] G.C. Prendergast, E.M. Jaffee, Cancer immunologists and cancer biologists: Why we didn't talk then but need to now, *Cancer Res.* **2007**, *67*, 3500-3504.

[3] P. Vineis, Definition and classification of cancer- monothetic or polythetic, *Theor. Med.* **1993**, *14*, 249-256.

[4] C. Leonetti, G. Zupi, Targeting different signaling pathways with antisense oligonucleotides combination for cancer therapy, *Current Pharmaceutical Design* **2007**, *13*, 463-470.

However, some kind of normal cells, like the bone marrow ones, grow fast and they can easily interact with antitumoral drugs. This relevant problem causes some collateral effects that can weaken the immune system and make intolerable the therapy for the patients. Another problem of chemotherapy is the issue of multidrug resistance (MDR) *Tabella 1*.

Mechanism	Individual process
Cell kinetic resistance	Tumor growth
Pharmacokinetic Resistance	Poor absorption
	Excessive metabolism
	Poor penetration to certain sites
	Blood supply of the tumor
	Drug diffusion
Cellular drug Resistance	Increased drug efflux
	Decreased drug uptake
	Sequestration of drugs
	Alterations in drug targets
	Activation of detoxifying systems
	Increased repair of drug-induced DNA damage
	Blocked apoptosis
	Disruption in signaling pathways
	Alterations of factors involved in cell cycle regulation

Table 1: *Mechanism of drug resistance.*

MDR occurs when cells, which have been once destroyed by a particular drug, they no longer respond to the treatment. It can be intrinsic, referred to tumors that are naturally unaffected by such a kind of drugs, or acquired, when it appears after some treatments because of an evolution of the tumor cells. For this reason the activity of the drug decreases. A tumor cell can express this phenomenon in different ways such as a reduced uptake of the drug, an increase in the production of proteins that repair the DNA-drug adducts, a different metabolic pathway that activates the tumoral cell or a development of drug expulsion mechanisms.[5]

[5] D.B. Zamble, S.J. Lippard, Cisplatin and DNA repair in cancer chemotherapy, *Trends Biochem. Sci.* **1996**, *21*, 38-38.

For this reason the discovery of new targets for cancer therapies is very important, for instance:

- DNA,
- protein tyrosine kinases (PTKs)
- tubulin and microtubules
- enzymes like Topoisomerase II or Histone Deacetylases

In the following *Table 2* is summarized a recent classification of anticancer drugs based on their biological target.[6]

Target		
Tumor	DNA	*Non-specific* DNA break: chemotherapy DNA related proteins: chemotherapy *Specific* Hormonal therapy, retinoids Interferon α Gene therapy
	RNA	Antisense oligonucleotides
	Proteins	*Membrane receptors* Extracellular domain: MoAb Intracellular domain: small molecules *Cytoplasm* Intracellular pathways: small molecules Tubulin: chemotherapy
Endothelium	DNA	Combretastatin
	Proteins	Monoclonal antibodies Small molecules
Extracellular matrix	MMPs	MMPs inhibitors
	Other elements	Monoclonal antibodies and small molecules
Immune system	Lymphocytes and macrophages	Interferons Interleukin 2 Vaccines
Hoste cells	Bone cells	Bisphosphonates, osteoprotogerin

Table 2: *New proposed classification of anticancer drugs.*

[6] X.Z. Wu, A new classification system of anticancer drugs - Based on cell biological mechanisms, *Medical Hypotheses* **2006**, *66*, 883-887.

Depending from the desired target, it can be appeared a different mechanism of action. Some drugs do not directly act with DNA and cause cell apoptosis by inhibiting other targets. Examples of these anticancer drugs are taxanes and Vinca alkaloids (for example Vinblastin and Vincristin), which interfere with the polymerization or depolymerization of microtubules. The consequence is the alteration of the mitotic spindle, causing inhibition of the cellular proliferation.[7] Other drugs act on particular enzymes that regulate the replication processes like Topoisomerase II or Histone deacetylase.[8] Finally, anticancer drugs can interact directly with the DNA in different ways. For example they can bind the nucleobases, like alkylating agents,[9] cisplatin and derivatives,[10] causing distortion and blocking the process of the DNA replication. Moreover, they can also cleave the DNA strands like some metals complexes such as Bleomycin,[11] Rutenium dimers[12] and so on. In the end, anticancer drugs can act on protein tyrosine kinases (PTKs), which are involved in several cellular functions leading to cancer. In particular they have a main role in new blood vessels formation, a phenomenon well known as angiogenesis. This is a fundamental key step in the formation and growth of solid tumors.

1.3 Angiogenesis

Angiogenesis, the sprouting of new capillaries from the pre-existing blood vessels, is a complex process involving many biological and cellular functions. Angiogenesis is a biological protocol that has a relevant role in many diseases. It happens in normal physiological processes, such as embryonic development, the female menstrual cycle, bone remodelling and wound healing. On the other hand, angiogenesis also plays a crucial role in many pathological conditions, including ocular diseases, such as diabetic retinopathy, retinopathy of prematurity and age-related macular degeneration; vascular diseases such as ischemic heart disease and atherosclerosis; chronic inflammatory disorders such as psoriasis and rheumatoid arthritis and tumor growth.[13] For all these reasons angiogenesis is an important biological target in drug discovery.

---

[7] S. Sharma, T. Ganesh, D.G.I. Kingston, S. Bane, Promotion of tubulin assembly by poorly soluble taxol analogs, *Anal. Biochem.* **2007**, *360*, 56-62.

[8] J.M. Mehnert, W.K. Kelly, Histone deacetylase inhibitors: Biology and mechanism of action**,** *Cancer J.* **2007**, *13*, 23-29.

[9] J.T. Millard, R.J. Spencer, P.B. Hopkins, Effect of nucleosome structure on DNA interstrand cross-linking reactions, *Biochem.* **1998**, *37*, 5211-5219.

[10] D. Lebwohl, R. Canetta, Clinical development of platinum complexes in cancer therapy: an historical perspective and an update, *Eur. J. Cancer* **1998**, *34*, 1522-1534.

[11] R.M. Burger, Cleavage of nucleic acids by bleomycin, *Chem. Rev.* **1998**, *98*, 1153-1169.

[12] T.K. Janaratne, A. Yadav, F. Ongeri, F.M. MacDonnell, Preferential DNA cleavage under anaerobic conditions by a DNA-binding ruthenium dimer, *Inorg. Chem.* **2007**, *46*, 3420-3422.

[13] L.K. Shawver, K.E. Lipson, T.A.T. Fong, G. McMahon, G.D. Plowman, L.M. Strawn, Receptor tyrosine kinases as targets for inhibition of angiogenesis, *DDT* **1997**, *2*, 50-63.

1.3.1 Angiogenesis and cancer

The role of angiogenesis in tumor growth was firstly described by Folkman (1971).[14] He found that in most cases solid tumors growth is accompanied by neovascularisation: new capillary growth is induced by diffusible growth factor generated by malignant tumor cells.[15] Results obtained in the 1970s have led to the conclusion that new blood vessel formation is essential for the growth and metastasis of solid tumors. Angiogenesis is a vital process in the progression of cancer from small and localized neoplasms to larger, growing and potentially metastatic tumors. To grow beyond 1 to 2 mm in diameter, a tumor needs an independent blood supply, which is acquired by expressing growth factors that recruit new vasculature from existing blood vessels and This process continues even the tumor matures. Thus, upregulation of angiogenesis is a key step in sustained tumor growth and may also be critical for tumor metastasis.[16] Folkman studies showed that angiogenesis depends on the tight regulation of factors that promote or inhibit this biological event (*Table 3*).

Angiogenic factors	Anti-angiogeic factors
Basic fibroblast growth factor (bFGF)	Plateled factor 4
Acidic fibroblast growth factor (aFGF)	Thrombospondin-1
Transforming growth factor (TGF)	Transforming growth factor-b
Plateled-derived growth factor (PDGF)	Interferon-a
Insulin-like growth factor (IGF)	Prolactin fragment
Vascular endothelial growth factor (VEGF)	Angiostatin
Hepatocyte growth factor (HGF)	Tissue inhibitors of metalloproteinases
Angiogenin	TIMP-1
Prostaglandine E_1 and E_2	TIMP-2
Tumor necrosis factor-a (TNF-a)	TIMP-3
Growth hormona	bFGF soluble receptor

Table 3: *Angiogenic and anti-angiogenic factors.*

1.3.2 Angiogenic switch-on

It has been proposed by Hanahan and Folkman[17] (1996) that there is a "switch" that perturbs the balance between pro-angiogenic and anti-angiogenic factors (*Figure 2*).

[14] J. Folkman, Tumor Angiogenesis: Therapeutic Implications, *N. Engl. J. Med.* **1971**, *285*, 1182-1186.

[15] J. Folkman, Anti-Angiogenesis: New Concept for Therapy of Solid Tumors, *Ann. Surg.* **1972**, *175*, 409-416.

[16] N. Ferrara, K.J. Hillan, H.P. Gerber, W. Novotny, Discovery and development of bevacizumab, an anti-VEGF antibody for treating cancer, *Nat. Rev. Drug. Discov*. **2004**, *3*, 391-400.

[17] J. Folkman, D. Hanahan, Patterns and emerging mechanisms of the angiogenic switch during tumorigenesis, *Cell* **1996**, *86*, 353-364.

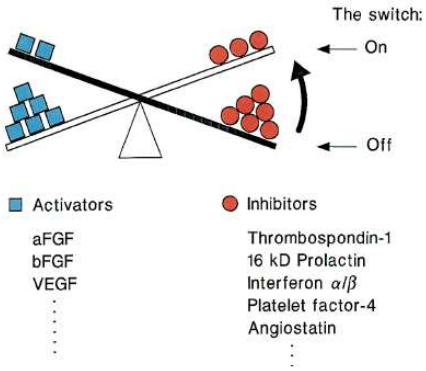

Figure 2: *The balance hypothesis for angiogenic switch-on.*

The *angiogenic switch-on* has been suggested to be a component of the tumor phenotype that is often activated during the preneoplasic step in tumor development. When the balance is perturbed, uncontrolled angiogenic factors, released from hypoxic tumor cells, migrate to nearby blood vessel endothelium, which signals the activation of biochemical events leading to the angiogenic process. Endothelial cells are stimulated to proliferate, migrate to the tumor site and form new capillaries to supply oxygen and nutrients to the growing tumor (*Figure 3*).

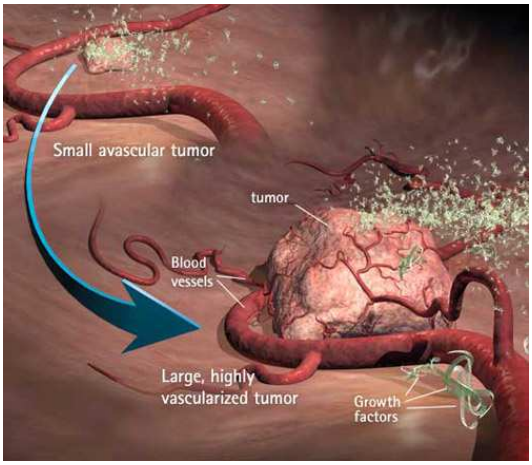

Figure 3: *To grow beyond 1 to 2 mm in diameter, a tumor needs an independent blood supply, which is acquired by expressing growth factors that recruit new vasculature from existing blood vessels. This process continues even as the tumor matures.*

An adequate supply of oxygen and nutrients is critical for homeostasis of virtually all human cells and tissues. This delivery of oxygen and nutrients, and the corresponding elimination of metabolic waste and carbon dioxide, depends on the vascular system. Accordingly, the formation of new tissues is systematically coordinated with the

formation of a new vasculature. In this process, endothelial cells, the primary building blocks of vasculature, must undergo four major steps (*Figure 4*): [18]

- Breaking through of the basal lamina that envelopes existing blood vessels
- Migration toward a source signal
- Proliferation
- Formation of tubes

Figure 4: *Angiogenesis is a complex mechanism involving several biological processes. a) small non-angiogenic tumor; b) invasion and migration of endothelial cells through the basement membrane; c) extension of vessels into the tumor.*

A large number of pro-angiogenic growth factors have been identified, many of which are able to induce all the four of the above steps mentioned. One of the primary factors among them is a protein known as vascular endothelial growth factor (VEGF).

[18] C. Sturk, D. Dumont, *The Basic Science of Oncology* - fourth edition **2005**.

1.3.3 Angiogenesis inhibition

Without the supplement of blood circulation and with the angiogenesis inhibition, tumor growth is dramatically impaired. With the absence of an adequate vascularisation, tumor cells become necrotic[19] and apoptotic[20]. Conversely, if a tumor becomes vascularised, its mass can rapidly expand. These newly formed vessels not only promote tumor growth, but also cause the tumor cells to become malignant and metastatic. Due to the reasons previously cited, the inhibition of angiogenesis has become an attractive target in anticancer treatment. The concept of the anti-angiogenic therapy of cancer is based on tumor growth prevention.[21] Subsequently, it was also recognized, that metastasis can be affected by angiogenesis. For these reasons, inhibitors of angiogenesis are expected to be valuable drugs for cancer therapy. Importantly, because endothelial cells have a stable genome, acquired drug resistance is not expected,[22] and, in addition, the possible side effects of an anti-angiogenic therapy should be limited. Inhibitors of angiogenesis may represent not only new anticancer agents but also may offer the possibility for therapeutic intervention in several diseases like rheumatic diseases, endometriosis, psoriasis and diabetic retinopathy. In this context, protein kinases (PKs) possessed a central role because they are involved in several genetic programs like: tumor growth, invasive growth, metastatic process, suppression of apoptosis and angiogenesis. Extensive efforts have been made to identify and develop small-molecule inhibitors of these central signalling proteins. Some of these compounds have already been approved or are currently in clinical trials to examine their applicability as anticancer drugs (*Table 4*). In particular the angiogenesis inhibitors have an important role in combined anticancer therapies. They show their maximum effect in combination with classical anticancer agents or others techniques like radiotherapies or surgeries.

[19] S. Brem, H. Brem, J. Folkman, D. Finkelstein, A. Patz, Prolonged Tumor Dormancy by Prevention of Neovascularization in the Vitreous, *Cancer Res.* **1976**, *36*, 2807-2812.

[20] L. Holmgren, M.S. Oreilly, J. Folkman, Dormancy of Micrometastases - Balanced Proliferation and Apoptosis in the Presence of Angiogenesis Suppression, *Nat. Med.* **1995**, *1*, 149-153.

[21] R. Kerbel, J. Folkman, Clinical translation of angiogenesis inhibitors, *Nat. Rev. Cancer.* **2002**, *2*, 727-739.

[22] R. Karbel, A cancer therapy resistant to resistance, *Nature* **1997**, *390*, 335-336.

With this double approach, the use of an angiogenesis inhibitor combined with a chemotherapic treatment is possible to maximize the inhibition of cancer growth and metastasis.

Generic name	Brand name	Number	Date approved	Known targets	Disease
Fasudil	-	HA-1077	1999	ROCK	Cerebral vasospasm
Imatinib	Gleevec	STI-571	2001	Abl, ARG, PDGFR, Kit	CML, gastrointestinal stromal tumors
Nilotinib	Tasigna	AMN107	2007	Abl, ARG, Kit, PDGFR	CML with resi stance to imatinib or intolerance
Dasatinib	Sprycel	BMS-354825	2007	Abl, ARG, Kit, PDGFR, Src and oth.	CML with resi stance to imatinib or intolerance
Gefitinib	Iressa	ZO-1839	2004	EGFR	Non-small-cell lung cancers (especially adenocarcinomas)
Erlotinib	Tarceva	OSI-774	2004	EGFR	Non-small-cell lung and pancreatic carcinomas
Lapatinib	Tykerb	GW572016	2007	EGFR (Erb8-1, Erb8-2)	Breast cancer, Her2-positive
Sorafenib	Nexavar	BA 43-9006	2006	8-Raf, VEGFR, PDGFR, FLT3, c-Kit	Renal cell carcinoma
Sunitinib	Sutent	SU11248	2006	VEGFR, PDGFR, FLT3, c-Kit	Renal cell carcinoma, gastrointestinal stromal tumors
Temsirolimus	Torisel	CCI-779	2007	mTOR	Renal cell carcinoma

Table 4: *small-molecule inhibitors of PKs approved by FDA.*

1.4 *Judah Folkman*

Moses Judah Folkman: 1933 - 2008

Born in Cleveland in 1933, Folkman graduated *cum laude* from The Ohio State University, Columbus, Ohio, in 1953. He continued his education at Harvard Medical School, where he graduated *magna cum laude* in 1957. Folkman began his surgical residency at the Massachusetts General Hospital and served as chief resident in surgery from 1964-1965.

As a student, Folkman co-authored papers describing a new method of hepatectomy for liver cancer and developed the first atrio-ventricular implantable pacemaker for which he received the Boylston Medical Prize, Soma Weiss Award and Borden Undergraduate Award in Medicine.

While serving as a lieutenant in the U.S. Navy from 1960-1962, Folkman and a colleague at the National Naval Medical Center, Bethesda, MD, first reported the use of silicon rubber implantable polymers for the sustained release of drugs. Their findings became the basis for development of Norplant, the contraceptive used internationally, and initiated the field of controlled release technology. At this time, Folkman also began to grow tumors in isolated perfused organs, which led to the idea that tumors are angiogenesis-dependent.

In 1971 Folkman published a seminal paper in the New England Journal of Medicine, proposing the hypothesis that all tumor growth is angiogenesis-dependent. This founded the field of angiogenesis research and opened a field of investigation now pursued by scientists in many fields worldwide. Folkman's laboratory purified the first angiogenic protein from a tumor, discovered the first angiogenesis inhibitors and initiated clinical trials of antiangiogenic therapy. Today, angiogenesis inhibitors have received FDA approval in the U.S. for cancer and for the treatment of macular degeneration and are also approved in 27 other countries. Largely because of Folkman's research, the possibility of antiangiogenic therapy is now on a firm scientific foundation, not only in the treatment of cancer, but of many non-neoplastic diseases as well.

Folkman is the author of 389 original peer-reviewed papers and 106 book chapters and monographs. He also holds honorary degrees from fifteen universities and is the recipient of numerous national and international awards. He has been elected to the National Academy of Sciences, the American Academy of Arts and Sciences, the American Philosophical Society and the Institute of Medicine of the National Academy of Sciences.

In addition to his distinguished accomplishments in research, Folkman has served as a surgeon and teacher. He began his career as an instructor in surgery for Harvard's Surgical

Service at Boston City Hospital Boston, was promoted to Professor of Surgery at Harvard Medical School, and became the Julia Dyckman Andrus Professor of Pediatric Surgery in 1968. From 1967 he served as Surgeon-in-Chief at the Children's Hospital Boston for 14 years. Dr. Folkman is also a Professor of Cell Biology at Harvard Medical School and is currently Director of the Vascular Biology Program at Children's Hospital Boston.

Angiogenesis inhibitors are now approved by the FDA in the U.S., for cancer and for macular degeneration and have received approval in 27 other countries. They have developed specific and sensitive angiogenesis-based biomarkers in blood and urine capable of detecting microscopic human cancers in mice. In pre-clinical studies, antiangiogenic therapy of these mice is guided by biomarkers until the biomarkers decline to normal levels. These results suggest the possibility of treating human cancer years before it becomes symptomatic, and before it can be anatomically located.

1.5 *Aim of the project*

The topic of this thesis is part of a multidisciplinary project that regards the preparation of selective anticancer compounds. In particular we faced the design, synthesis and biological exploitation of new tyrosine kinase inhibitors (TKIs). We focused our attemption and two different TKs:

- Met (chapter III);
- Abl (chapter IV).

The importance of Abl and Met against cancer and angiogenesis led several research groups to look for small molecules able to interact and block the dangerous activity of these kind of TKs.

In both cases we considered the situations of well known inhibitors and the three-dimensional structure of the biological targets. We designed new scaffolds to be decored to generate different quality collections of possible inhibitors.

The biological evaluation was developed in strict collaboration with different research groups. The activity toward cancer cells was considered as first instance. Then we moved to evaluate the activity toward single biological targets. The compounds with appreciable performance were selected for *in vivo* tests. For this reason the preparation in grams scale of the selected compounds was developed.

The biological studies were faced to confirm the activity of any new compound and to ascertain the biological mechanism of action. Further, the biological evaluation resulted useful to confirm the reliability of the modelling study.

Chapter II: Tyrosine kinases

2.1 Tyrosine kinases (TKs)

Over 500 human genes encode protein kinases, and these can be grouped into a number of subsets based primarily on sequence and structural similarities.[23] In general, protein kinases catalyze the transfer of the terminal phosphoryl group of ATP to specific hydroxyl groups of serine, threonine or tyrosine residues of their protein substrates. The protein phosphorylation controls a wide range of cellular and pathogenic processes, thus even subtle changes in protein kinase activity can lead to a variety of diseases, including cancer.[24] In this family, protein tyrosine kinases (PTKs) have a relevant place, because they play an essential role in signalling pathways involved in the control of cellular proliferation and growth. *Figure 5* shows the six hallmarks which lead to cancer.[25] Biologists suggest that the most part of cancers have acquired the same set of functional capabilities during their development, although through various mechanistic strategies. PTKs have a relevant role in the most part of these functions.

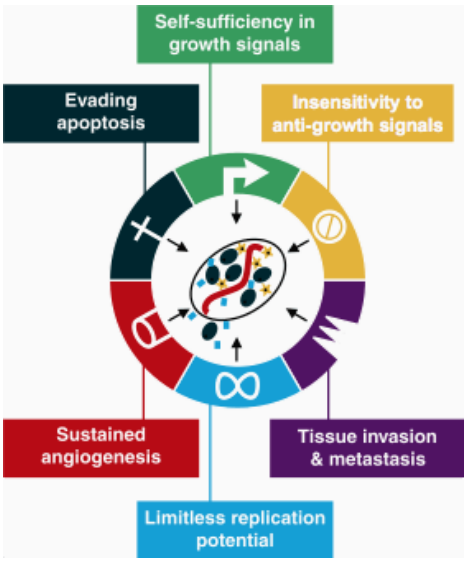

Figure 5: *Six hallmarks leading to cancer.*

PTKs function is the transmission of extracellular signals through a complex signalling pathway, to induce a specific genetic program like growth and migration. TKs can be subdivided into two large families: receptor tyrosine kinases (RTKs) and non-receptor tyrosine kinases (NRTKs). RTKs span the plasma membrane and contain an extracellular portion, which binds the ligands, and an intracellular portion, which possesses the

[23] G. Manning, D.B. Whyte, R. Martinez, T. Hunter, S. Sudarsanam, The protein kinase complement of the human genome, *Science* **2002**, *298*, 1912-1934.
[24] M.A. Bogoyevitch, D.P. Fairlie, A new paradigm for protein kinase inhibition: blocking phosphorylation without directly targeting ATP binding, *DDT* **2007**, *12*, 622-633.
[25] D. Hanahan, R.A. Weinberg, The hallmarks of cancer, *Cell* **2000**, *100*, 57-70.

residues responsible for catalytic activity and some regulatory sequences (*Figure 6*). The RTKs family includes the insulin receptor and the receptors for many growth factors such as epidermal (EGF), platelet-derived (PDGF), fibroblast (FGF) and vascular endothelial (VEGF). On the other hand, NRTKs are cytoplasmic proteins, without an extracellular or transmembrane portion but with modular domains that are responsible for subcellular targeting and regulation of the catalytic activity. The NRTK family includes Src, Abl, FAK and many others.

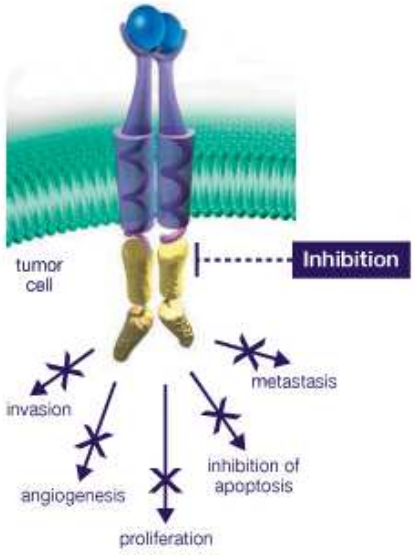

Figure 6: *Receptor tyrosine kinase (RTK).*

2.1.1 Receptor tyrosine kinases (RTKs)

More than 16 distinct RTKs families are known and the members are grouped on the base of their structure (*Figure 7*). The RTKs can be broadly divided into two groups depending on the covalent organization of the receptor. Most RTKs possess a single polypeptide chain and are monomeric in the absence of a ligand. Members of the insulin receptor subfamily, which includes insulin-like growth factor-1 receptor, are disulfide-linked dimers of two polypeptide chains, forming a heterotetramer.

The ligand which binds to the extracellular portion of RTKs leads to the dimerization of the monomeric receptors or to a rearrangement within the quaternary structure of the heterotetrameric receptors, resulting in auto-phosphorylation of specific tyrosine residues in the cytoplasmic portion.

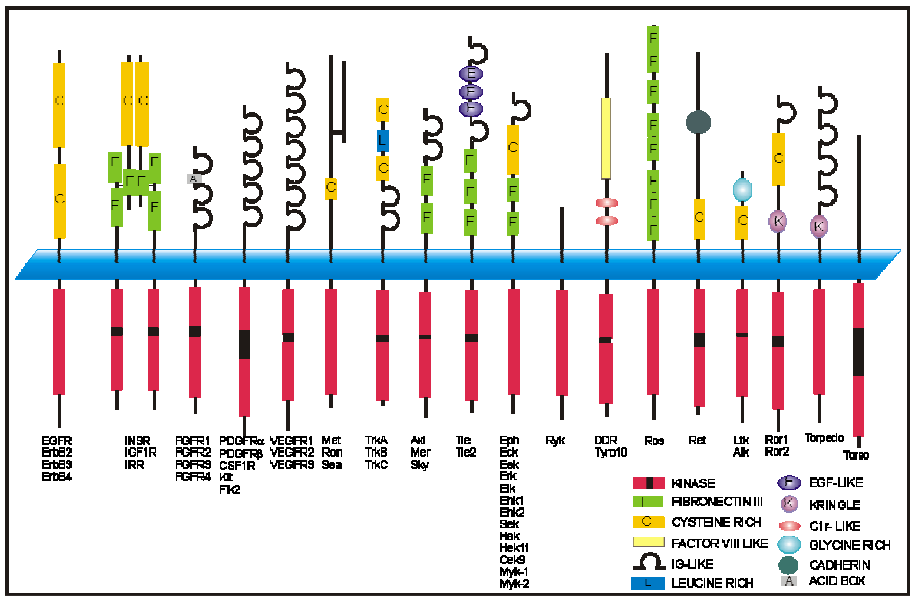

Figure 7: *RTKs families.*

In every case each RTKs has a comparable skeleton that could be classified as below: [26]

- extracellular domain
- transmembrane domain
- juxtamembrane domain
- catalytic domain
- *C*-terminal domain

The *extracellular domain* region contains the high-affinity binding site for the growth factor proteins. This domain diverges among the different receptor families, and appears with various structural motifs which have two basic functions. Some motifs participate in the formation of tridimensional configurations to ensure binding site stability and specificity for growth factors and others mediate receptor dimerization, which is critical for kinase activation and signal transduction. Every receptor family has a corresponding growth factor and each receptor generally binds one single factor with high affinity.

[26] P. Longati, P.M. Comoglio, A. Bardelli, Receptor tyrosine kinases as therapeutic targets: The model of the MET oncogene, *Curr. Drug Targets* **2001**, *2*, 41-55.

The *Transmembrane Domain* region contains about twenty-five hydrophobic residues which included in the cellular lipid bilayer. Single point mutations in this domain can dramatically alter the tyrosine kinase activity of the receptor.

Juxtamembrane Domain region is located in the cytoplasm. This region is involved in the modulation of receptor activity by adjacent signalling molecules, receptors or transducers.

The *Catalytic Domain* region is responsible for the tyrosine kinase activity and it is composed of about 250 aminoacids. The kinase domain is composed of two lobes delimiting a central cleft. In the central cleft, the protein substrate and the complex ATP-Mg^{++} ions are brought together and the phosphotransfer reaction takes place. The N-terminal lobe contains a glycine-rich motif and the lysine residue critical for ATP binding. Protruding onto the central cleft is the *catalytic loop*, in which an aspartic residue is the catalytic base and other residues allow recognition of tyrosine substrate. The C-terminal lobe contains a second loop, known as the *activation loop*, frequently including 1 to 3 tyrosine residues with regulatory functions. Mutations in the kinase activation loop are responsible for the kinase activity switch on in the absence of ligands.

C-Terminal Tail includes up to 200 aminoacid residues. Its length and function are variable in different receptors. This segment binds the intracellular signal transducer after the receptor activation.

2.1.2 RTKs activation[27] and signal transduction

The activation loop of RTKs is relatively mobile and probably adopts numerous conformations (*Figure 8*). In the absence of a ligand, such as a growth factor, the steric hinderance around the catalytic site inhibits the tyrosine(s) phosphorylation mediated by ATP. This conformation (*Figure 8 in red*) prevents the binding of protein substrates and ATP.

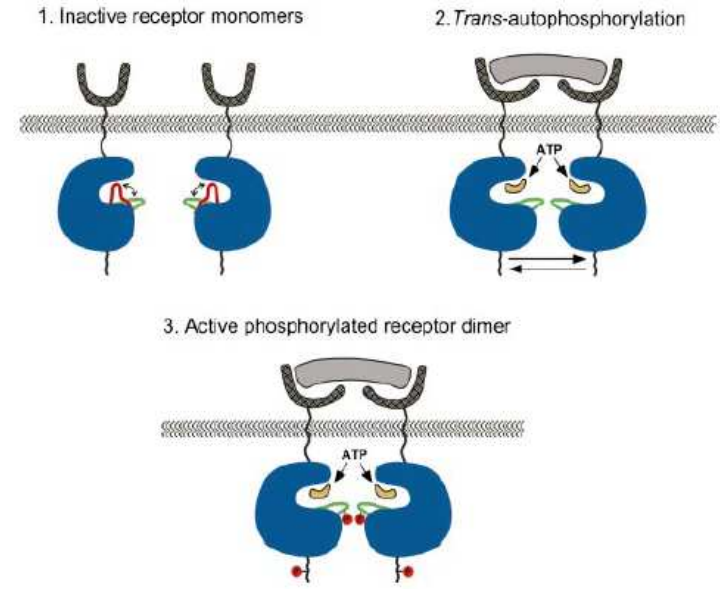

Figure 8: *RTK activation mechanism.*

But when a ligand binds to the extracellular domain, induces the dimerization of the receptor and changes in the conformation of the activation loop (*Figure 8 in green*) which lead to the redaction of the catalytic site steric hinderance. Then ATP is able to get into the activation loop and the transphosphorylation can be occured. Transphosphorylation of the activation-loop tyrosine(s) residues shifts the receptor from inactive to the active state. Once an RTK is activated it triggers the *signal transduction*. This downstream signal (recruitment and activation of cytoplasmic signalling molecules) induces the appropriate cellular response: tumor growth, invasive growth, metastatic process, apoptosis inhibition, angiogenesis and so on. The knowledge of the RTKs activation mechanism can be used for the design of three different approaches to block the signal transduction:

- *inhibition of ligand binding* with a specific receptor-binding antagonist,
- *interference with the RTKs activation loop* to prevent the transphosphorylation,
- *interference with the downstream signal* on cytoplasmic signalling molecules.

[27] S.R. Hubbard, M. Mohammadi, J. Schlessinger, Autoregulatory mechanisms in protein-tyrosine kinases, *J. Biol. Chem.* **1998**, *273*, 11987-11990.

A number of RTKs are also involved in angiogenesis, directly or indirectly. Of particular interest is the vascular endothelial growth factor receptor (VEGFR), which plays a relevant and direct role in angiogenesis. Other RTKs of potential interest in angiogenesis are: the epidermal growth factor receptor (EGFR), the platelet derived growth factor receptor (PDGFR) and hepatocyte growth factor receptor HGFR) better known as Met receptor. These last three RTKs play an indirect role for the production of VEGF.

2.2 Vascular endothelial growth factor (VEGF) and its receptor (VEGFR)

In the last thirty years a number of inducers of angiogenesis have been detected. The first which discovered in 1982 was the basic fibroblast growth factor (bFGF or FGF-2) followed shortly by the acid analogues[28] (aFGF or FGF-1). At about the same time, a secreted protein was identified by its ability to elicit vascular permeability. Subsequently this factor, called vascular endothelial growth factor[29] (VEGF), showed to be the most potent inducer of angiogenesis. VEGF is commonly expressed in a wide variety of human and animal cancer. Recently, two related endothelial growth factors, VEGF-B and VEGF-C, have been identified. An important point to take into consideration is that VEGF production and subsequent angiogenesis can be triggered by a number of factors in the cellular microenvironment but hypoxia (*Figure 9*) remains one of the most important trigger of VEGF expression even once a tumor becomes vascularized.

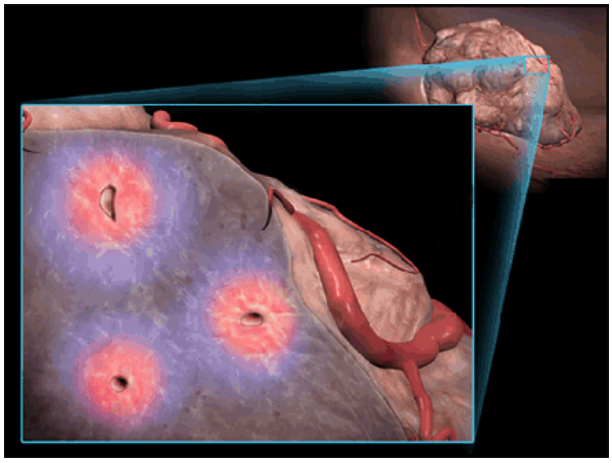

Figure 9: *This image illustrates hypoxic conditions in a tumor: cells closest to vasculature have a sufficient supply of oxygen, whereas oxygen supply diminishes further from blood vessels. As the oxygen supply decreases, cells become hypoxic (light purple areas) and later necrotic (grey areas).*

[28] J. Folkman, Y. Shing, Angiogenesis, *J. Biol. Chem.* **1992**, 267, 10931-10934.
[29] N. Ferrara, Vascular Endotelial Growth-Factor, *Trends. Cardiovasc. Med.* **1993**, *3*, 244-250.

Without an independent blood supply, tumors must depend on diffusion to obtain oxygen and other nutrients and typically cannot proliferate. Thus, a growing tumor without sufficient vasculature will be in hypoxic state, which is the lack of oxygen. In response to hypoxic conditions, tumors secrete, with several strategies involving PKs and VEGF in order to recruit new vasculature, which then provides a supply of oxygen.[30] As the tumor grows, continually outgrows its existing blood supply, leaving an area of necrotic and hypoxic tissue. Due to its main and direct role in vascularization processes VEGF and its receptors are one on the key targets against angiogenesis. Particularly, the inhibition occurs with the use of small molecules which blocks the receptor signal transduction (*Figure 10*).

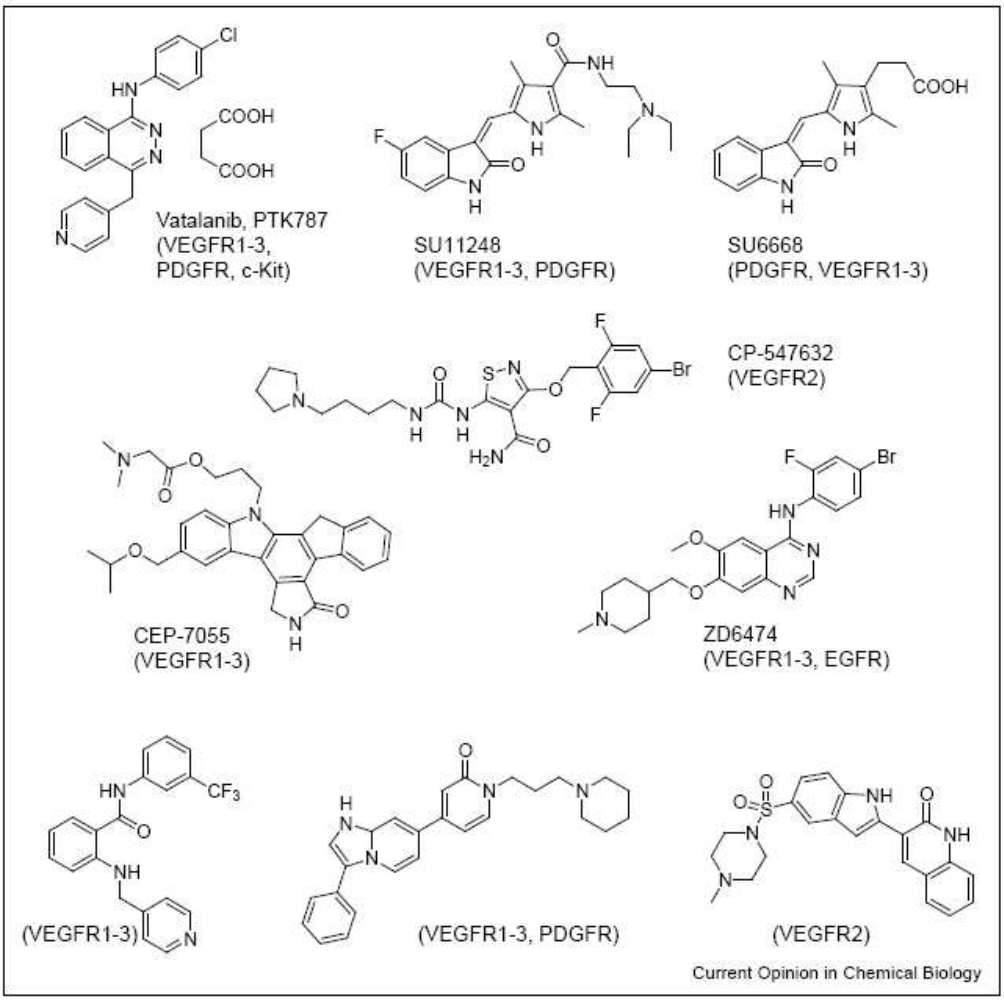

Figure 10: *VEGFR small molecule inhibitors.*

[30] M.A. Gimbrone, S.B. Leapman, R.S Cotran, J. Folkman, Tumor Dormancy in vivo by Prevention of Neovascularization, *J. Exp. Med*. **1972**, *136*, 261-276.

2.3 Met receptor

Met receptor (*Figure 11*) is a RTK based on a dimeric molecule composed of a 50 kDa α-chain disulfide linked to a 145 kDa β-chain in an α-β complex of 190 kDa.[31] Met is activated by its corresponding ligand hepatocyte growth factor (HGF), that triggers specific program leading to invasive growth, cell migration, cell survival, embryogenesis, organ regeneration, and neoplasia.[32]

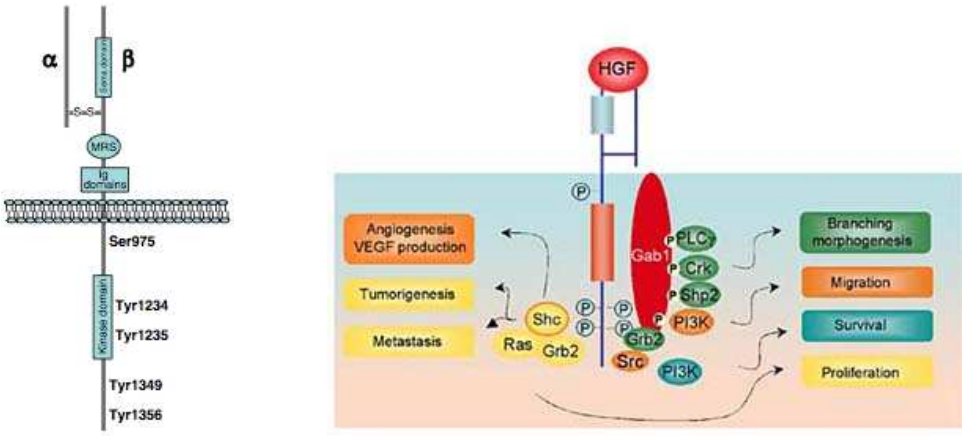

Figure 11: *Met receptor.*

In addition, it was demonstrated that HGF-Met is a powerful inducer of angiogenesis,[33] which is mediated through their mitogenic effect on endothelial cells. HGF-Met is also able to stimulate the expression of pro-angiogenic factors like VEGF (*Figure 12*) and to downregulate angiogenesis inhibitors like thrombospondin-1 (TSP-1).[34] HGF is a heparin binding glycoprotein that consists of a 60 kDa α-chain and 30-kDa β-chain linked by disulfide bonds. In particular HGF, also known as scatter factor (SF), has the main function to induce cellular migration. This cellular spreading is a fundamental requirement for the metastatic process and for angiogenesis. The overexpression[35] of Met has been demonstrated in several malignant tumors such as breast, esophagus, prostate, pancreas,

[31] E.M. Rosen, I.D. Goldberg, Scatter factor and angiogenesis. *Adv. Cancer Res*. **1994**, *67*, 257-279.

[32] E.M. Rosen, S.K. Nigam, I.D. Goldberg, Scatter factor and the c-Met receptor: a paradigm for mesenchymal-epithelial interaction, *J. Cell. Biol.* **1994**, *127*, 1783-1787.

[33] S. Wagatsuma, R. Konno, S. Sato, A. Yajima, Tumor angiogenesis, hepatocyte growth factor, and c-Met expression in endometrial carcinoma, *Cancer* **1998**, *82*, 520-530.

[34] G. Dong, Z. Chen, Z.Y. Li, N.T. Yeh, C.C. Bancroft, C. Van Waes, Hepatocyte growth factor/scatter factor-induced activation of MEK and PI3K signal pathways contributes to expression of proangiogenic cytokines interleukin-8 and vascular endothelial growth factor in head and neck squamous cell carcinoma, *Cancer Res.* **2001**, *61*, 5911-5918.

[35] S. Patane, N. Pietrancosta, H. Hassani, V. Leroux, B. Maigret, J.L. Kraus, R. Dono, F. Maina, A new Met inhibitory-scaffold identified by a focused forward chemical biological screen, *Biochem. Biophys. Res. Commun.* **2008**, *375*, 184-189.

kidney and bon.[36] Also, in *in vivo* models Met has showed to induce invasiveness and metastasizing capacity. For all these reasons and in particular for its over expression, the use of selective Met inhibitors, could lead to new anticancer therapies with more selectivity then the classic chemotherapy and, consequently, with less side effects for the patients.

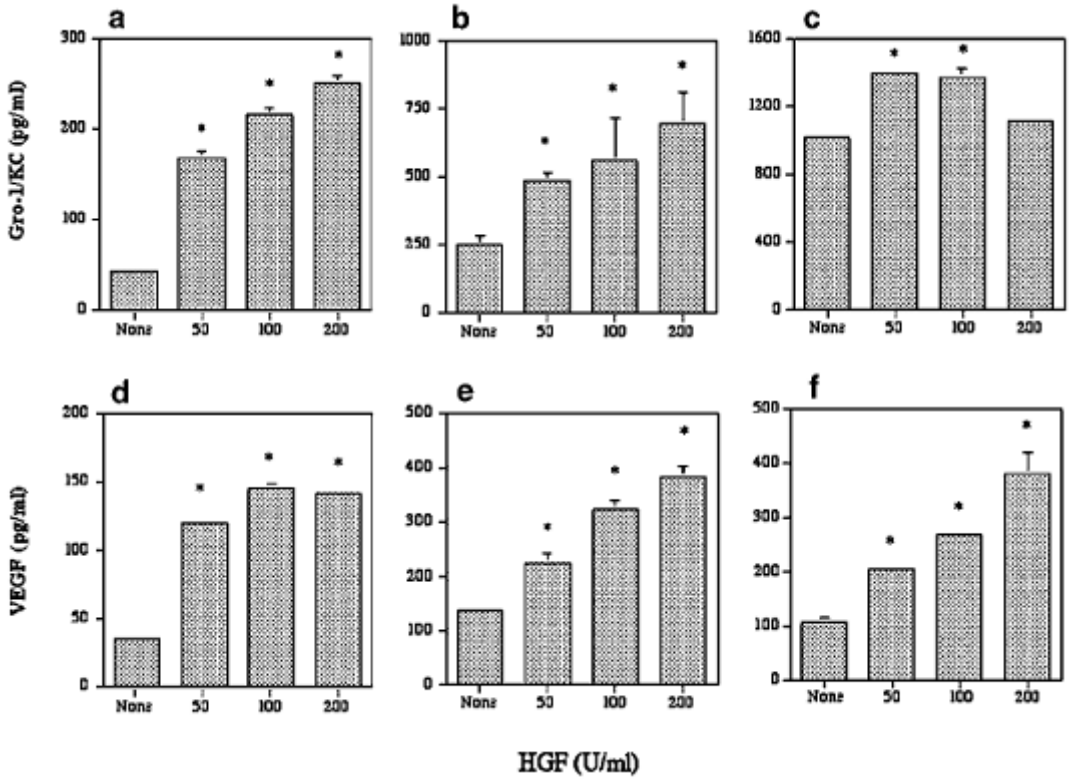

Figure 12: Dose dependent induction of VEGF and Gro-1/KC by HGF-Met in Pam 212 and LY cell lines.

[36] C. Kuhnen, T. Muehlberger, M. Honsel, E. Tolnay, H.U. Steinau, K.M. Muller, Impact of c-Met expression on angiogenesis in soft tissue sarcomas: correlation to microvessel-density, *J. Cancer Res. Clin. Oncol.* **2003**, *129*, 415-422.

2.4 Abelson tyrosine kinase (Abl)

Abelson Tyrosine Kinase (Abl)[37] is a non-receptor of about 1150 residues. The *N*-terminal half (about 530 residues) contains two peptide binding units (the SH2 and SH3 domains) followed by a tyrosine kinase domain, whereas the *C*-terminal half contains DNA-binding domains interspersed with sites of phosphorylation and other short recognition motifs (*Figure 13*).

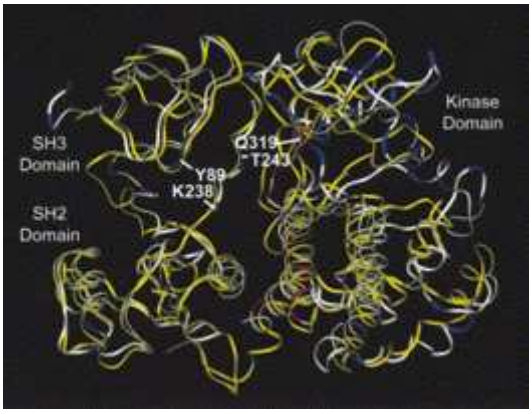

Figure 13: *Abl protein.*

The kinase domain presents a bilobal structure: the N-lobe contains a β-sheet and one conserved α-helix, the C-lobe is largely helical. At the interface between the two lobes, a highly conserved sequence of aminoacidic residues forms the ATP-binding pocket and the catalytic site. It was showed[38] that Abl is involved in the transduction of signals initiated by T-cell antigen receptor (TCR), a transmembrane receptor associated to T-cells (Thimus cells), a particular kind of lymphocytes. When an antigen is present inside a cell, it's able to generate a pathogen-derived antigenic peptide, and this peptide is the ligand of a specific kind of TCR. When a TCR is engaged by its ligand, it initiates a signal cascade that results in the proliferation and activation of T-cells specific for the infectious agent and a consequent immune response. It was recognized that, as a consequence of the engagement of the TCR, a large number of phosphorylated tyrosine residues is accumulated in some cellular proteins. Nevertheless none of the component polypeptide chains of the TCR complex have intrinsic tyrosine kinase activity, so the TCR needs to recruit various non-receptor tyrosine kinases into the microenvironment.

[37] B. Nagar, W.G. Bornmann, P. Pellicena, T. Schindler, D.R. Veach, W.T. Miller, B. Clarkson, J. Kuriyan, Crystal structures of the kinase domain of c-Abl in complex with the small molecule inhibitors PD173955 and Imatinib, *Cancer Res*. **2002**, *62*, 4236-4243.

[38] R.L. Wange, TCR signaling: another Abl-bodied kinase joins the cascade, *Curr. Biol.* **2004**, *14*, R562-R564.

Besides Abl, other three non-receptors of the Src family are involved: Lck, Fyn e ZAP-70 (*Figure 14*).

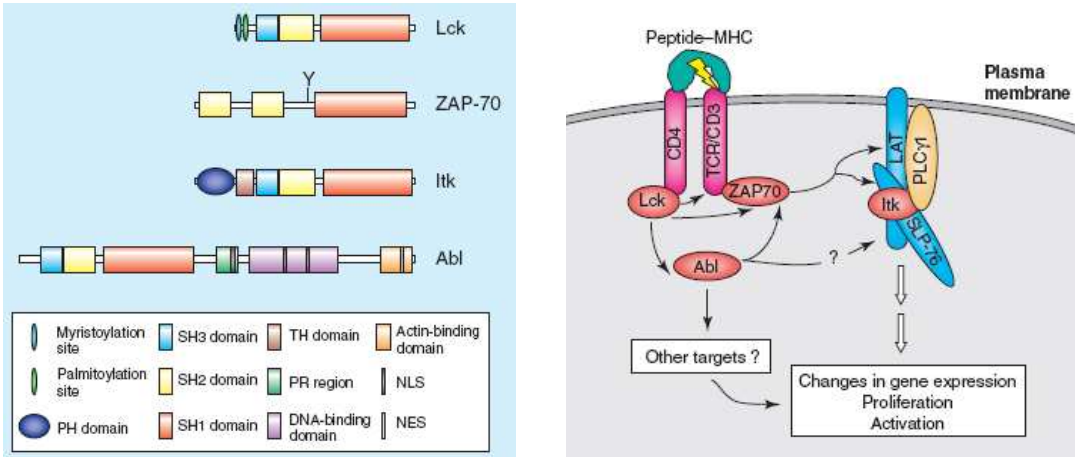

Figure 14: *Intracellular signal cascade involving Abl.*

Abl seems to act downstream of Lck and upstream of ZAP-70, although is not yet clear whether it acts exclusively through ZAP-70 or whether it might directly target other TCR signaling proteins downstream of ZAP-70. Under normal conditions, Abl exists in a highly regulated state with very low kinase activity. In most of the patients affected by chronic myeloid leukemia (CML), however, the accidental fusion of Bcr to the NH_2 terminus of Abl results in the constitutive activation of Abl kinase activity: Bcr-Abl phosphorylates cellular proteins extensively and transforms cells, making them growth factor independent. Recently, some small-molecule tyrosine kinase inhibitors were discovered that are able to bind to the kinase domain at the interface between the two lobes, displacing ATP. The expansion of tumor cell populations must depend not only on the rate of proliferation but also on the rate of cell death. Abl protein tyrosine kinase activity provides hemopoietic cells with a survival advantage via the suppression of apoptosis. In the hemopoietic system, programmed cell death plays a key role in the maintenance of a homeostatic supply of mature blood cells from the bone marrow. There is, however, some evidence to suggest that cells from patients with CML exhibit an enhanced survival potential, *in vitro*, in the absence of hemopoietic growth factors. CML is associated with a chromosomal translocation which results in the formation of a fusion gene (bcr-Abl) which encodes a membrane associated, activated Abl protein tyrosine kinase. Reconstitution of the murine hemopoietic system with stem cells infected with the activated Abl tyrosine protein kinase has showed that there is a positive correlation between this oncogene and leukemogenesis. A possible role for activated Abelson tyrosine kinase on the suppression of apoptosis.[39]

[39] C.A. Evans, P.J. Owen-Lynch, A.D. Whetton, C. Dive, Activation of the Abelson Tyrosine Kinase Activity Is Associated with Suppression of Apoptosis in Hemopoietic Cells, *Cancer Res.* **1993**, *53*, 1735-1738.

Chapter III: Met receptor

3.1 Met inhibitors

We have considered Met receptor, as a specific target for anticancer therapies because it is involved in several cellular functions leading to cancer. It is crucial for genetic program causing cellular scattering, angiogenesis and metastatic process. In particular, in cancer cells, oncogenic Met triggers the ‘‘invasive growth” program underlying cancer invasion and metastasis that occurs when neoplastic cells leave the primary tumor and infiltrate adjacent compartments to colonize distant organs.[40] For this reason Met inhibition is an important step in anti-cancer and also in anti-angiogenic therapy. *Figure 15* shows few examples of known Met inhibitors.

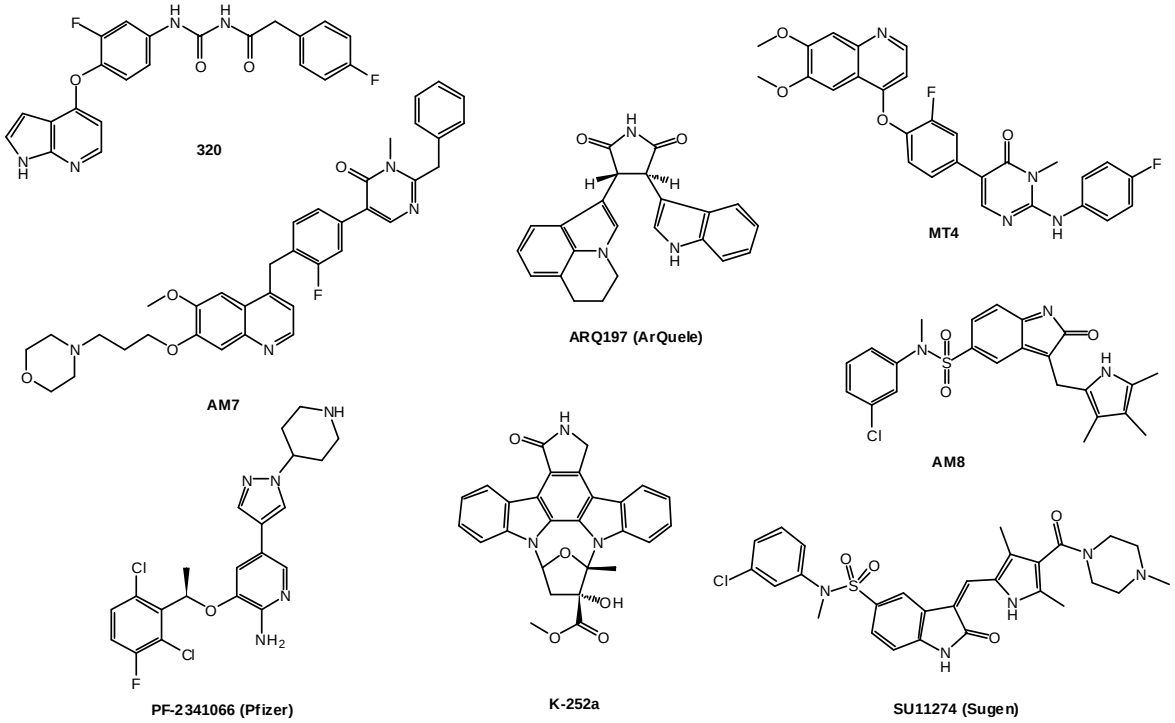

Figure 15: *Small molecules Met inhibitors.*

3.2 Modeling studies

To find new inhibitors we screened a chemical library of bioactive molecules to identify distinct chemical scaffolds with inhibitory properties towards Met. Selected compounds included analogues with physical-chemical parameters in partial or total agreement with the Lipinski’s rule of five[41] and belonged to different families corresponding to heterocycles, peptides, polyamines and natural products. Seventeen crystallographic

[40] S. Corso, P.M. Comoglio, S. Giordano, Cancer therapy: can the challenge be MET?, *Trends. Mol. Med.* **2005**, *11*, 284-292.

[41] C.A. Lipinski, F. Lombardo, B.W. Dominy, P.J. Feeney, Experimental and computational approaches to estimate solubility and permeability in drug discovery and development settings, *Adv. Drug. Deliv. Rev.* **2001**, *46*, 3-26.

complexes between Met tyrosine kinase domain and several structurally different inhibitors are available in Protein Data Bank. Such kinase complexes can be classified in three distinct conformational clusters.[42]

Cluster 1

Complexes 2RFS, 3I5N, 3CCN, 3CD8, 3F66, 2WGJ, 1R0P and 3A4P[43] show the so called active conformation of Met that is the conformation adopted by the protein when binds the ATP. As an example, *Figure 16 a* shows the binding mode of compound **AM8** within the binding site (PDB code: 2RFS). **AM8** makes favorable hydrogen bond contacts with residues Met1160 and Pro1158 belonging to the "hinge region" (residues 1159-1164). Furthermore, the *m*-chloro-phenyl portion of the ligand interacted with the activation loop (residues 1221-1251) establishing a π-π interaction with Tyr1230. In this conformation of Met, the phenylalanine of the DFG motif (residues 1222-1224) makes several hydrophobic interactions with residues Phe1200, Phe1134, Met1131, Leu1195 and Val1220 (*Figure 16 a-b*).

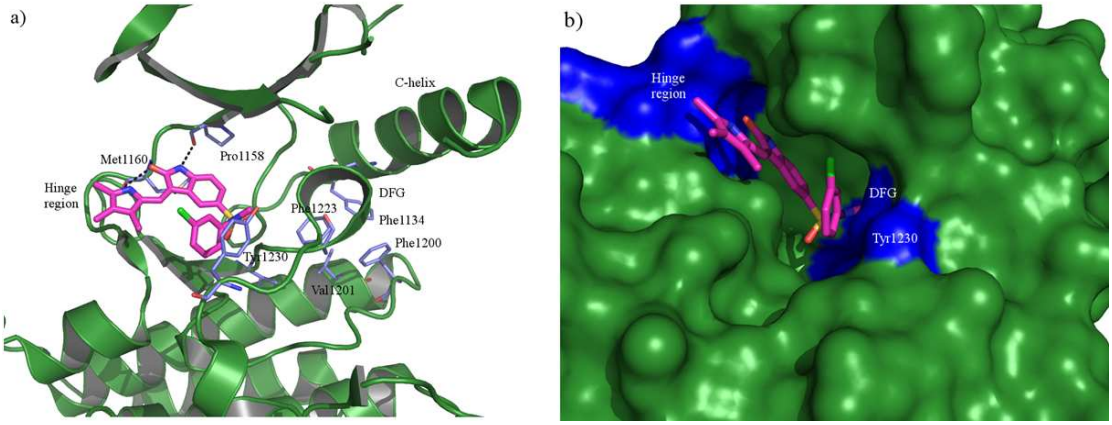

Figure 16 a-b: *Binding mode of **AM8** (reported as in stick with the carbon atoms in purple) in the active conformation of Met (2RFS).*

[42] Asses, .Y, Leroux, V., Tairi-Kellou, S., Dono, R., Maina, F., Maigret, B. Analysis of c-Met kinase domain complexes: a new specific catalytic site receptor model for defining binding modes of ATP-competitive ligands. *Chem. Biol. Drug Des.,* **2009**, *74*, 560-70.

[43] a) S.F. Bellon *et. al.*, c-Met inhibitors with novel binding mode show activity against several hereditary papillary renal cell carcinoma-related mutations, *J. Biol. Chem.* **2008**, *283*, 2675-2683. b) A.A. Boezio *et. al.*, Discovery and optimization of potent and selective triazolopyridazine series of c-Met inhibitors, *Bioorg. Med. Chem. Lett.*, **2009**, *19*, 6307-6312. c) J. Porter *et. al.*, Discovery of 4-azaindoles as novel inhibitors of c-Met kinase. *Bioorg. Med. Chem. Lett.,* **2009**, *19*, 2780-2784. d) B.K. Albrecht *et. al.*, Discovery and optimization of triazolopyridazines as potent and selective inhibitors of the c-Met kinase, *J. Med. Chem.*, **2008**, *51*, 2879-2882. e) J. Porter *et. al.*, Discovery of a novel series of quinoxalines as inhibitors of c-Met kinase. *Bioorg. Med. Chem. Lett.*, **2009**, *19*, 397-400. f) N. Schiering *et. al.*, Crystal structure of the tyrosine kinase domain of the hepatocyte growth factor receptor c-Met and its complex with the microbial alkaloid K-252a. *Proc. Natl. Acad. Sci. USA*, **2003**, *100*, 12654-12659. g) H. Nishii *et. al.*, Discovery of 6-benzyloxyquinolines as c-Met selective kinase inhibitors. *Bioorg. Med. Chem. Lett.*, **2010**, *20*, 1405-1409.

Cluster 2

Complexes 3C1X, 3CE3, 3CTH, 3CTJ, 3F82[44] present the activation loop of the protein in an inactive, DFG-out conformation. In all these complexes, the DFG motif, which is conserved among kinases and marks the beginning of the activation loop (Asp1222-Leu1245), is observed in the structure, but most of the remaining loop is undefined. The activation loop folds back toward the ATP-binding pocket opening in this way a hydrophobic pocket (Phe1134, Phe1200, Met1131, Leu1195 and Val1220), herein called DFG pocket. Within this cluster, the DFG pocket is always occupied by a *p*-F-phenyl ring of the co-crystallized inhibitor **320**. In addition, because of the displacement of the activation loop, the C-helix (Asp1117-Phe1134) is shifted toward the DFG pocket. In this way, the C-helix pocket, defined by hydrophobic residues Phe1124, Val1155, Leu1142, Ile1145, and Gly1128 and existing because of the movement of the C-helix away from the small domain, is closed (*Figure 16 c-d*).

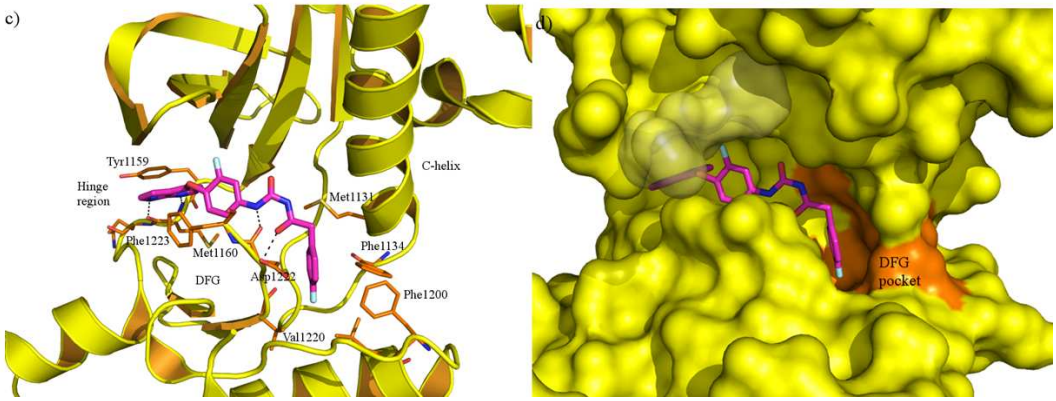

Figure 16 c-d: *Binding mode of **320** (reported as in stick with the carbon atoms in purple) in the inactive conformation of Met (3CTJ).*

[44] a) G.M. Schroeder *et. al.,* Identification of pyrrolo[2,1-f][1,2,4]triazine-based inhibitors of Met kinase, *Bioorg. Med. Chem. Lett*., **2008**, *18*, 1945-1951. b) K.S. Kim *et. al.*, Discovery of pyrrolopyridine-pyridone based inhibitors of Met kinase: synthesis, X-ray crystallographic analysis, and biological activities, *J. Med. Chem.*, **2008**, 51, 5330-5341. c) Z.W. Cai *et. al.*, Discovery of orally active pyrrolopyridine- and aminopyridine-based Met kinase inhibitors, *Bioorg. Med. Chem. Lett.*, **2008**, *18*, 3224-3229. d) G.M. Schroeder *et. al.*, Discovery of N-(4-(2-Amino-3-chloropyridin-4-yloxy)-3-fluorophenyl)-4-ethoxy-1-(4-fluorophenyl)-2-oxo-1,2-dihydropyridine-3-carboxamide (BMS-777607), a Selective and Orally Efficacious Inhibitor of the Met Kinase Superfamily, *J. Med. Chem.*, **2009**, *52,* 1251-1254.

Cluster 3

Complexes 2RFN, 3EFK and 3EFJ[45] show the activation loop of the protein in an inactive conformation, but, on the contrary to cluster 2, the C-helix pocket is open and able to receive the hydrophobic moiety of the co-crystallized ligand **MT4** (*Figure 16 e-f*).

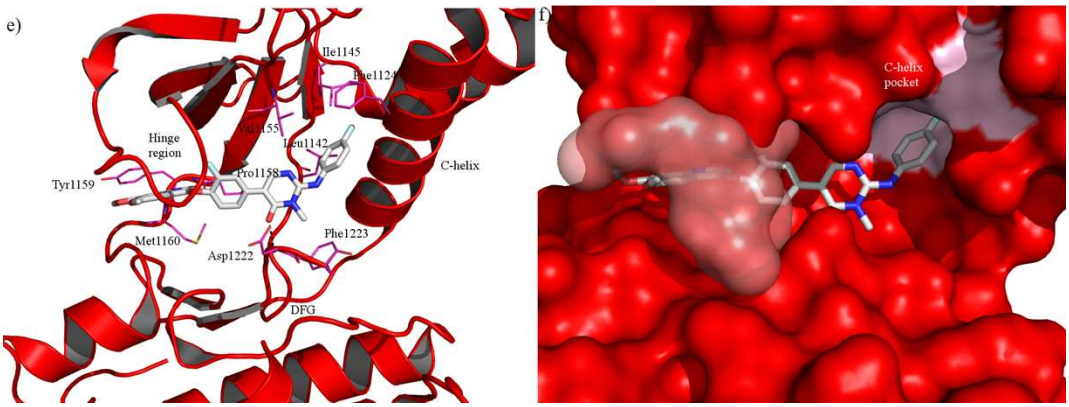

Figure 16 e-f: *Binding mode of **MT4** (reported as in stick with the carbon atoms in white) in the inactive conformation of Met (3EFK).*

The docking studies and the molecular dynamic simulations previously reported showed the generic scaffold **1** (*Figure 17*) as potential Met inhibitors. *Figure 17* shows also the possible interaction between ligand and protein.

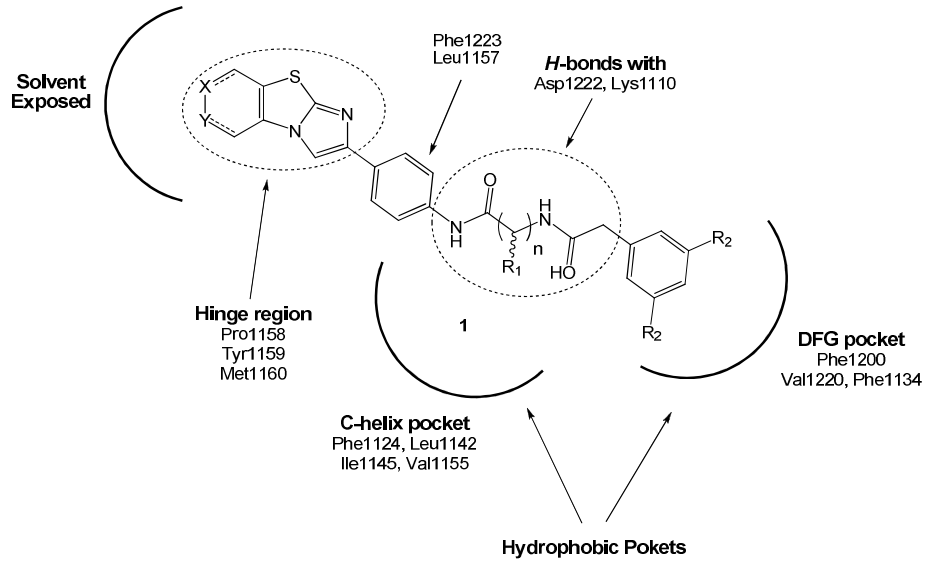

Figure 17: *Interaction between Met and the generic structure **1** suggested by modeling.*

[45] D`Angelo, N. D., Bellon, S. F., Booker, S. K., Cheng, Y., Coxon, A., Dominguez, C., Fellows, I., Hoffman, D., Hungate, R., Kaplan-Lefko, P., Lee, M. R., Li, C., Liu, L., Rainbeau, E., Reider, P.J., Rex, K., Siegmund, A., Sun, Y., Tasker, A. S., Xi, N., Xu, S., Yang, Y., Zhang, Y., Burgess, T. L., Dussault, I., Kim, T. S. Design, synthesis, and biological evaluation of potent c-Met inhibitors. *J. Med. Chem*, **2008**, *51*, 5766-5779

This class of compounds bind within the Met ATP-binding pocket in the inactive, DFG out conformation (see *claster 2*), with the thiazole moiety at the entrance of the binding pocket, near the residues forming the hinge region (Pro1158, Tyr1159 and Met1160). The disubstitued-benzene occupied the DFG hydrophobic pocket and the R^1 residue occupied the C-helix hydrophobic pocket. The ligand was also involved in hydrogen bond interaction with the Lys62 side chain. Taking into consideration the binding mode of such hit compound, the available crystallographic structures of Met in complex with different inhibitors and all the known anticancer compounds reported in IMS and Becker's data banks, we design a new collection of compounds based on this characteristics:

- presence of tetrahydropyridine, benzene or a cyclohexyl ring condensed on the thiazole moieties. The aromatic ring of Tyr1159, belong to hinge region, could favorably interact with the aromatic portion of the benzothiazole.
- introduction of a second hydrophobic group R^1 on the pseudo-peptide chain large enough to occupy the activation loop pocket making these compounds able to simultaneously interact with the two hydrophobic pockets.

We planned the preparation of four series of compounds characterized by a different tricyclic scaffold and using a convergent approach (*Scheme 1*).

3.3 Chemistry

In our approach, we took into consideration the information deriving from molecular modeling studies and we designed a synthetic path with a convergent approach. The retro-synthetic strategy, showed in *Scheme 1* proceeds through the separated preparation of the thiazole **2** and pseudo-dipeptide **3** portions bonded with an amide bound to afford analogues of generic structure **1**.

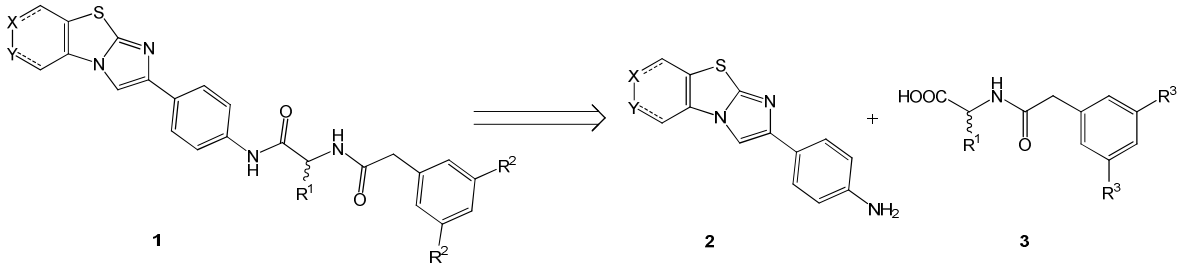

Scheme 1: *Convergent retrosynthetic approach.*

3.3.1 Thiazole portion synthesis

Following the molecular modeling guideline we have synthesize four different thiazole scaffolds (*Scheme 2*) based on the skeleton **2**:

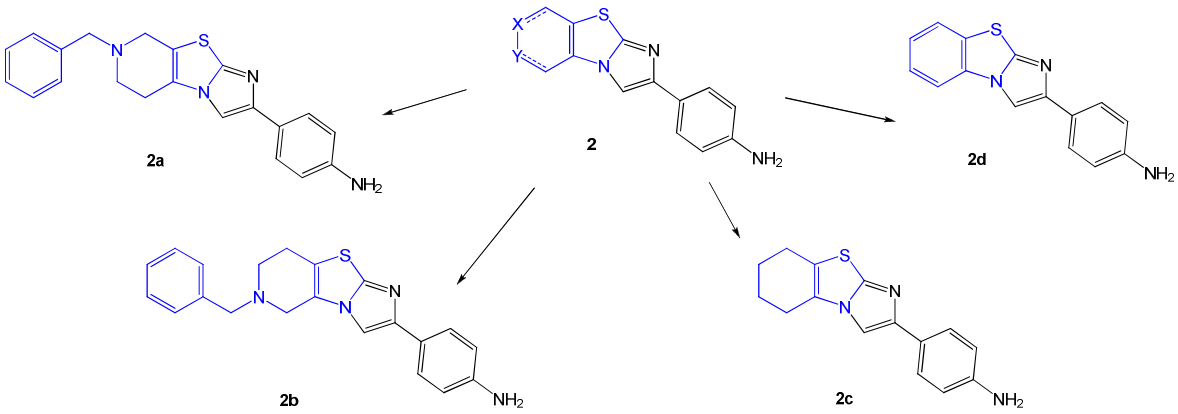

***Scheme 2**: Thiazoles portion synthesized.*

Each of these was synthesized starting from the corresponding 2-aminothiazole **4a-d**, commercially available, with the exception of **2c**. In this case the starting 2-aminotetrahydro benzothiozole **4c** was obtained by reaction of cyclohexanone with thiourea in the presence of iodine (*Scheme 3*).[46] This particular reaction is solvent free and leads to **4c** without any purification.

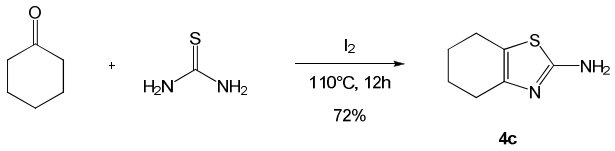

***Scheme 3:** Synthesis of 2-Amino-4,5,6,7-tetrahydrobenzothiazole **4c**.*

Reaction of **4** with 2-bromo-4'-nitroacetophenone in EtOH or *i*-PrOH provided the corresponding nitro-derivatives **5** by alkylation of the ring nitrogen and successive dehydration.[47] The use of a polar solvent secured the successive second step while the

[46] A. Singh, J. Mohan, H.K. Pujari, Heterocyclic systems containing a bridgehead nitrogen atom: Part XXV. Syntheses of imidazo[2,1-*b*]benzothiazoles and quinoxalino[2,3:4',5']imidazo-[2',1'-*b*] benzothiazoles, *Indian J. Chem.* **1976**, *14B*, 997-998.

[47] M. Amat, A. Kövér, D. Jokic, O. Lozano, M. Pérez, N. Landoni, F. Subrizi, J Bautista, J. Bosch, Synthesis of a tetrahydroimidazo- [2',1':2,3]thiazolo[5,4-*c*]pyridine derivative with Met inhibitory activity, *ARKIVOC* **2010**, *3*, 145-151.

use of toluene induces only the first step of the reaction (*Scheme 4*) that lead to compounds **6**.

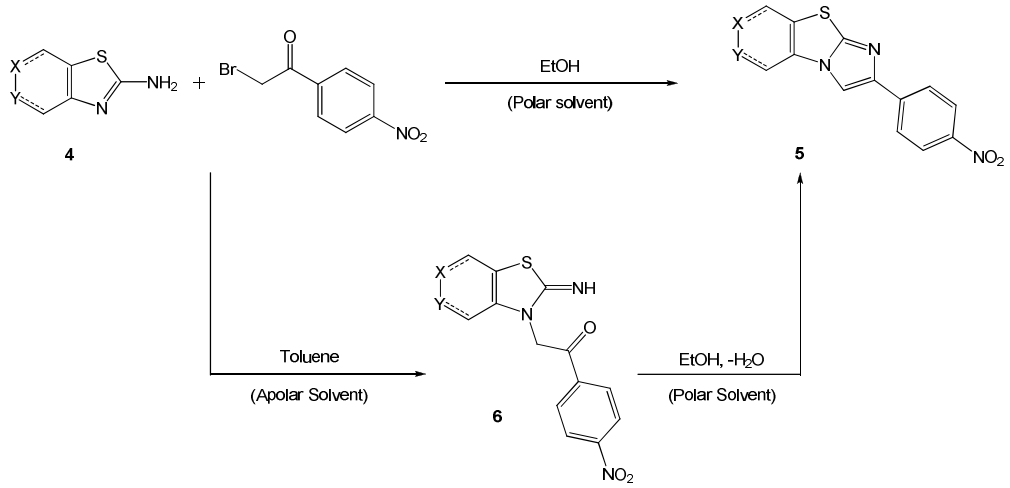

Scheme 4: *Synthesis of* ***5****.*

The following reduction of the nitro group presents some problems. We tried with hydrogenation catalyzed by palladium using both THF and acetic acid as solvent but only the starting reagent was recovered. No reaction was detected probably due to the presence of sulfur that poisons the catalyst. The next attempt was done with $SnCl_2$ in MeOH and concentrated HCl. In this case we isolated **2** in a variable yields (*Scheme 5*).

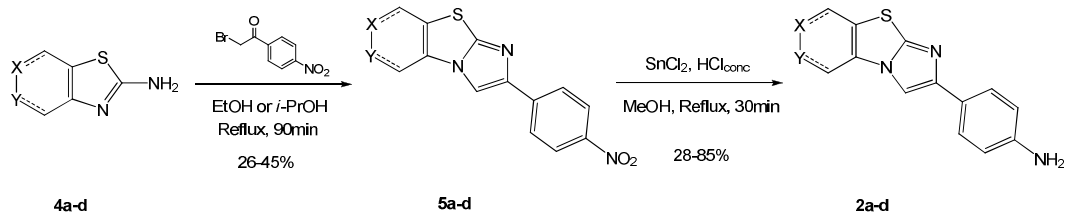

Nome	Thiazole
a	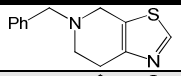
b	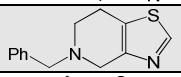
c	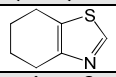
d	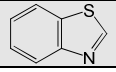

Scheme 5: *Synthesis of compounds* ***2a-d****.*

The reason is the presence of a secondary reaction (*Scheme 6*) that led to a chlorine insertion at position 3 of the tricyclic core (compounds **7**).

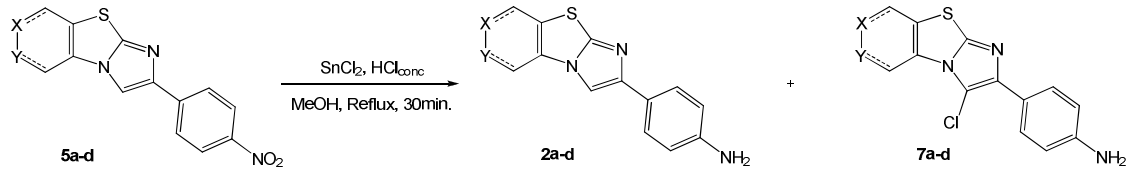

Scheme 6: *Formation of side products **7** in the reduction of **5** using $SnCl_2$.*

This side reaction was acceptable in the **2a-b** synthesis because it is slower than the reduction. But in the case of **2c-d** the chlorine insertion was faster and that gave an unsatisfactory yield, lower than 50%. This problem was overcome using Fe-powder in the presence of H_2SO_4 concentrated that leads to **2c-d** in good yields and without any further purification (*Scheme 7*).

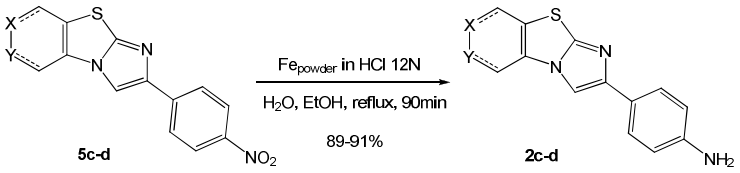

Scheme 7: *Reduction of **5c-d** using iron.*

3.3.2 Pseudo-dipeptide portion synthesis

Glycine, *R*- and *S*-alanine, *R*- and *S*-phenylalanine, and *S*-tyrosine were selected for the generation of the pseudo-dipeptidic chain (*Scheme 8*) that was subsequently condensed with the tricyclic scaffolds. The methyl esters of the aminoacids were reacted with 3,5-dimetylphenyl-, 3,5-difluorophenyl- and 3,5-ditrifluorometylphenyl-acetic acids in the presence of DCC or DCI to give the methyl esters **8**. The hydrolysis of **8** (LiOH, MeOH, 0°C, 1h) took place without any racemization[48] as reported in literature, and permitted to obtain the desired acids **3** (*Table 5*) that was recovered without any further purification.

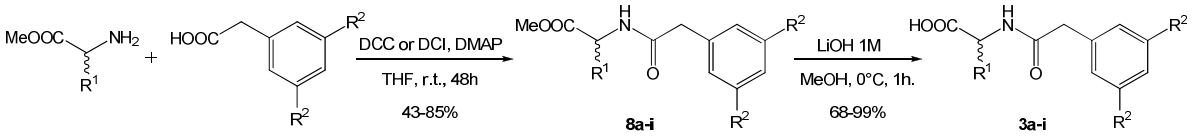

Scheme 8: *Generic synthesis of pseudo-dipeptide **3**.*

Compound	R^1	R^2
a	(*S*)-Bn	CH_3
b	(*R*)-Bn	CH_3
c	(*S*)-Bn	CF_3
d	(*R*)-Bn	CF_3
e	(*S*)-Bn	F
f	H	CH_3
g	(*S*)-*p*OH-Bn	CH_3
h	(*S*)-Me	F
i	(*R*)-Me	F

Table 5: *Pseudo-dipeptide **3** synthesized.*

[48] a) C. Benhaim, L. Bouchard, G. Pelletier, J. Sellstedt, L. Kristofova, S. Daigneault, Enantioselective Synthesis of beta-Trifluoromethyl alpha-Amino Acids *Org. Lett.* **2010**, *12*, 2008-2011; b) J.E. Green, D.M. Bender, S. Jackson, M.J. O'Donnell, J.R. McCarthy, R. James, Mitsunobu Approach to the Synthesis of Optically Active alpha,alpha-Disubstituted Amino Acids *Org. Lett.* **2009**, *11*, 807-810; c) L. Gentilucci, L. Cerisoli, R. De Marco, A. Tolomelli, A simple route towards peptide analogues containing substituted (S)- or (R)-tryptophans *Tetrahedron Lett.* **2010**, *51*, 2576-2579.

*3.3.3 Synthesis of compounds **1***

We synthesized four families with scaffold **1** classified by the thiazole building block **2a-d** employed (*Scheme 9*).

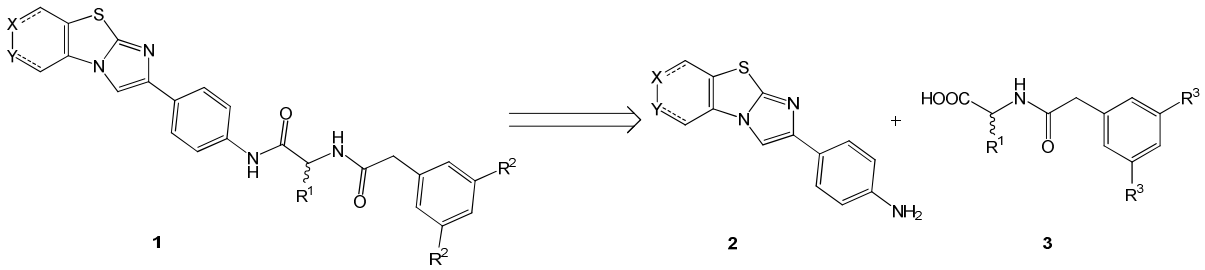

Scheme 9: *Convergent retrosynthetic approach.*

In the first approach we tried to form the acyl chloride of dipeptides **3** using firstly thionyl chloride and then with oxalyl chloride but in both cases we had a rapid degradation of **3** that made impossible them employs. Reject this strategies we decided to follow the condensating agents way. For this purpose we tried several conditions. The first coupling agents employed, DCC, DIC, EDC and DMC (*Figure 18*) gave back **1** in a very low yield, lower than 20%, and with a complex profile of side products that make hardly the purification of the desired product. Then we tried with a stronger agent named BOP-Cl. In this case we obtain the series of compounds **1** with a quite good yield of 45-70% but again with a bad profile of side products.

Not pleased with these results we tried again the coupling using HATU. These last conditions led to final products in good yields (70-90 %).

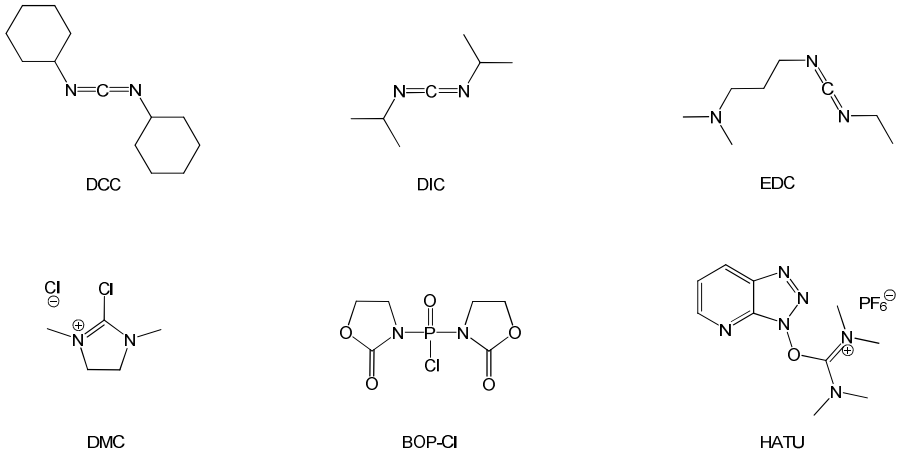

Figure 18: *Condensing agents employed in the synthesis of final compounds **1**.*

The building blocks **2a** and **2b** were used for the formation of the corresponding compounds **9** and **10** using HATU or BOP-Cl as condensing agent.

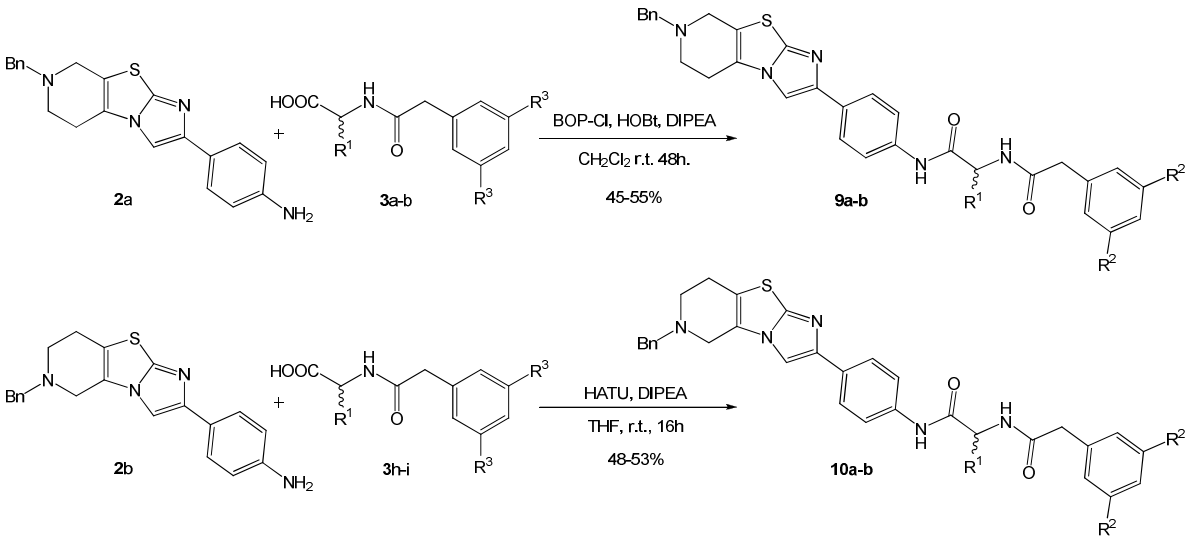

Compound	R^1	R^2
9a	(*S*)-Bn	CH_3
9b	(*R*)-Bn	CH_3
10a	(*S*)-Me	F
10b	(*R*)-Me	F

The use of **2c** and **2d** permitted the obtainment of **11** and **12** respectively. In these cases only HATU was used due to its high reaction yields. All the obtained compounds resulted stable as solid and in solution (DMSO, $CHCl_3$, MeOH). All the structures were confirmed on the base of the NMR and MS spectra.

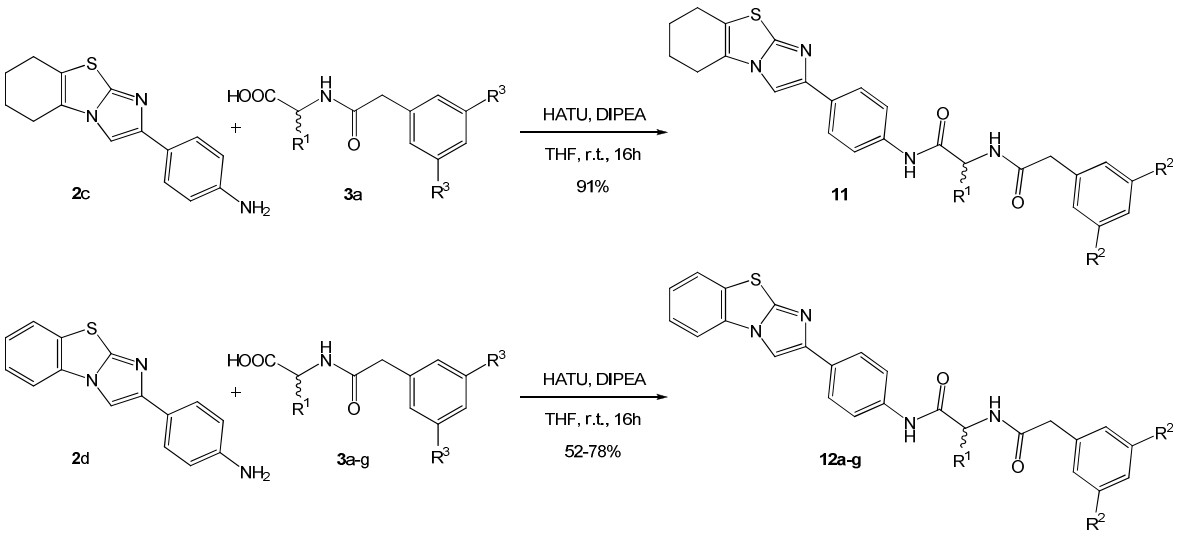

Compound	Code	R^1	R^2
11	CF054	(*S*)-Bn	CH_3
12a	CF022	(*S*)-Bn	CH_3
12b	CF056	(*R*)-Bn	CH_3
12c	CF052	(*S*)-Bn	CF_3
12d	CF081	(*R*)-Bn	CF_3
12e	CF082	(*S*)-Bn	F
12f	CF083	H	CH_3
12g	CF023	(*S*)-*p*OH-Bn	CH_3

Each compound was synthesized in hundreds milligrams scale except **12a** and **12c** that, for their high activity, were synthesized in grams scale necessary for *in vivo* biological trials.

3.3.4 Importance of central chain

Till this point we tried to change the different R^1 and R^2 residues and the thiazole scaffold but no affords was done to check the importance of the central chain conformation (*Figure 19*).

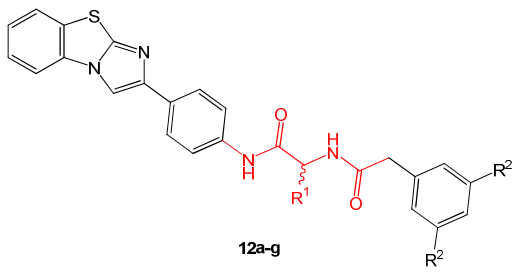

Figure 19: *In red is showed the central pseudo-dipeptide chain.*

We took as a candidate our lead compound CF052 (**12c,** see biological section, scattering test pag 69) and we introduced some modification in the central portion of the molecule. Ever following the prediction of molecular modeling studies, we synthesized the corresponding benzylamine of **2d**, compound **14**, using the procedure reported below in *Scheme 10*.

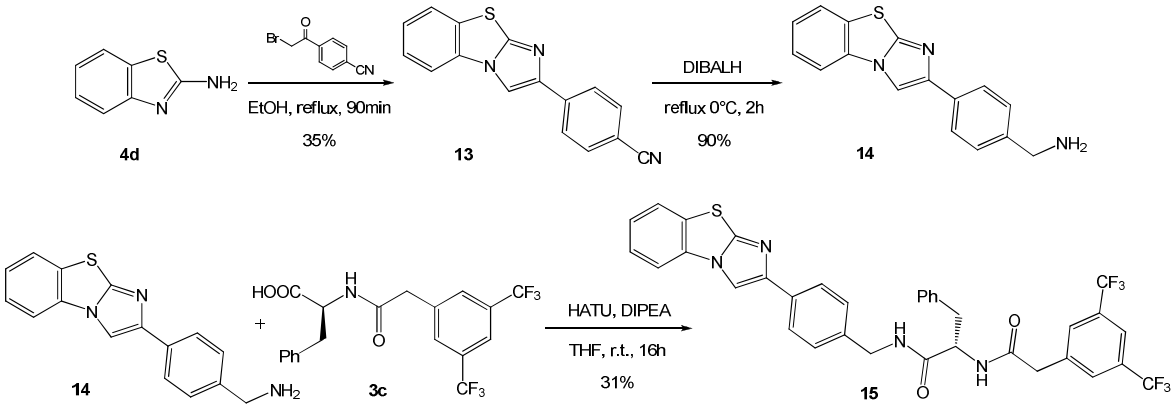

Scheme 10: *Synthesis of modified analogues **15**.*

The modeling showed that the analogue **15** has a worse binding affinity compared to **12c**. But our idea was to check the importance of central chain and the program prediction ability. Furthermore a chemical diversity is fundamental for the improvement of the molecular model.

Following the same idea we synthesized two different analogs (**18** and **19**) using a pseudo-peptide portion based on β-alanine (*Scheme 11*).

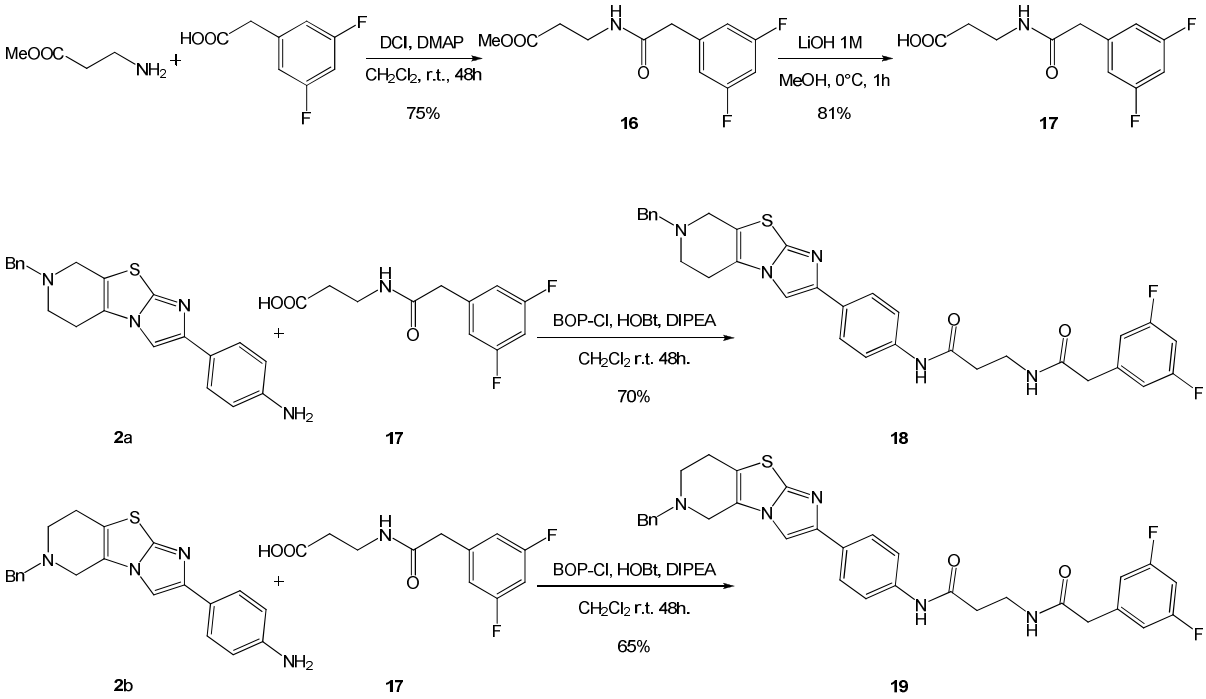

Scheme 11: *Synthesis of modified analogues **18** and **19** based on β-alanine.*

3.4 BIACORE: Surface plasmon resonance (SPR)

Working on TKIs an important point is to know the selectivity of our compounds, in particular if they are able to interact significantly only with the prefixed biological target or with a more number of targets. To do this kind of screening several tests are available but BIACORE: Surface Plasmon Resonance (SPR) seemed particularly interesting (*Figure 20*).

Figure 20: *BIACORE Surface Plasmon Resonance (SPR) instrument.*

The surface plasmon resonance (SPR) phenomenon occurs when polarized light, under conditions of total internal reflection, strikes an electrically conducting gold layer at the interface between media of different refractive index: the glass of a sensor surface (high refractive index) and a buffer (low refractive index). A wedge of polarized light, covering a range of incident angles, is directed toward the glass face of the sensor surface. Reflected light is detected within a Biacore system. An electric field intensity, knowed as an evanescent wave, is generated when the light strikes the glass. This evanescent wave interacts with, and is absorbed by, free electron clouds in the gold layer, generating electron charge density waves called plasmons and causing a reduction in the intensity of the reflected light. The resonance angle at which this intensity minimum occurs is a function of the refractive index of the solution close to the gold layer on the opposing face of the sensor surface. As molecules are immobilized on a sensor surface, the refractive index at the interface between the surface and a solution flowing over the surface changes, altering the angle at which reduced-intensity polarized light is reflected from a supporting glass plane. The change in angle, caused by binding or dissociation of molecules from the sensor surface, is proportional to the mass of bound material and is recorded in a sensorgram. When sample is passed over the sensor surface, the sensorgram shows an increasing response as molecules interact. The response remains constant if the interaction reaches equilibrium. When the sample is replaced by buffer, the response decreases as the interaction partners dissociate. Complete profiles of recognition, binding and dissociation are generated in real time. From these profiles, data such as specificity, affinity, kinetic behavior and sample concentration can be determined. For most applications, a dextran matrix covering the gold layer enables molecules to be immobilized to a sensor surface and provides a hydrophilic environment for interactions. Surface specificity is determined by the nature of the immobilized molecule. Since light does not penetrate the sample, interactions can be followed in colored, turbid or opaque samples. No labels are required and detection is instantaneous.

3.5 Selectivity on Met receptor

To carry out SPR screening it is necessary to support the under examination compound on a surface. Following this aim we synthesized the bromo-derivatives **20**. The presence of bromine on the benzothiazole ring could be an important anchor point for the introduction of a spacer, conveniently functionalized, necessary for the binding with the surface.

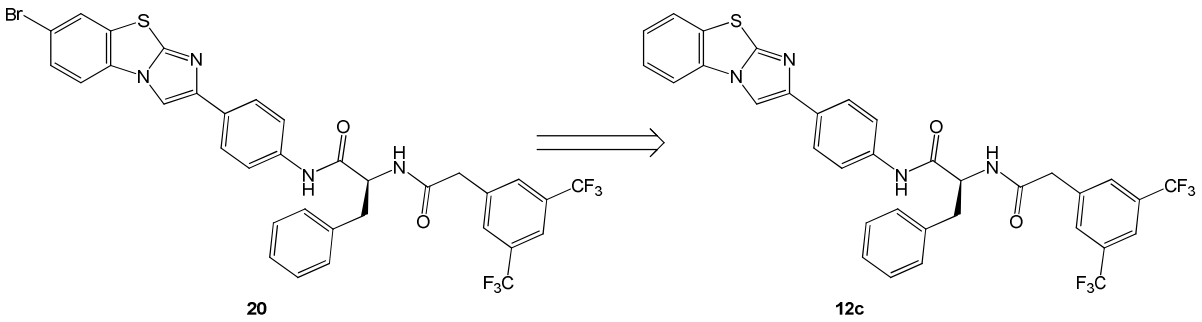

Firstly we tried directly with a direct halogenation on **12c** using both bromine and NBS. Unluckily both attempts failed. That forced us to restart a new synthesis as showed in *Scheme 12*.

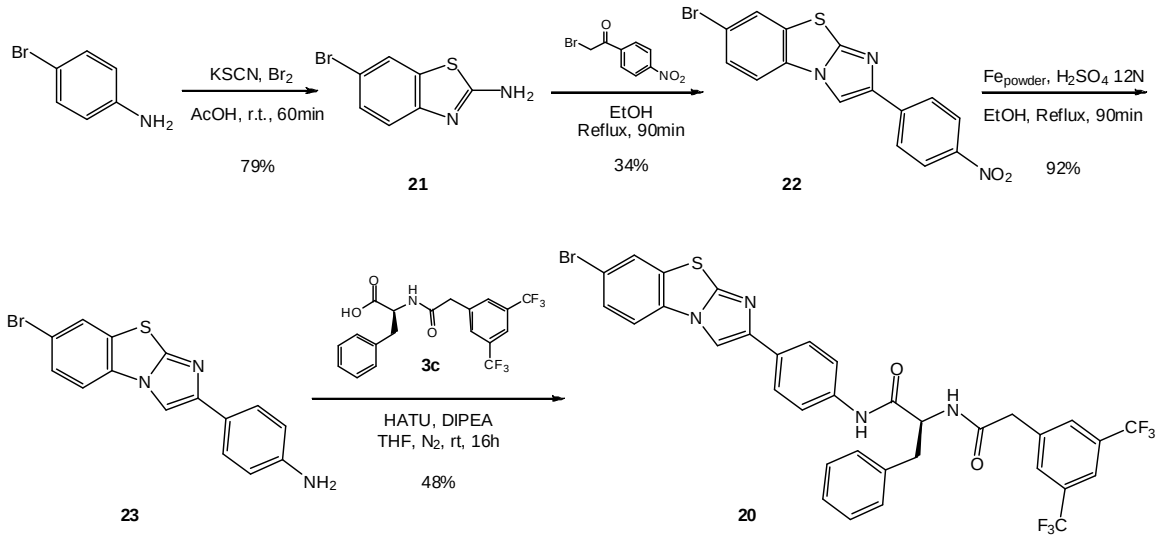

Scheme 12: *Synthesis of bromine derivatives* ***20****.*

The construction of the benzothiazole derivative **21** proceeded through the *o*-position of *p*-bromoaniline bromination followed by potassium thiocyanate nucleophilic-substitution of bromine in *o*-position. Finally, it took place the second heterocycle formation induced by aniline nitrogen (*Scheme 13*).

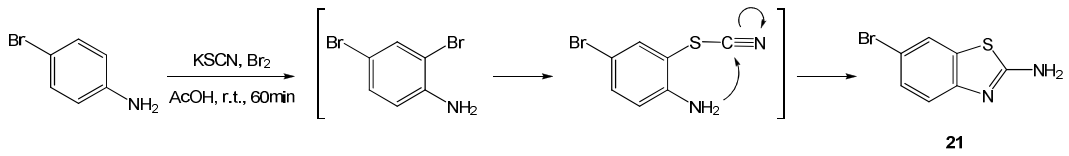

Scheme 13: *Reaction mechanism in the synthesis of* ***21****.*

The synthesis of **20** proceeded as showed previously (*Scheme 12*) through the reaction of **21** with 2-bromo-4'-nitroacetophenone in EtOH, a reduction catalyzed by Fe-powder and the final condensation with pseudo-dipeptide **3c** using HATU. Reached **20**, we tried to functionalize it played on bromine just inserted. We employed different reaction conditions like Suzuki coupling, Stille coupling, Heck reaction but no trace of functionalized product was detected. We tried also with the insertion of a nitrile moiety using following conditions:

- $Zn(CN)_2$, $Pd(PPh_3)_4$, DMF, MW, 150 °C;
- CuCN, DMF, 140 °C;

Even in these last two attempts no trace of desired product was obtained. The bromine seems unreactive. This consideration was confirmed by the same results obtained using identical reaction conditions on the precursors **22** and **23**. The only way for the introduction of the spacer seems the directly functionalization of *p*-bromoaniline.

3.6 1,2,3-Triazole and amide bioisosterism

Bioisosterism is a widely accepted principle in medicinal chemistry used to make changes in a lead structure with the aim of achieving various goals such as improved chemical stability or better pharmacokinetic properties while maintaining or even enhancing biological activity.[49] In relation to the recent widespread use of the copper(I)-catalyzed azide-acetylene cycloaddition reaction for the regioselective formation of 1,4-disubstituted 1,2,3-triazole derivatives, a lot of examples show the similarity of the amide moiety and the 1,2,3-triazole ring (*Figure 21*). The similitudes of the two moieties can be

[49] E.D. Chrysina, E. Bokor, K. Alexacou, M. Charavgi, G.N. Oikonomakos, S.E. Zographos, D.D. Leonidas, N.G. Oikonomakos, L. Somsàk, Amide-1,2,3-triazole bioisosterism: the glycogen phosphorylase case, *Tetrahedron:Asymmetry* **2009**, *20*, 733-740.

seen in the size (distance between substituents 3.8–3.9 Å in amides, 5.0–5.1 Å in triazoles), the dipolar character (amide: 4 Debye, triazole: 5 Debye) and the H-bond acceptor capacity (lone pairs of the amide oxygen as well as of the triazole nitrogens):

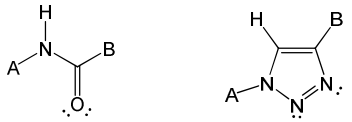

Figure 21: *Bioisosterism between amide bond and 1,2,3-triazole.*

The triazole C(5)-H can act as a H-bond donor, in a similar manner to the hydrogen of the amide, as it was showed by X ray crystallography, in which the 1,2,3-triazole can participate in the H-bond network of an α-helical peptide. These findings raise the possibility of a broader use of the 1,2,3-triazole moiety as a bioisosteric replacement for the amide group. This is also supported by the high chemical stability of the 1,2,3-triazole ring, especially under hydrolytic as well as reductive and oxidative conditions. However, the outcome of such a replacement may depend on the biological target, that is, this kind of isosterism may not be considered to be obvious and it should be verified in each case.

3.6.1 Click reaction

Looking at the environment around us, all synthetic chemists can easily understand nature's greatness: using carbonyl chemistry, nature was, and still is, able to create about 35 simple "building blocks" and to assemble them into biopolymers. But to do that, nature could rely on a whole planet and a few billion years: it means that mimicking nature's carbonyl chemistry doesn't suit a rapid discovery of new molecules with desired properties. For this reason one of synthetic organic chemists' goals is to develop an expanding set of powerful, selective and modular reactions that work reliably in both small- and large-scale applications. Sharpless and coworkers[50] termed this approach "click chemistry" and defined a set of stringent criteria that a process must meet to be useful in this context. The reaction must be modular, wide in scope, give very high yields, generate only inoffensive byproducts that can be removed by non-chromatographic methods, and be stereospecific (but not necessarily enantioselective).

[50] a) H.C. Kolb, M.G. Finn, K.B. Sharpless, Click chemistry: diverse chemical function from a few good reactions *Angew. Chem. Int. Ed.* **2001**, *40*, 2004-2021. b) M. Colombo, I. Peretto, Chemistry strategies in early drug discovery: an overview of recent trends *D.D.T.* **2008**, *13*, 677-684. c) J.E. Moses, A.D. Moorhouse, The growing applications of click chemistry *Chem. Soc. Rev.* **2007**, *36*, 1249-1262.

The required process characteristics include simple reaction conditions (ideally, the process should be insensitive to oxygen and water), readily available starting materials and reagents, the use of no solvent or a solvent that is benign (such as water) or easily removed, and simple product isolation. Purification, if required, must be by non-chromatographic methods, such as crystallization or distillation, and the product must be stable under physiological conditions. It is important to recognize that click reactions achieve their required characteristics by having a high thermodynamic driving force, usually greater than 20 kcal mol^{-1}. Click chemistry ideals are beautifully represented among cycloaddition reactions involving heteroatoms, such as hetero-Diels-Alder and, especially, 1,3-dipolar cycloadditions. These modular reactions unite two unsaturated reactants and provide fast access to an enormous variety of interesting five- and six-membered heterocycles. In this family of reactions, the most useful in organic chemistry are Huisgen dipolar cycloadditions of azides and alkynes.[51] Concerns about the safety of azide moiety have always been an obstacle to a wide use of these reactions, but the azide group is by far the most convenient of the 1,3-dipolar components to introduce and probably the only one which is stable toward dimerization and/or hydrolysis. In addition, a wide variety of alkynes can participate to this reaction, with the EWG-substituted terminal alkynes being the most reactive.

3.6.2 Huisgen cycloaddition

The Huisgen cycloaddition reactions products are 1,2,3-triazoles and they are very interesting moieties in medicinal chemistry since they can act like rigid linkers mimicking the atom placement and electronic properties of a peptide bond, but without the same liability in hydrolytic cleavage. The drawback of these reactions is that a mixture of regioisomers is obtained:

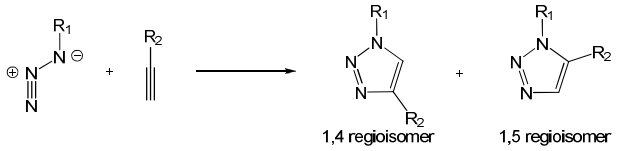

In 2002 Sharpless' and Meldal's groups reported independently the advantages of Cu(I)-catalyzed alkyne-azide cycloaddition (CuAAC). Copper(I) catalysis improves the regioselectivity, affording exclusively the 1,4-regioisomer, and increases the reaction rate up to a 10^7 factor, thus avoiding also the necessity of high temperatures.

[51] M. Meldal, C.W. Tornoe, Cu-Catalyzed Azide-Alkyne Cycloaddition *Chem. Rev.* **2008**, *108*, 2952-3015.

Since copper(I) salts are quite labile, the active catalytic species is usually generated *in situ*. Two are the most used protocols:

- Copper(II)/ascorbate system: the active catalyst is generated from the Cu(II) salts (0.25-2.0 mol %) via reduction with sodium ascorbate or ascorbic acid (5-10 mol %). A slight excess of ascorbate is generally used in order to prevent the formation of the oxidative coupling products that are often observed when a Cu(I) source is used directly:

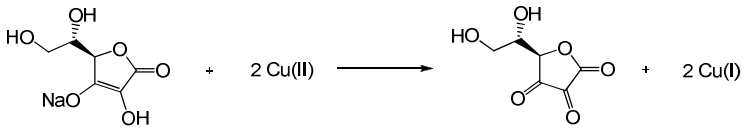

- Copper metal system: the active Cu(I) catalyst is formed via comproportionation of the Cu(II)/Cu(0) couple:

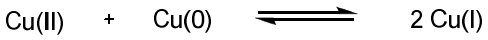

This procedure is especially convenient in parallel synthesis applications or when the substrates do not tolerate ascorbate or its oxidation products.

3.6.3 Mechanism

Density functional theory (DFT) calculations[52] revealed that the reaction proceeds through a stepwise mechanism and not through a concerted one.

- Concerted pattern (uncatalyzed)

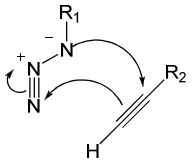

The activation barriers for the concerted reaction leading to both 1,4- and 1,5-regioisomers of the 1,2,3-triazole are 25.7 and 26.0 kcal/mol, respectively. Both reactions are highly exothermic, -60.8 and -60.6 kcal/mol, for the 1,4- and 1,5-regioisomers, respectively.

[52] F. Himo, T. Lovell, R. Hilgraf, V. V. Rostovtsev, L. Noodleman, K. B. Sharpless, V.V. Fokin, Copper(I)-catalyzed synthesis of azoles. DFT study predicts unprecedented reactivity and intermediates *J. Am. Chem. Soc.* **2005**, *127*, 210-216.

- Stepwise pattern (Cu(I)-catalyzed, regiospecific)

Conversion of the alkyne **24** to the acetylide **26** is known to be involved in many C-C bond-forming reactions. In this case the initial coordination of acetylene leads to the formation of a π-complex **25** that lowers the pK_a of alkyne C-*H* by up to 9.8 units. This makes the second step (**25**-->**26**) accessible in an aqueous environment (*Scheme 14*).

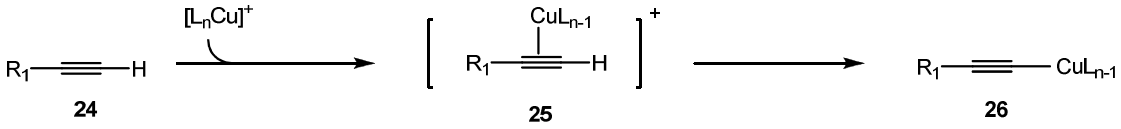

Scheme 14: *Formation of copper(I) acetylide*

A mechanism in which coordination of the acetylene to the copper(I) (without its deprotonation) activates it toward a 1,3-dipolar cycloaddition is not realistic since the calculated barrier for this process is 27.8 kcal/mol, even higher than that without the copper catalyst. The concerted cycloaddition of acetylide **26** has a high activation barrier too, 23.7 kcal/mol. In the most likely hypothesis (*Scheme 15*), it doesn't happen a concerted cycloaddition: the azide replaces one of the Cu ligands forming intermediate **27**. After that, the distal nitrogen of the azide in **27** attacks the C-2 carbon of the acetylide, forming the unusual six-membered copper(III) metallacycle **28**: the calculated barrier is 14.9 kcal/mol, considerably lower than the barrier for the uncatalyzed reaction (26.0 kcal/mol).

This explains the enormous rate acceleration of the copper(I)-catalyzed process, 7 to 8 orders of magnitude, as compared to the purely thermal cycloaddition.

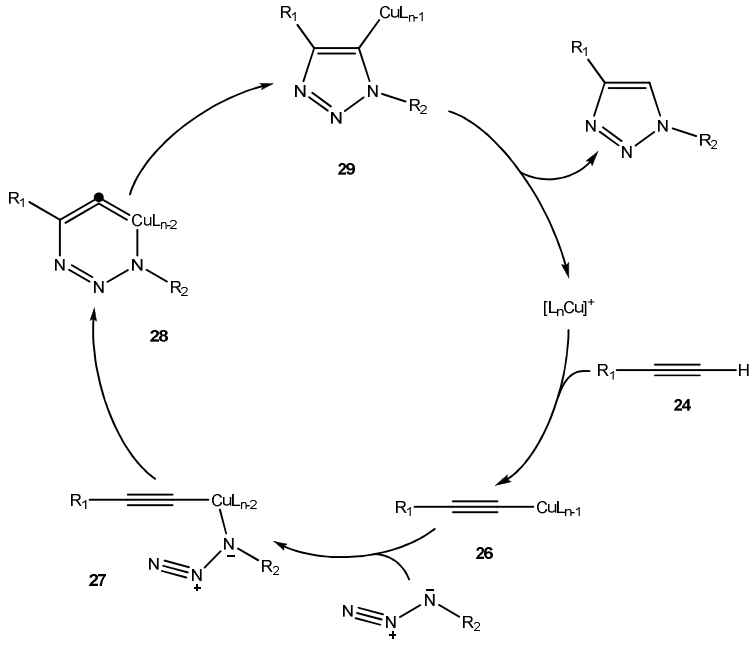

***Sheme 15**: Cycloaddition in Sharpless conditions mechanism.*

From **28**, the barrier for ring contraction, which forms the triazolyl-copper derivative **29**, is very low (3.2 kcal/mol). Proteolysis of **29** releases the triazole product, thereby completing the catalytic cycle.

3.6.4 1,2,3-Triazole analogues of CF052

Knowing the bioisosterism between 1,2,3-triazole and amide bond we considered interesting the synthesis of compound **30** (*Figure 22*). It is based on the structure of our lead compound CF052 (**12c**), the most active compound in our quality collection.

The excellent relationship between these two groups was also confirmed by molecular modeling studies.

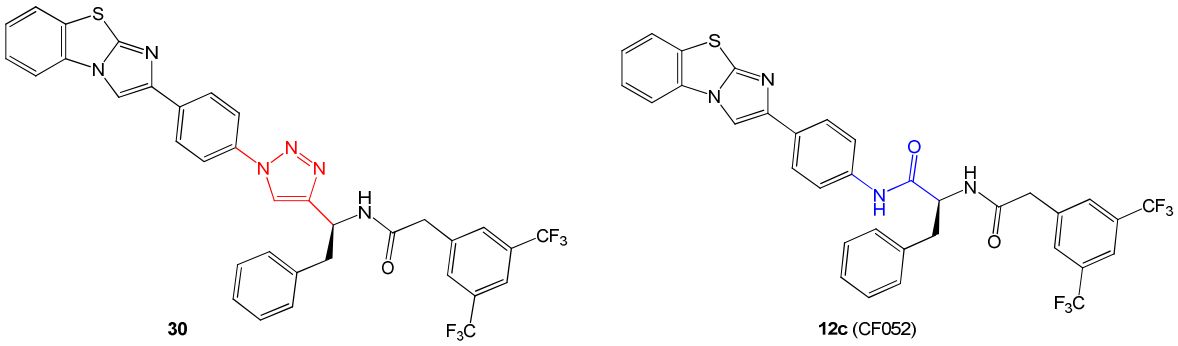

***Figure 22**: Lead compound CF052 (**12c**) and its 1,2,3-triazole analogue **30**.*

To reach **30** our affords were focused on the design of a new synthesis based on our knowledge in the field of these kind of analogues. In *Scheme 16* is showed the retrosynthetic approach. We hypothesized a key step based on a cycloaddition reaction in Sharpless conditions to afford **30** starting from azide **31** and alkyne **32**.

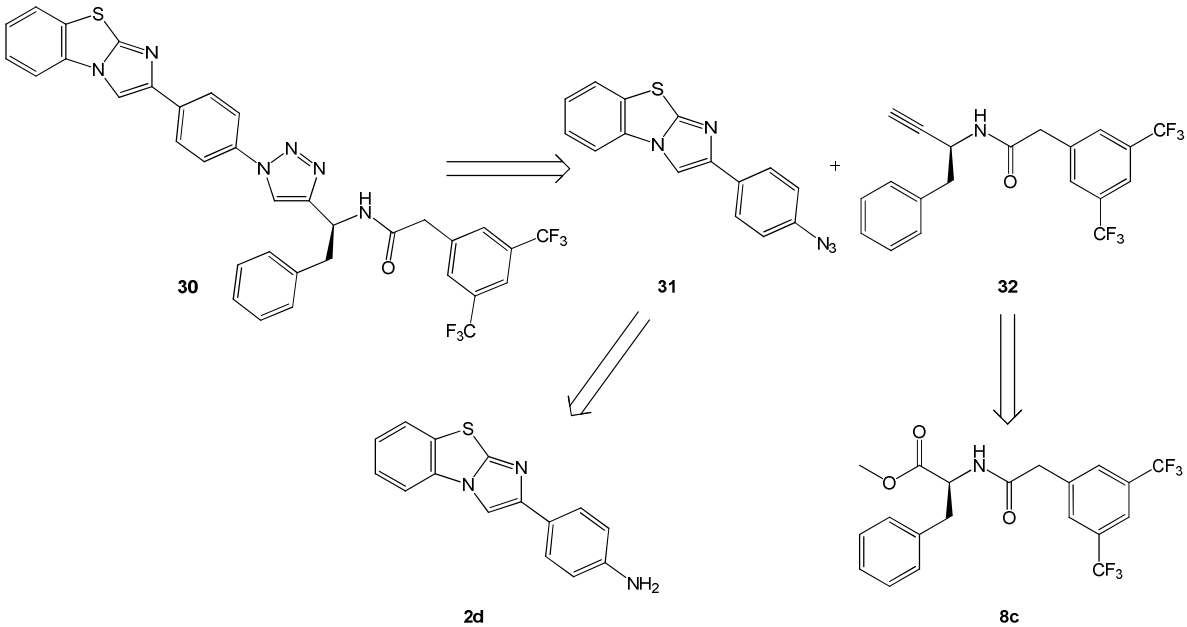

***Scheme 16**: Retrosynthetic approach for the synthesis of 1,2,3-triazole analogue **30**.*

The synthesis of azide **31** proceeded through the *in situ* formation of the diazonium salt **33**, using sodium nitrite in acid conditions and water, and subsequent reaction with sodium azide.

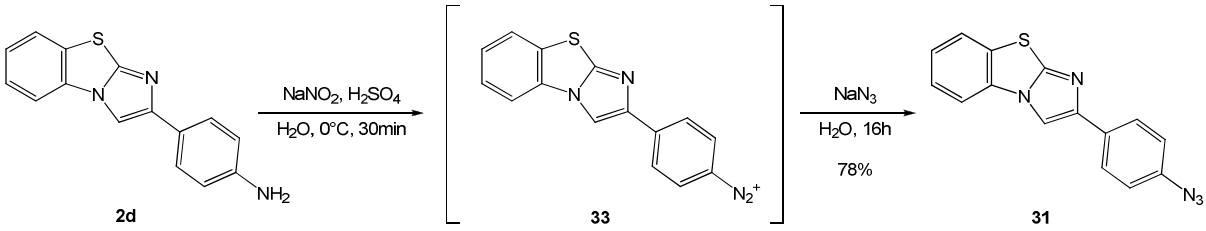

The synthesis of **32** resulted more complicated. In this case we decided to start from the methylester **8c** for its analogies with **32**. The main problem following this kind of approach was the necessity to synthesize an alkyne homologue of **8c**. Took into consideration this aspect we designed the synthesis as show below, which has a Bestmann-Ohira reaction as a key step (*Scheme 17*).

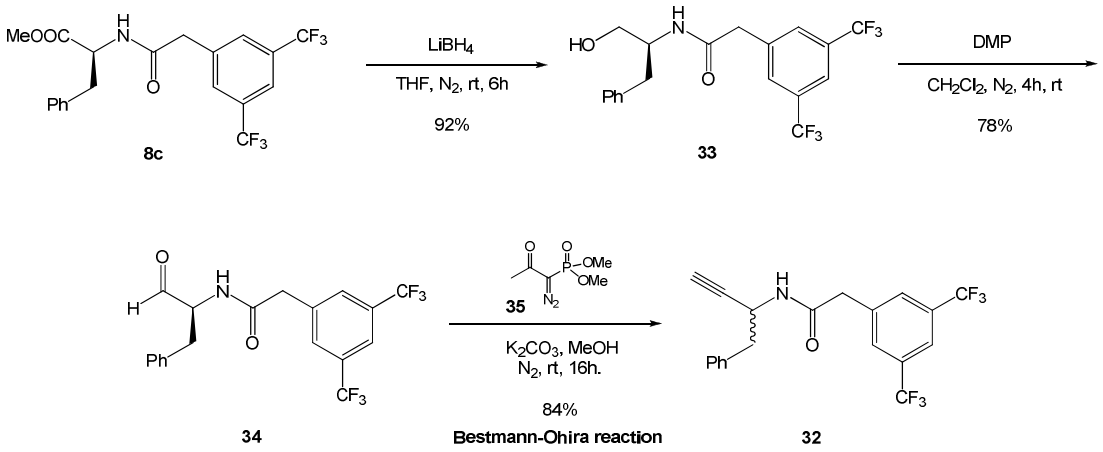

***Scheme 17**: Synthesis of alkyne **32**.*

The Bestmann-Ohira reaction allows the conversion of an aldehyde to the homologues alkyne in mild conditions using Bestmann-Ohira reagent **35**. To obtain the desired aldehyde **34** (necessary for the Bestmann-Ohira key step), we tried firstly different reductive conditions on ester **8c**. We tried using $NaBH_4$ but the reduction agent was too weak. Surely, the employment of $LiAlH_4$ should lead to the reduction of both esters and amide groups contained in structure **8c**. For this reason we used $LiBH_4$ in THF that gave the alcohol **33** in a very good yield (92 %). The reduction was followed by alcohol re-oxidation using Dess-Martin periodinane (DMP) in DCM that afford **34** in good yield (78

%). Finally the alkyne **32** was reached with the employment of Bestmann-Ohira reaction using the homonym reagent **35** and K_2CO_3 in methanol for 16 h at room temperature. Unluckily despite the mild conditions of this last step we observed the racemization of alkyne **32** due to the contemporary presence of a base and a protic solvent. The final step in the synthesis of **30** is a cyclocondensation in Sharpless conditions using azide **31** and alkyne **32** as showed in *Scheme 18*.

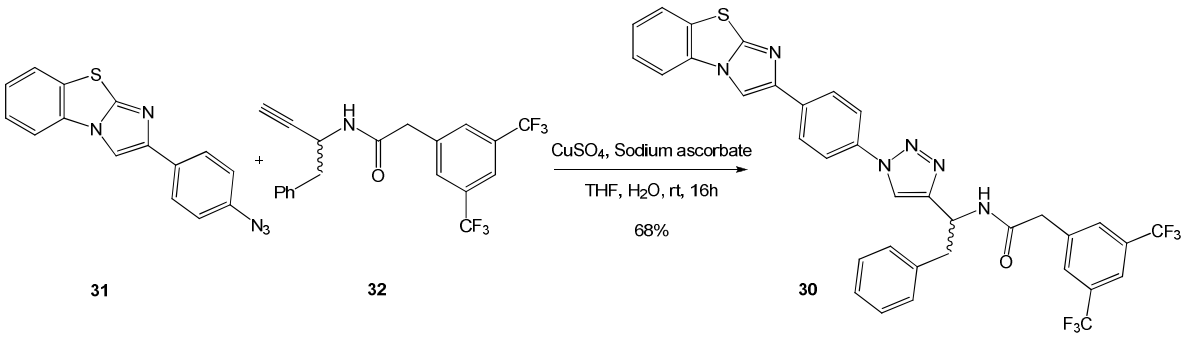

Scheme 18: *Synthesis of **30** through cycloaddition in Sharpless conditions.*

3.6.5 Bestmann-Ohira reaction

Terminal alkynes are extremely valuable synthetic intermediates and their formation from aldehydes is a widely used preparative procedure. Initially, the *Corey-Fuchs*[53] sequence has been employed, consisting in the formation of a terminal alkyne by an homologation of the corresponding aldehyde through a 1,1-dibromo alkenyl intermediate:

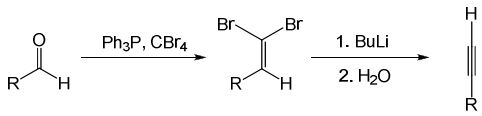

The first step is comparable to a Wittig reaction and leads to a dibromoalkene. In the formation of the ylide from CBr_4, two equivalents of triphenylphosphine are used.

[53] E.J. Corey, P.L. Fuchs, A synthetic method for formyl→ethynyl conversion (RCHO→RC≡CH or RC≡CR′), *Tetrahedron Lett.* **1972**, *13*, 3769-3772.

One equivalent forms the ylide while the other acts as reducing agent and bromine scavenger:

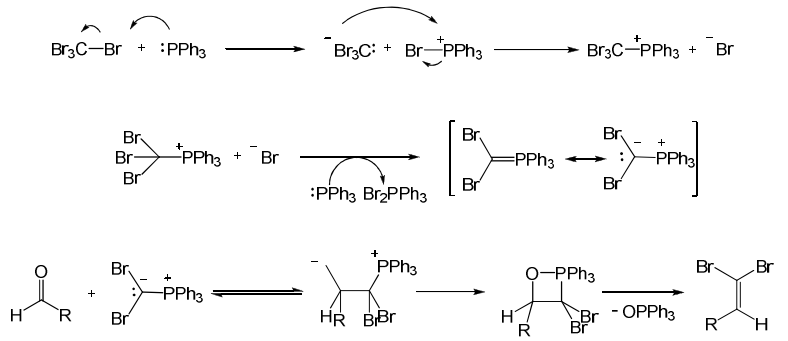

By treatment with BuLi the corresponding bromoalkyne is generated, which undergoes metal-halogen exchange and yields the terminal alkyne after work-up:

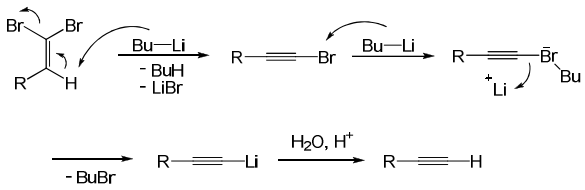

The need for a strong base like BuLi for the dehydrohalogenation of the intermediate 1,1-dibromoalkenes can limit the applicability of this procedure.

The ***Seyferth-Gilbert***[54] homologation has been revealed as a very effective alternative to this method. It consists in the base-promoted reaction of dialkyl diazomethylphosphonates with aldehydes and arylketones at low temperatures to give alkynes:

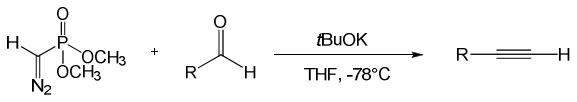

[54] D. Seyferth, R.S. Marmor, P. Hilbert, Reactions of dimethylphosphono-substituted diazoalkanes. (MeO)2P(O)CR transfer to olefins and 1,3-dipolar additions of (MeO)2P(O)C(N2)R, *J. Org. Chem.* **1971**, *36*, 1379-1386.

The deprotonated Seyferth-Gilbert reagent adds to the carbonyl compound forming an alkoxide that closes to give an oxaphosphetane. Comparable to the Wittig reaction, a cycloelimination yields a stable dimethyl phosphate anion and a diazoalkene:

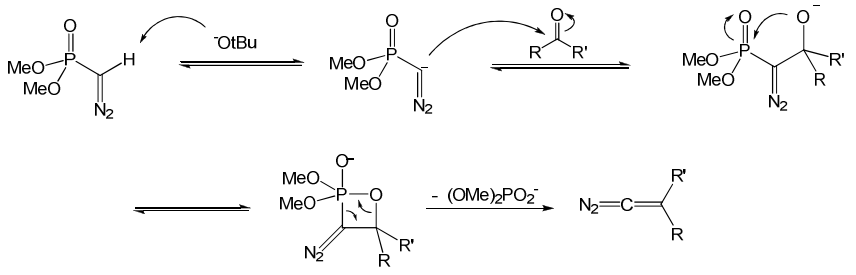

Upon warming of the reaction mixture to room temperature, loss of nitrogen gives a vinylidene carbene that yields the desired alkyne after 1,2-migration of one of the substituents:

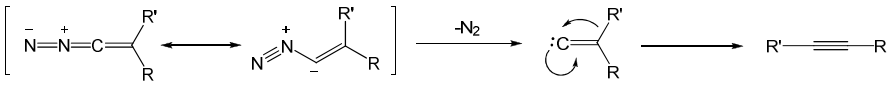

The major disadvantage of this procedure is the fact that the Seyferth-Gilbert reagent is not commercially available and has to be prepared by a multistep procedure that requires a strong base for deprotonation, low temperatures and inert gas techniques.

Recently, *Bestmann and Ohira*[55] reported a valuable procedure in which dimethyl-1-diazo-2-oxopropylphosphonate **35** is employed:[56]

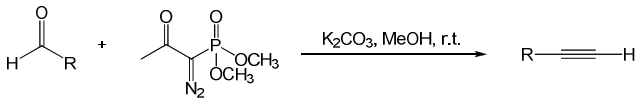

35

[55] S. Ohira, Methanolysis of dimethyl (1-diazo-2-oxopropyl) phosphonate - generation of dimethyl (diazomethyl) phosphonate and reaction with carbonyl-compounds, *Synth. Commun.* **1989**, *19*, 561-564.

[56] A.K. Gosh, A. Bischoff, J. Cappiello, Asymmetric total synthesis of the gatroprotective microbial agent AI-77-B, *Eur. J. Org. Chem.* **2003**, 821-832.

The Bestmann-Ohira reagent is stable and readily prepared in high yields from commercially available precursors:

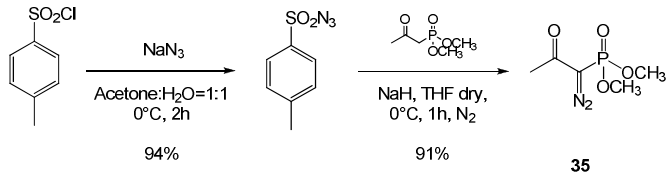

In this way, it is possible to obtain the dimethyl(diazomethyl)phosphonate anion by mild acyl cleavage of dimethyldiazo-2-oxopropylphosphonate:

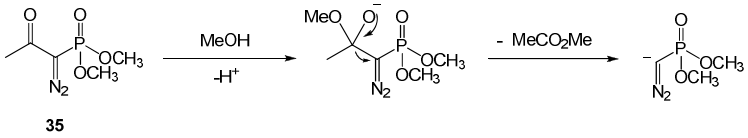

These mild reaction conditions allow the conversion of even enolizable aldehydes.[57]

Furthermore, a new procedure has been described in which the commercially available dimethyl-2-oxopropylphosphonate can directly be used as reagent:[58]

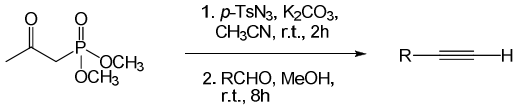

Nevertheless, this simpler procedure gave the desired alkynes in lower yields.

[57] S. Muller, B. Liepold, G.J. Roth, H.J. Bestmann, An improved one-pot procedure for the synthesis of alkynes from aldehydes, *Synlett.* **1996**, 521-522.

[58] G.J. Roth, B. Liepold, S.G. Muller, H.J. Bestmann, Further improvements of the synthesis of alkynes from aldehydes, *Synthesis* **2004**, *1*, 59-62.

3.7 Biology

3.7.1 Scattering test on MDCK cells

Efficiency of newly synthetized thiazol-based inhibitors was primarily assessed by checking their ability to block HGF-induced madin darby canine kidney (MDCK) scattering (*Figure 23*).[59] MDCK are epithelial cells forming cohesive clusters which scatter in response to Hepatocyte Growth Factor/Scatter Factor (HGF/SF) and thus represent an interesting model to study the ability of compounds to inhibit Met activity.[60] This assay is the most widely used to screen for Met inhibitors because of the clear answers it provides. It allowed us to identify among our family of compounds those which are able to inhibit Met-driven scattering, and to compare their relative efficiency by calculating their IC_{50}, corresponding to the compound concentration at which HGF-induced cell scattering was half that in the control condition. For these studies, the Met inhibitor SU11274 was used as a reference compound in all assays.[61]

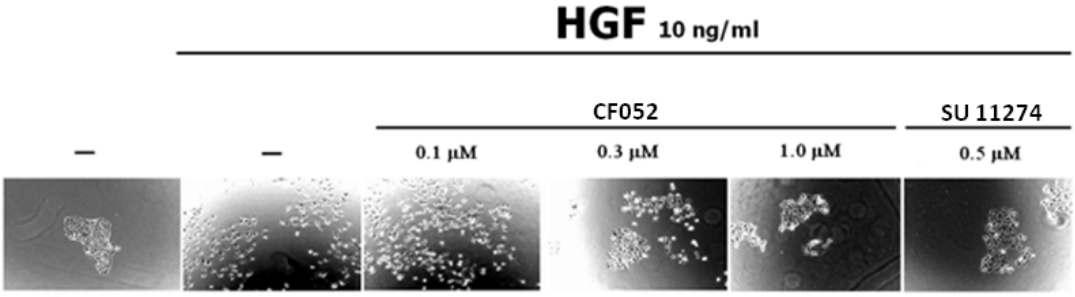

Figure 23: 12c *(CF 052) scattering test on MDCK cell.*

Among around 20 new synthesised compounds (*Scheme 19*), we found that CF022, CF052, CF054, CF056 CF081, CF082, and CF120 elicited inhibitory activity on Met-triggered cell scattering (*Table 6*).

[59] Patane, S.; Pietrancosta, N.; Hassani, H.; Leroux, V.; Maigret, B.; Kraus, J. L.; Dono, R.; Maina, F., A new Met inhibitory-scaffold identified by a focused forward chemical biological screen. *Biochem Biophys Res Commun* **2008**, *375*, 184-189.

[60] Chan, G. K.; Lutterbach, B. A.; Pan, B. S.; Kariv, I.; Szewczak, A. A., High-throughput analysis of HGF-stimulated cell scattering. *J Biomol Screen* **2008**, *13*, 847-854.

[61] Schiering, N.; Knapp, S.; Marconi, M.; Flocco, M. M.; Cui, J.; Perego, R.; Rusconi, L.; Cristiani, C., Crystal structure of the tyrosine kinase domain of the hepatocyte growth factor receptor c-Met and its complex with the microbial alkaloid K-252a. *Proc Natl Acad Sci U S A* **2003**, *100*, 12654-12659.

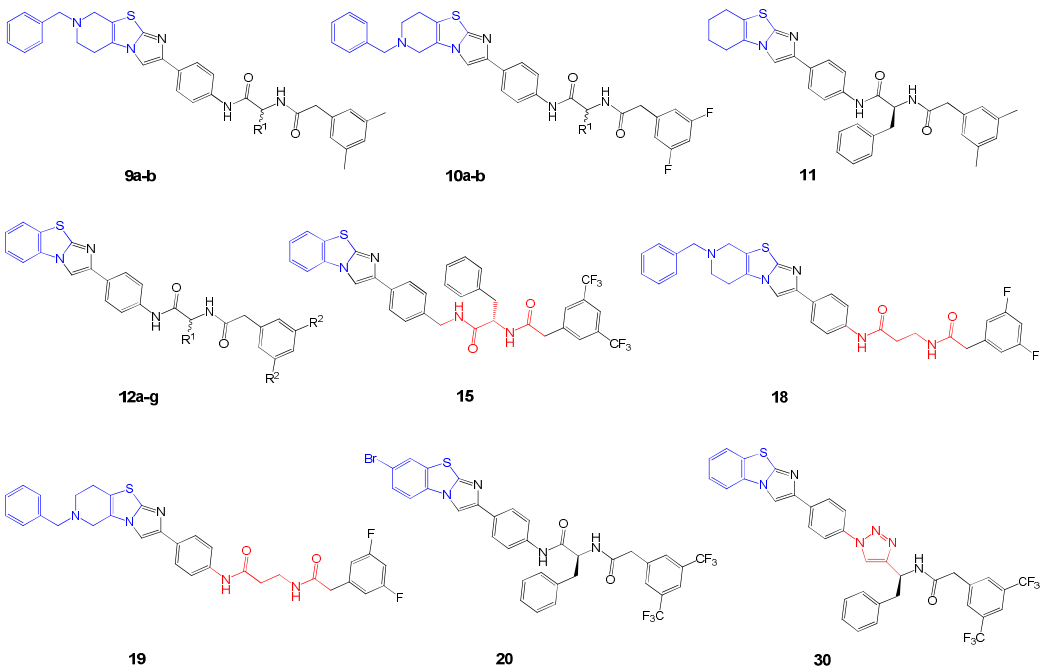

Scheme 19: *List of compounds tested on MDCK cells for HGF induced scattering test.*

Compound	Code	Thiazole	R^1	R^2	IC_{50} (μM)
9a	-	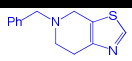	(*S*)-Bn	CH_3	Not active
9b	-	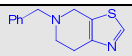	(*R*)-Bn	CH_3	Not active
10a	-	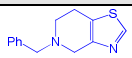	(*S*)-Me	F	Not active
10b	-	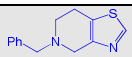	(*R*)-Me	F	Not active
11	CF054		(*S*)-Bn	CH_3	0.8
12a	CF022		(*S*)-Bn	CH_3	0.6
12b	CF056		(*R*)-Bn	CH_3	0.6
12c	CF052		(*S*)-Bn	CF_3	0.2
12d	CF081		(*R*)-Bn	CF_3	0.2
12e	CF082		(*S*)-Bn	F	0.8
12f	CF083		H	CH_3	Not active
12g	CF023		(*S*)-*p*OH-Bn	CH_3	Not active
15	CF070		(*S*)-Bn	CF_3	Not active
18	-	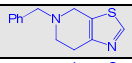	-	F	Not active
19	-	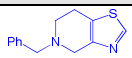	-	F	Not active
20	CF203	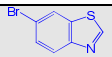	(*S*)-Bn	CF_3	Not active
30	CF120		Bn	CF_3	0.6

Table 6: *Concentration of 50 % scattering inhibition on MDCK cells. Selected CF compounds tested for their action on HGF-induced scattering of MDCK cells. The IC_{50} value (μM) for the most active compounds is reported. R^1 and R^2 residues are referred to the positions showed on generic structure* ***12a-g****.*

By evaluating the IC_{50} of the most active compounds, we found that CF052 and CF081 impaired Met-triggered cell scattering at concentration comparable to SU11274 (CF052: 0,17 µM; CF081: 0,20 µM; SU11274: 0,15 µM; *Figure 24*).

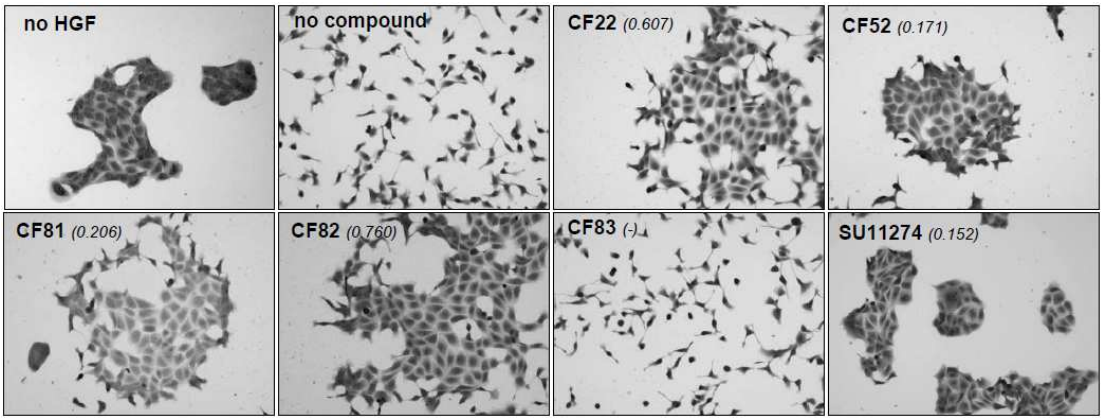

Figure 24: *HGF-induced scattering of MDCK cells is blocked by CF22, CF52, CF81, CF82, and not by CF83. SU11274 was used as positive control. The IC_{50} is indicated in µM.*

No toxic effects were observed at biologically active concentrations and they only appeared when the doses rang from 50 to 100 fold higher. The toxicity can be explained due to the presence of a little quantity of DMSO necessary for the first dissolution of the CF compounds. We could see that compound CF022 was indeed a good inhibitor of Met-induced scattering. Dehydrogenation of the thiazol ring in compound CF054 slightly decreased its activity, as well as introduction of fluorine atoms in R^2 positions in CF082, while the steriogenic center configuration doesn't lead to variations in the activity as showed by CF052 and CF081. This last modification was conceived in order to use non-natural aminoacids, which may be more resistant to proteolysis. Strikingly, the presence of CF_3 groups in R^2 substituents (compound CF052) greatly improved the inhibition by our compounds of Met-triggered scattering. The benzyl group in R^1 position proved to be critical for Met inhibition since attempts to replace it by hydrogen atom, CH_3 group or *p*-hydroxyl benzyl group resulted in inactive compounds. Further validations were obtained by testing CF compounds on human MCF10A breast cells and similar inhibitory properties on Met-triggered scattering were observed.

3.7.2 Double mechanism of action

Differently by the common Met inhibitors the interesting point of our CF series is the dual action mechanism: they impair Met signaling by interaction with the ATP binding pocket into the intracellular domain and, in addition to the classical inhibitors, prevent its restoration after degradation. This dual activity could lead to a synergic effect that makes

the CF family different by precedent Met inhibitors. In detail signalling by activated Met is attenuated through receptor endocytosis and proteasomal degradation in endosomal compartments. Subsequently, Met receptors are restored following gene transcription,[62] allowing fine tuning and delicate balance of Met functions. Upon HGF stimulation, Met is down-regulated after 6 h and its protein levels are restored after 24 h (*Figure 25*)

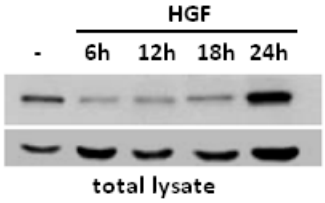

Figure 25: *Upon HGF stimulation, Met protein levels are down-regulated after 6 hours and restored by 24 hours in primary embryonic hepatocytes.*

Remarkably, CF series treatment impaired restoration of Met protein levels over time. In contrast to CF, SU11274 did not prevent up-regulation of Met protein levels (*Figure 26*), as previously showed.[63]

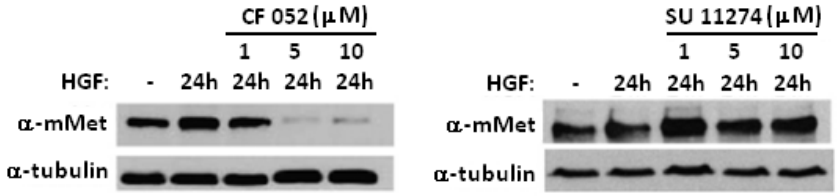

Figure 26: *restoration of Met protein levels in 293-T cells is impaired by the presence of CF052 (**12c**) at 5μM. In contrast, SU11274 does not prevent restoration of Met protein levels.*

3.7.3 Survival on HepG2 and GTL-16 cell lines

We next investigated the ability of CF compounds to prevent Met-triggered survival of cancer cells. These studies were performed on human hepatocellular liver carcinoma HepG2 cells, which tumorigenesis is Met-dependent,[64] and on human GTL-16 gastric carcinoma cells, in which Met gene amplification results in high Met protein levels and its

[62] A.C. Porter, R.R. Vaillancourt, Tyrosine kinase receptor-activated signal transduction pathways which lead to oncogenesis, *Oncogene* **1998**, *17*, 1343–1352.

[63] S. Arena, A. Pisacane, M. Mazzone, P.M. Comoglio, A. Bardelli, Genetic targeting of the kinase activity of the Met receptor in cancer cells, *Proc. Natl. Acad. Sci. USA* **2007**, *104*, 11412–11417.

[64] Heideman, D. A.; Overmeer, R. M.; van Beusechem, V. W.; Lamers, W. H.; Hakvoort, T. B.; Snijders, P. J.; Craanen, M. E.; Offerhaus, G. J.; Meijer, C. J.; Gerritsen, W. R., Inhibition of angiogenesis and HGF-cMET-elicited malignant processes in human hepatocellular carcinoma cells using adenoviral vector-mediated NK4 gene therapy, *Cancer Gene Ther.* **2005**, *12*, 954-962.

ligand independent activation. As consequences, GTL-16 cells are "Met-addicted" for survival, anchorage-independent growth, and tumor formation when injected in nude mice.[65]

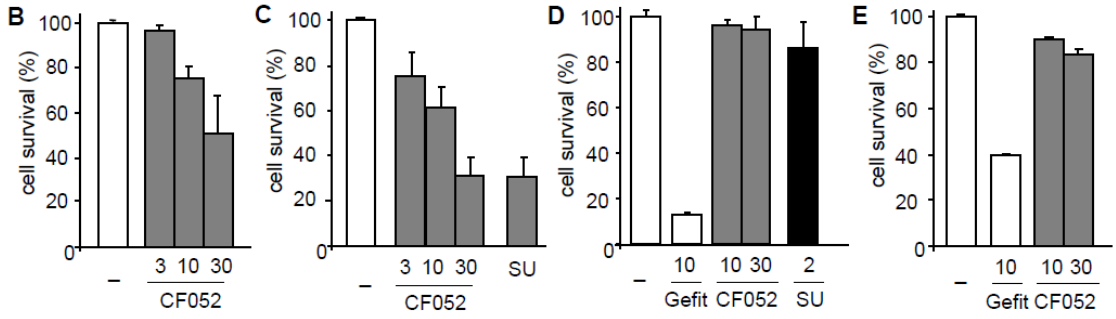

Figure 27: *(**B** and **C**) Survival of HepG2 (**B**) and GTL-16 (**C**) cells was reduced by CF052 (**12c**), in a dose dependent manner (µM). (**D** and **E**) Survival of BT474 (**D**) and MCF7-ErbB2 (**E**) cells, which are addicted to the ErbB oncogenes, was impaired by the ErbB inhibitor Gefitinib (Gefit), but not by CF052 (µM). For survival assays (n=3), cells were serum-starved for 24 hrs and then incubated with CF052 or Gefitinib for 48 h. Values are expressed as means ± s.e.m. *P<0.05; **P<0.01; Student's t-tests.*

We found that compounds CF022, CF052, CF081, and CF082 reduced survival of both HepG2 (*Figure 27 B*) and GTL-16 cells (*Figure 27 C and 28*) in a dose dependent manner.

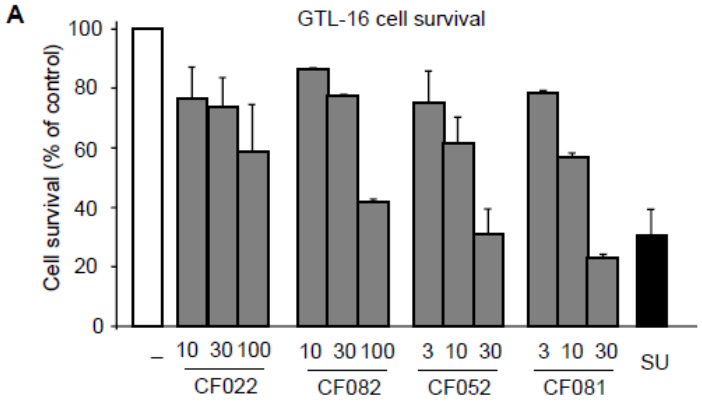

Figure 28: *CF compounds block Met-triggered cell survival and anchorage-independent growth. Survival of GTL-16 cells was reduced by CF022, CF052, CF081 and CF082, in a dose dependent manner (µM). GTL-16 cells were serum-starved for 24 h and then incubated in the presence or not of CF compounds for 48 h.*

[65] Zou, H. Y.; Li, Q.; Lee, J. H.; Arango, M. E.; McDonnell, S. R.; Yamazaki, S.; Koudriakova, T. B.; Alton, G.; Cui, J. J.; Kung, P. P.; Nambu, M. D.; Los, G.; Bender, S. L.; Mroczkowski, B.; Christensen, J. G., An orally available small-molecule inhibitor of c-Met, PF-2341066, exhibits cytoreductive antitumor efficacy through antiproliferative and antiangiogenic mechanisms. *Cancer Res* **2007**, *67*, 4408-4417.

In contrast, CF compounds did not restrain survival of cancer cell lines, such as BT474 and MCF7-ErbB2 (*Figure 27 D-E*), which are addicted to ErbBs oncogenes.[66]

3.7.4 CFs interfere with Met-triggered in vitro tumorigenesis

We next ascertained whether the identified CF compounds prevented also Met-triggered anchorage-independent growth, which is a hallmark of oncogenic transformation. Soft-agar growth of HepG2 cells requires intact Met as it is impaired by the Met inhibitor SU11274.[65] We found that compounds CF022, CF052, CF081, and CF082 impaired tumorigenesis of HepG2 cells, in a dose dependent manner (*Figure 29 A-B and 30 B*).

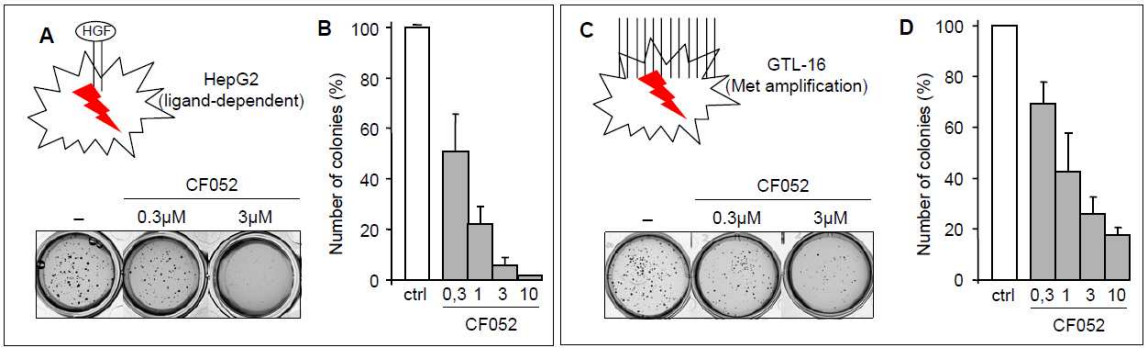

Figure 29: *CF052 blocks in vitro tumorigenesis by Met. CF52 impairs anchorage-independent growth of HepG2 (**A** and **B**) and GTL-16 (**C** and **D**) cells, in a dose dependent manner (μM; n=3). Values are expressed as means ± s.e.m. *P<0.05; **P<0.01; Student's t-tests.*

By evaluating the IC_{50} of the most active compounds, we found that CF052 and CF081 impaired Met-triggered anchorage-independent growth at concentration lower than those required for SU11274 (CF052: 0,321 μM; CF081: 0,620 μM; SU11274: 1,561 μM; *Figure 29 A-B and 30 B*).

[66] K.M. Nicholson, C.H. Streuli, N.G. Anderson, Autocrine signalling through erbB receptors promotes constitutive activation of protein kinase B/Akt in breast cancer cell lines, *Breast Cancer Res. Treat.* **2003**, *81,* 117–128.

CF compounds impaired effectively also tumorigenesis of GTL-16 cells addicted to the Met oncogene, in a dose dependent manner (*Figure 29 C-D and 30 C*).

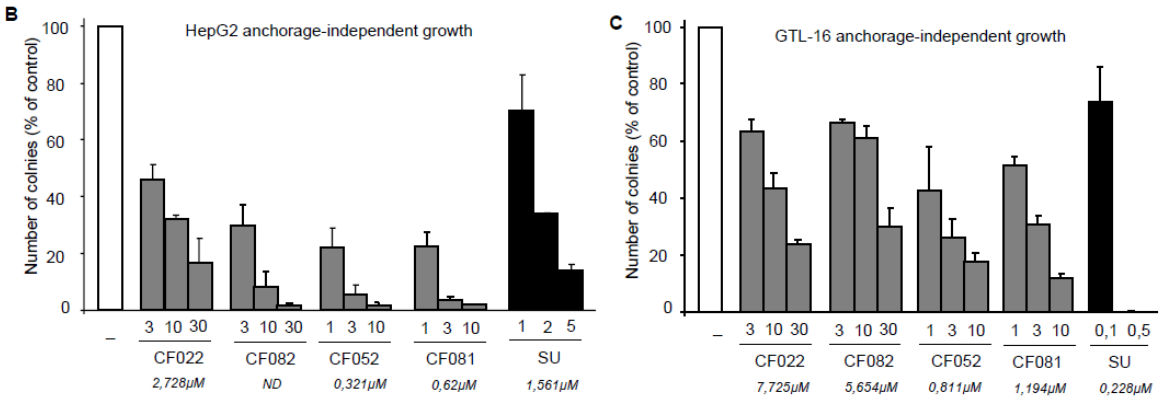

Figure 30: *CF compounds block Met-triggered cell survival and anchorage-independent growth. CF compounds impaired anchorage-independent growth of HepG2 (**B**) and GTL-16 (**C**) cells, in a dose dependent manner (µM). Values are expressed as means ± s.e.m. (n=3) *P<0.05; **P<0.01; Student's t-tests.*

The IC_{50} evaluation for the most active compounds revealed that CF052 and CF081 were also the most efficient to impair Met-triggered *in vitro* tumorigenesis (CF052: 0,811 µM; CF081: 1,194 µM; SU11274: 0,228 µM; *Figure 29 C-D and 30 C*). Altogether, these findings demonstrate that CF compounds restrain *in vitro* tumorigenesis of cells dependent or addicted to the Met oncogene. As CF052 appeared the most effective among all compounds, its properties were further investigated through a series of in vitro and in vivo assays.

3.7.5 CF052 interferes with Met phosphorylation and signalling in living cells

Activation of Met by HGF can be biochemically evaluated by following the phosphorylation levels of two tyrosine residues located in its kinase domain, namely Tyr_{1234} and Tyr_{1235}. We therefore characterised the inhibitory properties of CF052 by following Met phosphorylation in HepG2 cells. High levels of phospho-Met were observed upon HGF stimulation, and phosphorylation levels progressively decreased overtime (*Figure 31 A-B*).

Met phosphorylation was reduced by CF052 of approximately 30 to 50% overtime when compared to controls (*Figure 31A-B*).

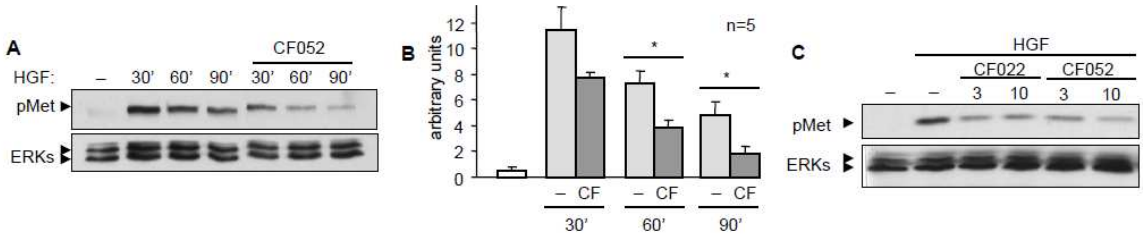

Figure 31: *CF052 interacts with Met (depending on in silico data) and interferes with Met phosphorylation. (**A**) Met phosphorylation following HGF stimulation in HepG2 cells was reduced in the presence of CF052. For western blot analyses, cells were treated with HGF for 30, 60, and 90 minutes in the presence or not of CF052 (10µM). Total cell lysates were analyzed using α-phosphoTyr$_{1234/1235}$-Met (pMet) (upper panel). ERK protein levels were used as loading controls (lower panel). (**B**) Quantification of Met phosphorylation in the presence or not of CF052 (n=5). Values are expressed as means ± s.e.m. *P<0.05; **P<0.01; Student's t-tests. (**C**) Met phosphorylation was also reduced by CF022 and CF052 applied at 3 and 10 µM in human MDA-MB231 breast cancer cells exposed to HGF stimulation for 15 minutes.*

Reduced Met phosphorylation by CF052 was observed also in other cell lines, such as in human MDA-MB231 breast cancer cells exposed to HGF stimulation (*Figure 31C*). Altogether, these results indicated that the new CF chemical scaffold interferes with Met phosphorylation.

3.7.6 CF52 impairs in vivo tumor growth

We next evaluated the ability of CF052 to impair tumor growth of cancer cells addicted to the Met oncogene. GTL-16 cells (10^6) were intra-peritoneally injected in nude mice and tumor growth was examined in mice treated with CF052 or vehicle alone. Intra-peritoneal injection of cancer cells leads to development of several nodules in the peritoneal cavity, offering the possibility to evaluate compound efficacy on tumor weight and nodule numbers. Notably, we found that both the total weight and the number of nodules were drastically reduced in mice injected with CF052, in a dose dependent manner (*Figure 32 A*). In particular, when CF052 was administered to mice at a dose of 30 mg kg^{-1} every two days, we found (see *Figure 32 B-C*):

- reduction in tumor weight of 60 % (control: 539,3 ± 209,6; CF052 injected: 214,3 ± 148,1; *P* = 0,0004);
- reduction of nodule numbers was 82 % for nodules smaller than 2 mm (control: 8,6 ± 4,6; CF052 injected: 1,6 ± 1,6; *P* = 4,4E-05);

- reduction of nodule numbers was 76 % for nodules between 2 to 5 mm (control: 10,6 ± 5,3; CF052 injected: 2,6 ± 1,8; *P* = 5,2E-05);

- reduction of nodule numbers was 59 % for nodules bigger than 5 mm (control: 2,3 ± 1,6; CF052 injected: 0,9 ± 0,6; *P* = 0,0099).

Moreover, when GTL-16 cells were subcutaneously injected, tumor growth was also reduced by approximately 35 % in mice treated with CF052.

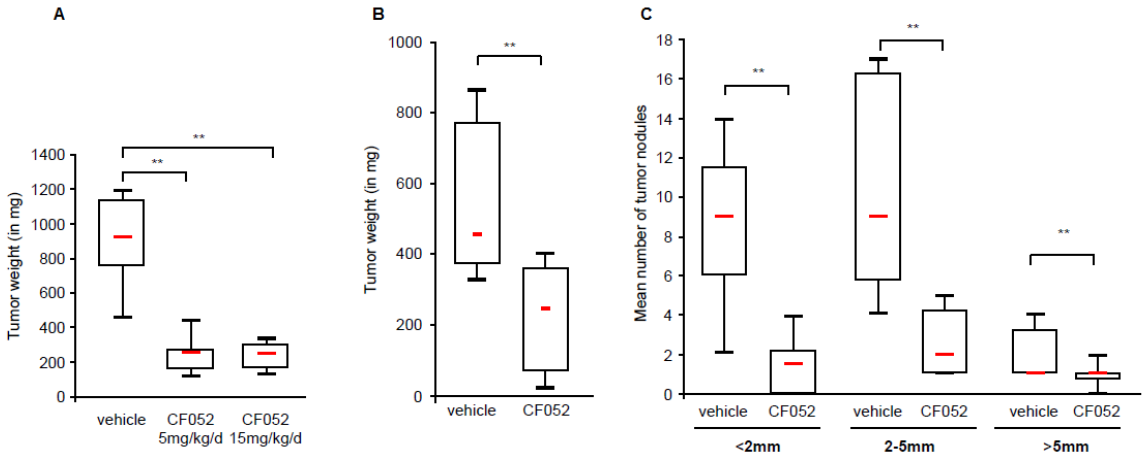

Figure 32: *CF052 interferes with growth of tumors triggered by cancer cells addicted to the Met oncogene. (**A**) Dose-response of CF052 (i.p. 10 or 30 mg kg^{-1} every 2 days) on tumor growth, evaluated by measuring tumor weight. (**B**) and nodule numbers (**C**) in nude mice injected intra-peritoneally with GTL-16 cells. Values are reported as boxplots. Two independent experiments were performed and 8 mice per group were used. Values are expressed as means ± s.e.m. *P<0.05; **P<0.01; Student's t-tests.*

Next was evaluated whether CF052 elicited toxic effects in vivo. As the body weight is a generic indicator of animal physiology influenced for example by body metabolism, activity and feeding behaviour, the weight of mice treated with CF052 was followed and no significant differences were found versus controls (*P* > 0.05; *Figure 33 A*). We measured also the weight of heart, spleen, kidney and liver of mice treated for 21 days with CF052. No differences were found between the two groups (*P* > 0.05; *Figure 33 B*). Taken together, these findings demonstrate that CF052 elicited in vivo tumor growth inhibition of cancer cells addicted to the Met oncogene. Moreover, the absence of side effects indicated that CF052 was well tolerated when injected in mice at doses required to elicit its anti-tumor effects.

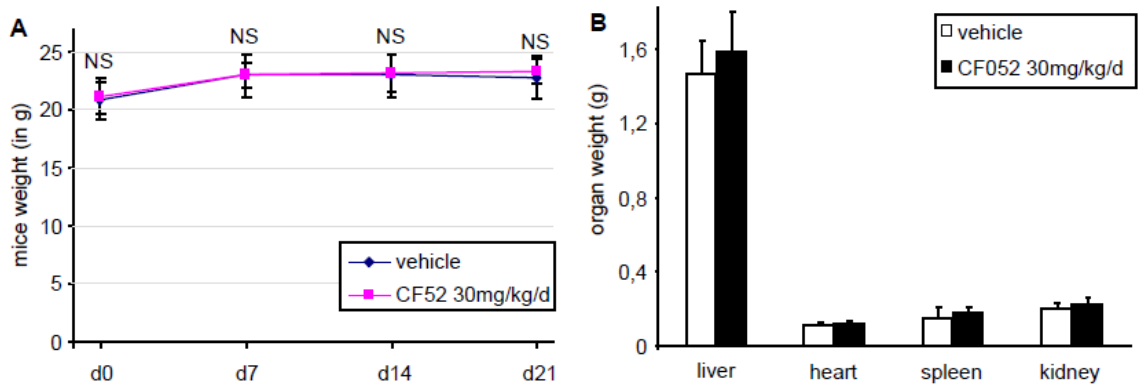

Figure 33: *In vivo administration of CF052 does not result in major side effects. (**A**) Evolution of the body weight in mice daily treated with CF052 (30 mg kg^{-1}) or vehicle showed no significant differences. Body weight is expressed as weight evolution over the 21 day's treatment. (**B**) The weight of heart, spleen, kidney and liver was evaluated in mice intra-peritoneally injected everyday with CF052 (30 mg kg^{-1}) or vehicle. No significant differences were observed. Values are expressed as means ± s.e.m. P>0.05; Student's t-tests.*

3.8 Modelling Studies

Docking studies were performed on all the new hypothesized compounds in order to predict their binding mode inside the ATP binding pocket of the protein. Two different inactive conformations of Met kinase have been used for docking calculations. The active conformation was immediately discarded because of its inability to accommodate such bulky ligands. Among the inactive conformations, we chose the 3CTJ and the 3EFK as representative of the second and the third X-ray cluster, respectively.

Docking on 3CTJ

The docking calculations performed in 3CTJ (*Figure 35*) showed a common binding mode for the left part of all inhibitors. The benzothiazole (A-ring) is located at the entrance of the ATP binding site, in close proximity of the residues constituting the hinge region and partially superimposed to the pyrrolopyridine of the crystallographic inhibitor (*Figure 34*).

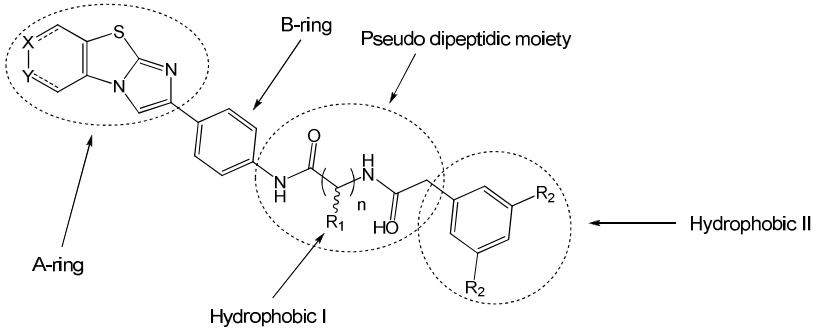

Figure 34: *General structure of the CF series of designed compounds.*

The *N*-benzyl ring of compounds **9**, **10**, **18** and **19** and bromine of compound **20** are solvent exposed, outside of the binding pocket and does not make any favorable interactions. The central aromatic ring (B-ring) π-stacks with Phe1223 (DFG motif) and is flanked on the opposite face by gatekeeper residue Leu1157. The peptidic moiety could be involved in *H*-bonds with Asp1222 of activation loop or *N* of Lys1110. The placement of Hydrophobic I and Hydrophobic II moieties is the most interesting element about the binding mode of all the studied compounds.

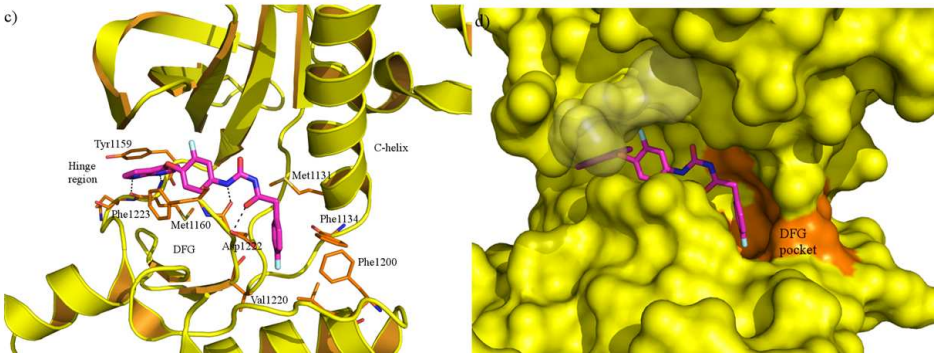

Figure 35: *Binding mode of* ***320*** *(reported as in stick with the carbon atoms in purple) in the inactive conformation of Met (3CTJ).*

Molecules **9**, **12a-e** and **12g**, having two hydrophobic residues bound to the peptidic moiety, occupy or with Hydrophobic I (**9a**, **12b**, **12d** and **12e**) or with Hydrophobic II (**9b**, **11**, **12a**, **12c** and **12g**) the DFG pocket. Since the C-helix is closed in this crystallographic complex, the other hydrophobic group (Hydrophobic I or II depending on the compound) is outside of the binding site and does not give any interaction with the protein.

Docking on 3EFK

The docking calculations performed in 3EFK (*Figure 36*) gave essentially the same results as the simulations carried out in 3CTJ. Again, the A-ring is in close proximity of hinge region. The B-ring is involved in lipophilic interactions with the side chain of Leu1157 and in the stacking with the side chain of Phe1089 that in 3EFK replaces Phe1223.

This replacement is extremely significant and demonstrates the flexibility of the binding pocket of Met.

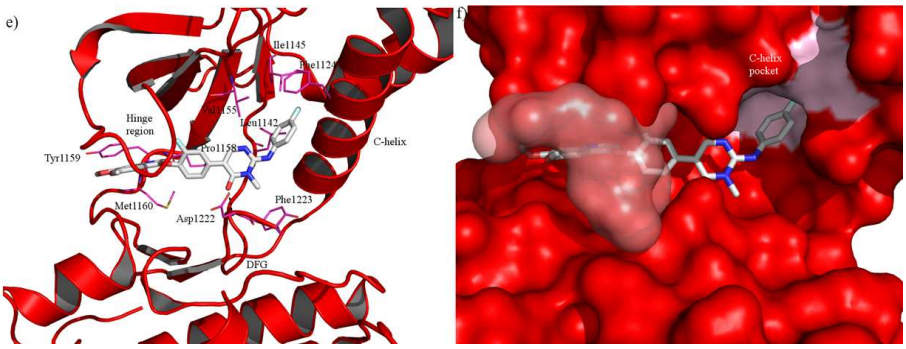

Figure 36: Binding mode of **MT4** (reported as in stick with the carbon atoms in white) in the inactive conformation of Met (3EFK).

In fact, while in 3CTJ the co-crystallized inhibitor is able to occupy the DFG pocket, in the 3EFK the inhibitor **MT4** occupies the C-helix pocket. In this way the activation loop shifts (see black arrow in *Figure 37*), with the Phe1223 that occupies the DFG pocket and cannot anymore interact with the inhibitor. However, the place of Phe1223 is taken by Phe1089 that "comes down" to interact with the central aromatic ring of ligand, moving the P-loop (*Figure 37*).

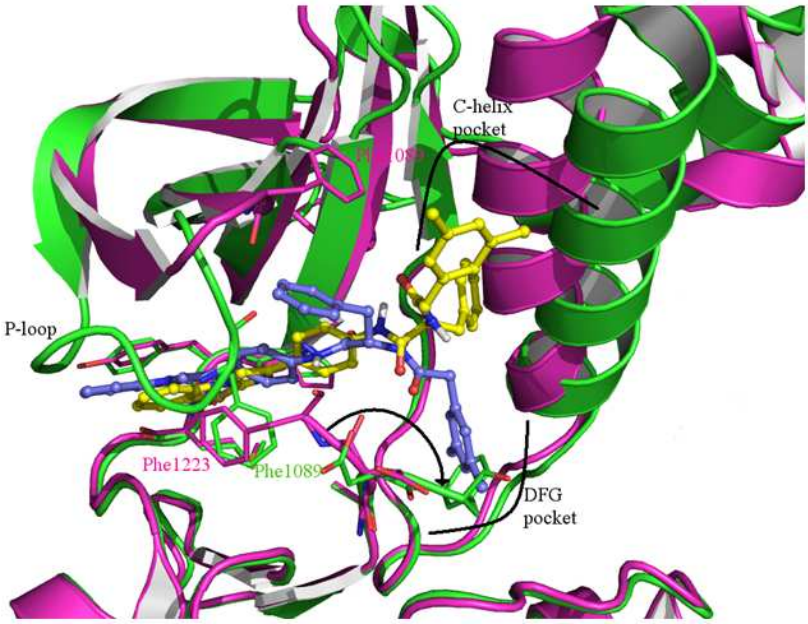

Figure 37: *Superposition of X-ray crystal structures 3CTJ in purple and 3EFK in green. Binding mode of compound CF022 (**12a**) as found by docking simulation in both 3CTJ and 3EFK (blue carbon atoms for CF022 into 3CTJ and yellow carbon atoms for CF022 into 3EFK). Some relevant residues are reported as stick for both the structures.*

In addition, the peptidic moiety could be involved in H-bond with Lys1110. In this crystallographic structure, since the closing of DFG pocket, Hydrophobic I fit into the *C*-helix pocket, while Hydrophobic II is outside the binding pocket, toward Glu1120.

3.9 Discussion

The binding mode just now described for the inhibitors in both the crystallographic complexes is able to rationalize the inactivity of compounds **9**, **10**, **18**, **19** and **20**. In fact these compounds are characterized by the presence of a benzyl group or a bromine bound to A-ring that is outside of the binding pocket and solvent exposed, giving unfavorable interactions. Anyway, this binding mode is not able to explain the inactivity of **12f**. Compound **12f** occupies with its unique hydrophobic group the C-helix pocket in 3EFK and the DFG pocket in 3CTJ. The only difference between **12f** and **12a** or **12b** (two of the most active compounds) is the lacking of the second hydrophobic group that, however, seems not to be involved in favorable interactions with Met neither in 3CTJ, nor in 3EFK. Furthermore, compound **12g** with a polar OH group in the Hydrophobic I is inactive against Met, demonstrating that two hydrophobic groups are necessary for the activity.

Merge of 3CTJ and 3EFK

The impossibility to rationalize the activity data using the X-ray complexes 3CTJ and 3EFK was overcome merging these two crystallographic structures. The new modelled protein (hereafter called *Merge protein*) had both the hydrophobic pockets open, with the DFG and the P-loop in the orientation of 3CTJ and the C-helix as 3EFK (*Figure 38*).

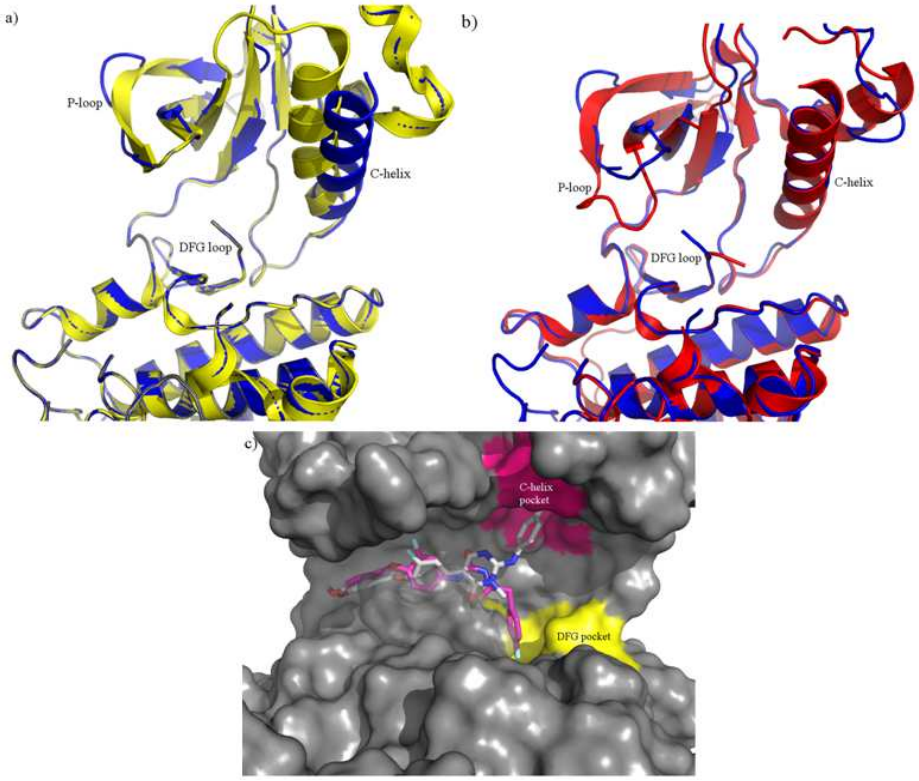

Figure 38: *(**a**) Superposition of 3CTJ (yellow cartoon) and Merge protein (blue cartoon). (**b**) Superposition of 3EFK (red cartoon) and Merge protein (blue cartoon). (**c**) The Merge protein showed as surface with DFG pocket in yellow and C-helix pocket in fuchsia. Inhibitors co-crystallized in 3CTJ and in 3EFK (white carbons and purple carbons, respectively) are also reported in stick representation.*

3.10 Docking on Merge protein

The docking calculations were repeated using the *merge protein* for all the prepared compounds. Each compound was found to bind Met in regular orientation, with A-ring toward the entrance of the binding site. The interactions and the binding mode of each compound are the same previously described in 3CTJ and 3EFK, with the only difference that in the Merge protein, since both the hydrophobic pockets are open, both Hydrophobic I and II give their contribution to the interactions with Met. In this context, it results clear the inactivity of **12f** that having only the Hydrophobic II is not able to fit in the same time both the pockets.

3.11 Conclusion

A convenient and versatile synthesis of a new collection of potential Met inhibitors based on thiazole scaffold was realised. The synthesis resulted flexible and permits to obtain a series of analogues. The synthesis is also scalable and gives the possibility to produce compounds in grams scale.

Biological evaluation showed interesting *in vitro* and *in vivo* activity for some compounds, in particular tetrahydro-benzothiazole and benzothiazole scaffolds resulted determinant for the activity on Met.

The reported activity data clearly showed that the incorporation of phenylalanine in the pseudo-dipeptide chain is fundamental for the activity of this class of inhibitors. Any others attempt to replace phenylalanine with others amino acids led to inactive products.

Biological tests and *in silico* studies confirmed also the bioisosterism between peptide bond and 1,2,3-triazole ring. The activity of our lead compound CF052 (**12c**) and the corresponding triazole derivatives CF120 (**30**) have a comparable activity.

Biological trials showed that the CF series compounds are able both to reduce Met phosphorylation and to prevent Met-triggered survival of Met-dependent HepG2 and GTL-16 cancer cell lines.

The study on biological mechanism of action showed an important point for this thiazole based inhibitors: the double ability to reduce Met phosphorylation and to prevent its re-synthesis. This dual mechanism of action could lead to more potent Met inhibitors.

The obtained results showed the good ability of the prediction coming from the modelling studies and these results confirmed the importance of the *in silico* studies in drug discovery.

3.12 Experimental details

3.12.1 Modeling

Building of merge protein

The backbone of 3CTJ and 3EFK crystallographic complexes was superimposed using the software Pymol version 1.2[67] by the implemented Shindyalov and Bourne algorithm,[68] obtaining a RMSD value of 0.31 Å. The crystallographic complex 3CTJ was taken as template from the first residue (Val1051) to Ser1111, then, to be able to insert the C-helix of 3EFK, residues Leu1112-Phe1134 were removed, while residues Ile1118-Phe1134, constituting the C-helix in the intended 3EFK orientation, were added. The remaining residues (Ser1135-Lys1360) of 3CTJ were conserved in the Merge protein. This chimeric protein was subjected to minimization using Macromodel 8.5/Maestro and OPLS_2005 force field (Polak-Ribiere conjugate gradient, 0.05 kJ/Å·mol convergence).[69-70] In particular, the backbone of the entire protein was frozen, while all the amino acid side chains were unconstrained during energy minimization to allow for reorientation and proper hydrogen-bonding geometries and van der Waals contacts. The obtained minimized Merge protein was used for the following docking calculation.

Docking simulations

Docking studies were performed on all the compounds by means of the GOLD 4.0 software.[71] The Kinase Scoring Function was chosen as fitness function. This particular kind of Chemscore keeps into account weak CHO interactions calculating a contribution for weak hydrogen bonds. This term can be useful when dealing with particular proteins, like most kinases that contain weak N-heterocycle CH...O hydrogen bonds. The GA parameter settings of Gold were employed using the Search efficiency set to 100%. The reliability of the docking protocol was tested by simulations of the binding mode of Met inhibitors co-crystallized in 3CTJ and 3EFK by a comparison of the modeled complexes with the available 3D structures derived by X-ray crystallography. Structures of inhibitors were built using Maestro 3D-sketcher, minimized with OPLS_2005 force field, using the

[67] DeLano, W. L. The PyMOL Molecular Graphics System; DeLano Scientific LLC: San Carlos, CA; http://www.pymol.org.

[68] Shindyalov, N., Bourne, P. E. Protein structure aligment by incremental combinatorial extension (CE) of the optimal path. *Protein Eng.,* **1998**, *11*, 739–747.

[69] Maestro, version 8.5; Schrodinger: New York, 2008.

[70] Jorgensen, W. L.; Maxwell, D. S.; Tirado-Rives, J. Development and testing of the OPLS all-atom force field on conformational energetics and properties of organic liquids. *J. Am. Chem. Soc*. **1996**, *118*, 11225– 11236.

[71] (a) Jones, G., Willett, P., Glen, R. C. Molecular Recognition of Receptor Sites Using a Genetic Algorithm with a Description of Desolvation, *J. Mol. Biol.* **1995**, *245,* 43-53; b) Jones, G., Willett, P., Glen, R. C., Leach, A. R., Taylor, R. Development and Validation of a Genetic Algorithm for Flexible Docking, *J. Mol. Biol*. **1997**, *267*, 727-748: c) Verdonk, M. L., Cole, J. C., Hartshorn, M. J., Murray, C. W., Taylor, R. D., Improved Protein-Ligand Docking Using GOLD, *Proteins,* **2003**, *52*, 609-623.

Polak-Ribiere conjugated gradient method (0.001 kJ/Å·mol convergence) and finally docked in the native protein. The experimental binding conformations of the reference compounds were successfully reproduced applying the already mentioned settings of GOLD, with 30 docking runs. In particular, the first ranked docked conformation was able to reproduce the X-ray conformation of **320** and **MT4** (ligand of 3CTJ and 3EFK, respectively) with a root-mean-square deviation (rmsd) of 0.7 Å and 0.3 Å, respectively, calculated on all heavy atoms coordinates. With a reliable docking procedure in our hands, in the next step of the computational work we used the 3CTJ, 3EFK and the Merge protein to dock the synthesized compounds.

3.12.2 Biology

Cell culture

MDCK cells were grown in Dulbecco's modified Eagle's medium (DMEM) (Gibco BRL) containing 4mM L-glutamine and supplemented with 2% (v/v) foetal bovine serum (Gibco BRL), 100 U/mL penicillin, and 100 µg/mL streptomycin. Cells were plated at a density of 1000 cells per well in 24-well microplates and allowed settling overnight at 37°C in a humidified atmosphere of 5% CO_2 prior to treatments. Human MCF10A breast cells, human MDA-MB231 breast cancer cells, human GTL-16 gastric carcinoma cells, human HepG2 hepatocellular carcinoma cells, human U-87 glioblastoma-astrocytoma cells and human LLC Lewis lung carcinoma cells were grown in RPMI medium (Gibco BRL) containing 4mM L-glutamine and supplemented with 10% (v/v) foetal bovine serum (Gibco BRL), 100 U/mL penicillin, and 100 µg/mL streptomycin and kept at 37°C in a humidified atmosphere of 5% CO_2.

Compound treatments

For scattering assays, MDCK cells were pre-incubated with compounds over-night at 0.1-100 µM concentrations at 37 °C in a humidified atmosphere of 5 % CO_2, followed by 24 hours stimulation with 20 ng/ml HGF (R&D Systems), as previously described.[59] Cells were further incubated at 37 °C in an atmosphere of 5 % CO_2 for 24-48 hours, washed with phosphate-buffered saline (PBS; Gibco BRL), and fixed with 4 % PFA (Sigma). The quantification of scattering response was performed by counting the number of cells with scattered morphology in 30 independent colonies. The IC_{50} corresponds to the concentration of compounds leading to a 50 % inhibition of Met-triggered cell scattering. Active compounds were assayed to impair scattering response also on MCF10A cells following the same procedure. For survival assays, GTL-16, HepG2 and U-87 cells were cultured in serum-free media for 24 hrs prior to compound addition for 48 hrs. Viability was assessed with the Cell Titer Glo Luminescent Assay (Promega). For in vitro tumorigenesis, soft agar growth assays were performed using GTL-16, HepG2, and U-87 cells, as previously described.[59] Data on biological assays are representative of three independent experiments performed in duplicate.

Biochemical evaluation of Met inhibitors

After starvation, cells were pretreated overnight with inhibitors, then stimulated with HGF, and total extracts were analyzed as described.[72] Antibodies used were anti-tubulin (Sigma), anti-phospho $Y_{1234-1235}$-Met, anti-Akt, anti-phospho-Akt, anti-phospho-Gab1, anti phosphor-ErbBs, anti-phospho-PDGFR, anti-PDGFRs, anti-ERKs (Cell Signaling), anti-ErbBs, anti-Met (Santa Cruz).

In vivo tumorigenesis assays

Xenografts of GTL-16 cells were established by intraperitoneal (i.p.) or subcutaneous (into the flank/leg region) injection of cells (10^6) in nude mice (S/SOPF SWISS NU/NU; Charles River). When GTL-16 cell were intra-peritoneally injected, mice were treated with CF052 (i.p. 10 or 30 mg kg^{-1}) or vehicle at day 1 and treatment was repeated every two days. Alternatively, CF052 treatment was started 7 days after cell injection and treatment was daily performed. When GTL-16 cell were sub-cutaneously injected, CF052 administration (i.p. 30 mg kg^{-1}) was daily performed starting from day 1. Mice were then sacrificed after 21 days of treatment. Tumor nodules present in the peritoneal cavity were isolated and quantified according to their diameter and their total weight. Similarly, sub-cutaneous tumors were isolated after 21 days of treatment and quantified as above. For CF052 in vivo treatment, the drug was formulated in Cremophor EL (polyethoxylated castor oil) and DMSO (1:1, v/v) and diluted in sterile 0.9% (w/v) sodium chloride for administration at dose levels of 10 and 30 mg kg^{-1}. Three independent tumorigenesis assays were performed (8 mice per group were used). Mice were kept at the IBDML animal facilities and all experiments were performed in accordance with institutional guidelines.

Toxicity evaluation of compounds in vivo

The weight of nude mice treated with CF52 compound (30 mg kg^{-1}) or vehicle was measured before, during and after treatment. To evaluate the weight of heart, spleen, kidney and liver, mice were sacrificed after 21 days of CF52 or vehicle treatments, organs were dissected, rinsed in PBS, and their weight was measured.

[72] F. Maina, G. Pante, F. Helmbacher, R. Andres, A. Porthin, A.M. Davies, C. Ponzetto, R. Klein, Coupling Met to specific pathways results in distinct developmental outcomes, *Mol Cell* **2001**, *7*, 1293-1306.

3.12.3 Chemistry

General

All non-aqueous reactions were performed under inert atmosphere with dry, freshly distilled solvents using standard procedures. Drying of organic extracts during the work-up of reactions was performed over anhydrous Na_2SO_4 or $MgSO_4$. Evaporation of solvents was accomplished with a rotatory evaporator. Thin-layer chromatography (TLC) was performed on Merck precoated 60F254 plates. Reactions were monitored by TLC on silica gel, with detection by UV light (254 nm) or by charring with 1 % permanganate solution. Flash chromatography was performed using Silica gel (240–400 mesh, Merck). NMR spectra were recorded with Brucker 300 and 400 MHz spectrometers using chloroform-d ($CDCl_3$), dimethylsolfoxide-d_6 (DMSO-d_6) and methanol-d_4 (CD_3OD). Chemical shifts are reported in parts per million (δ) downfield from tetramethylsilane (TMS). EI mass spectra were recorded at an ionizing voltage of 6Kev on a VG 70-70 EQ. ESI mass spectra were recorded on FT-ICR APEXII (Bruker Daltonics). All reactions were carried out in dry solvents. Specific rotations were misured by a polarimeter “P-1030 Jasco” with 10 cm of Optical path cells and 1 ml of capacity. The mesures were done between 18 and 22 °C at 589 nm Wavelength (Na lamp). The melting point was determined by “Digital Melting Point IA9100 series - Electrothermal”.

*General Procedure for Synthesis of (**2**)*

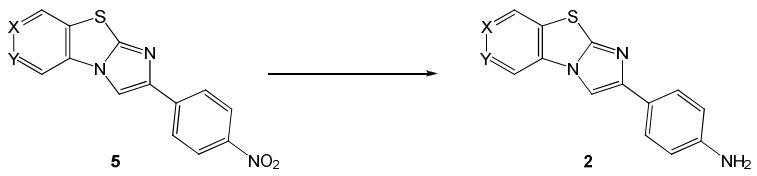

Procedure **A**:

Fe powder (7 g, 120 mmol) and H_2SO_4 12 N (0.7 ml, 30 mmol) were added to a solution of **5** (6 mmol) in ethanol/water (5:1, 50-100 ml) and the mixture was stirred at 90 °C for 1 h. The hot solution was filtered through celite and washed with hot ethanol. The solvent was removed in vacuo and the crude materials was extracted by satured solution of $NaHCO_3$ and AcOEt. The organic phase was dried with Na_2SO_4 anhydrous. Compound **2** was obtained without any further purification.

Procedure **B***:*

HCl (37 %, 100 ml) was slowly added to a mixture of **5** (3.4 mmol) and $SnCl_2$ (13 mmol) in MeOH (100 ml). The crude mixture was refluxed for 30 min. A solution of K_2CO_3 (2 M) was slowly added to reach pH 9. The precipitate was filtered and purified by flash chromatography.

2-(4-Aminophenyl)-7-benzyl-5,6,7,8-tetrahydroimidazo[2',1':2,3]thiazolo[5,4-*c*]pyridine - (**2a**)

ARKIVOC **2010**, *3*, 145-151.

From **5a** (1.92 g, 4.08 mmol) using procedure **B**. Crude material was purified by flash chromatography (AcOEt + 0.1 % NEt_3) to afford **2a** as pale yellow solid (0.38 g, yield 26 % over 2 steps).

^{1}H NMR ($CDCl_3$, 400 MHz): δ 7.60 (2H, d, *J* = 8.4 Hz), 7.39 (1H, s), 7.25-7.36 (5H, m), 6.69 (2H, d, *J* = 8.4 Hz), 3.73 (2H, s), 3.56 (2H, s), 2.95 (2H, t, *J* = 6.0 Hz), 2.71 (2H, t, *J* = 6.0 Hz).

EIMS 360 $[M]^+$.

2-(4-Aminophenyl)-6-benzyl-5,6,7,8-tetrahydroimidazo[2',1':2,3]thiazolo[4,5-*c*]pyridine - (**2b**)

ARKIVOC **2010**, *3*, 145-151.

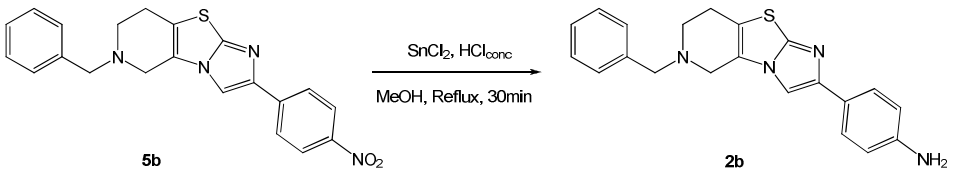

From **5b** using the procedure **B**. Crude material was purified by flash chromatography (CH_2Cl_2 to CH_2Cl_2:MeOH 98.5:1.5). to afford **2b** as pale yellow solid (yield 23%).

^{1}H NMR ($CDCl_3$ with drops of CD_3OD, 400 MHz): δ 7.89 (1H, s), 7.52 (2H, d, *J* = 8.8 Hz), 7.33-7.39 (5H, m), 6.73 (2H, d, *J* = 8.8 Hz), 3.80 (2H, s), 3.57 (2H, t, *J* = 1.5 Hz), 2.95 (2H, t, *J* = 5.2 Hz), 2.82 (2H, t, *J* = 5.2 Hz).

^{13}C NMR ($CDCl_3$ with drops of CD_3OD, 100.6 MHz): δ 148.22, 146.63, 145.77, 136.89, 128.80 (2C), 128.33 (2C), 127.45, 125.96 (2C), 124.27, 124.08, 119.34, 115.22 (2C), 104.16, 61.42, 49.94, 48.86, 24.27.

EIMS 360 $[M]^+$.

2-(4-Aminophenyl)-5,6,7,8-tetrahydroimidazo[2,1-*b*]benzothiazole - (**2c**)

Bioorg. Med. Chem. Lett. **2005**, *15*, 1561-1564.

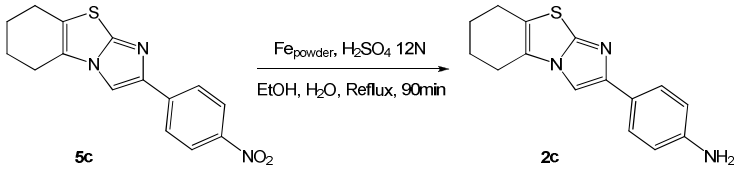

5c 2c

2c was prepared from **5c** (2.00g, 6.69 mmol) using general procedure **A** for synthesis of **2**. Yellow solid (1.58 g, yield 89 %).

^{1}H NMR (DMSO-d_6, 300 MHz): δ 7.87 (1H, s), 7.50 (2H, d, *J* = 8.2 Hz), 6.58 (2H, d, *J* = 8.2 Hz), 5.13 (2H, s), 2.69-2.64 (4H, m), 1.89-1.85 (4H, m).

EIMS 269 $[M]^+$.

2-(4-aminophenyl)imidazo[2,1-*b*]benzothiazole - (**2d**)

J. Med. Chem. **1986**, *29,* 386-394.

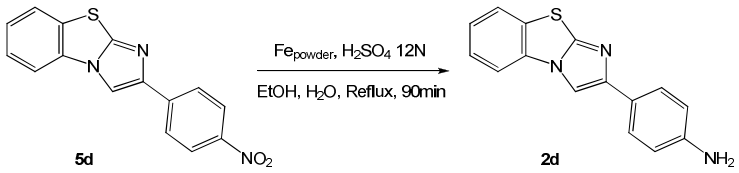

2d was prepared from **5d** (2.00 g, 6.78 mmol) using general procedure **A** for synthesis of **2**. Pale yellow solid (1.63 g, yield 91 %).

^{1}H NMR (DMSO-d_6, 300 MHz): δ 8.48 (1H, s), 8.05 (1H, d, *J* = 8.0 Hz), 7.93 (1H, d, *J* = 8.0 Hz), 7.61-7.51 (3H, m), 7.42 (1H, t, *J* = 8.0 Hz), 6.64 (2H, d, *J* = 9.0 Hz), 5.23 (2H, s);

EIMS 265 $[M]^+$.

*General Procedure for Synthesis of (**3**)*

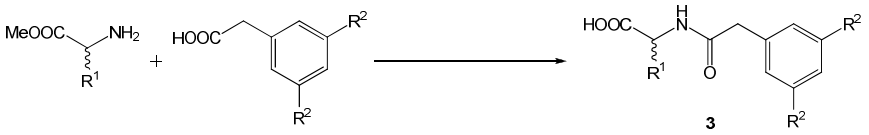

Procedure **C**:

A solution of a phenylacetic acid (3.7 mmol), DMAP (5.55 mmol) and DCC (5.55 mmol) in THF (40-70 ml) was stirred at rt for 30 min. The hydrochloride salt of the carboxy protected aminoacid (3.7 mmol) was added and the solution was stirred for 48 h at rt. The crude mixture was filtered over celite and the solvent was removed in vacuo. The product was purified by flash chromatography to afford the methylester of acid **8**. The methylester (1 mmol) was dissolved in methanol. A solution of LiOH 1N (4 mmol) was added and the reaction mixture was stirred for 1 h at 0 °C. H_2O was added and methanol only was evaporated under reduced pressure. The pH was reduced to 2 using HCl solution 1N. The crude materials was extracted with ethyl acetate and the organic phase was dried with Na_2SO_4 anhydrous. The solvent was removed in vacuo to afford **3** without any further purification.

Procedure **D**:

A solution of phenylacetic acid (6 mmol), DMAP (3 mmol) and DCI (10 mmol) in THF was stirred for 14h at rt. The crude mixture was filtered over celite and the solvent was removed in vacuo. The product was purified by flash chromatography. The product was purified by flash chromatography to afford the methylester of acid **8**. The methylester (1 mmol) was dissolved in methanol. A solution of LiOH 1N (4 mmol) was added and the reaction mixture was stirred for 1 h at 0 °C. H_2O was added and methanol only was evaporated under reduced pressure. The pH was reduced to 2 using HCl solution 1N. The crude materials was extracted with ethyl acetate and the organic phase was dried with Na_2SO_4 anhydrous. The solvent was removed in vacuo to afford **3** without any further purification.

(*S*)-2-[2-(3,5-dimethylphenyl)acetamido]-3-phenyl-propanoic acid - (**3a**)

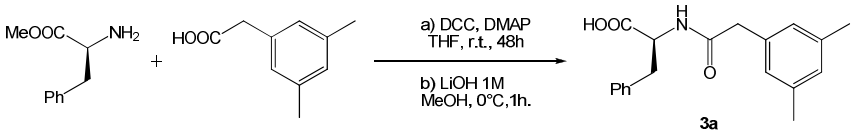

3a

The methylester of acid **3a** was prepared using L-Phenylalaninemethylester hydrochloride (0.80 g, 3.71 mmol) and 3,5-Dimethylphenylacetic acid (0.61 g, 3.71 mmol) using general procedure **C** for synthesis of **3**. The crude mixture was purified by flash chromatography (Hex:AcOEt 2:1) to afford the methylester as white solid (0.85 g, yield 70 %).

^{1}H NMR ($CDCl_3$, 400 MHz): δ 7.24-7.18 (3H, m), 6.94-6.91 (3H, m), 6.82 (2H, s), 5.83 (1H, d, *J* = 7.6 Hz), 4.91-4.83 (1H, m), 3.66 (3H, s), 3.52 (1H, d, *J* = 15.8 Hz), 3.48 (1H, d, *J* = 15.8 Hz), 3.09 (1H, dd, *J* = 13.8, 5.5 Hz), 3.04 (1H, dd, *J* = 13.8, 5.5 Hz), 2.19 (6H, s).

EIMS 325 $[M]^+$.

3a was prepared from the corresponding methylester (0.64 g, 1.96 mmol) using general procedure **C** for synthesis of **3**. White solid (0.58 g, yield 95 %).

m.p. 85-88°C,

$[\alpha]^{20}_D$ = +35.12 (Na, *c* = 0.80 in $CHCl_3$).

^{1}H NMR ($CDCl_3$, 400 MHz): δ 10 (1H, s), 7.24-7.19 (3H, m), 6.97 (2H, dd, *J* = 7.2, 1.6 Hz), 6.94 (1H, s), 6.78 (2H, s), 6.01 (1H, d, *J* = 7.6 Hz), 4.87-4.83 (1H, m), 3.52 (1H, d, *J* = 16.4 Hz), 3.48 (1H, d, *J* = 16.4 Hz), 3.16 (1H, dd, *J* = 14.0, 5.6 Hz), 3.06 (1H, dd, *J* = 14.0, 5.6 Hz), 2.3 (6H, s).

^{13}C NMR ($CDCl_3$, 100.6 MHz): δ 174.36, 172.18, 138.63 (2C), 135.44, 133.68, 129.67, 129.24 (2C), 128.54 (2C), 127.26 (2C), 127.08, 53.17, 43.20, 36.99, 21.23 (2C).

HR-EIMS Anal. Calcd for $[C_{19}H_{21}NO_3]^+$ 311.1521; found 311.1523.

(*R*)-2-[2-(3,5-dimethylphenyl)acetamido]-3-phenylpropanoic acid - (**3b**)

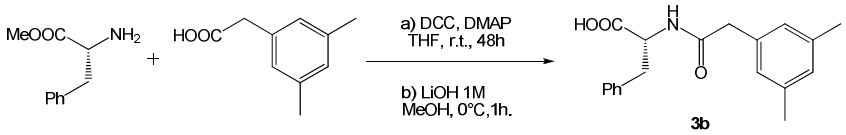

3b

The methylester of acid **3b** was prepared using D-Phenylalaninemethylester hydrochloride (0.80 g, 3.71 mmol) and 3,5-Dimethylphenylacetic acid (0.61 g, 3.71 mmol) using general procedure **C** for synthesis of **3**. The crude mixture was purified by flash chromatography (Hex:AcOEt 2:1) to afford the methylester as white solid (0.82 g, yield 68 %).

^{1}H NMR ($CDCl_3$, 400 MHz): δ 7.24-7.18 (3H, m), 6.94-6.91 (3H, m), 6.82 (2H, s), 5.83 (1H, d, *J* = 7.6 Hz), 4.91-4.83 (1H, m), 3.66 (3H, s), 3.52 (1H, d, *J* = 15.8 Hz), 3.48 (1H, d, *J* = 15.8 Hz), 3.09 (1H, dd, *J* = 13.8, 5.5 Hz), 3.04 (1H, dd, *J* = 13.8, 5.5 Hz), 2.19 (6H, s).

EIMS 325 $[M]^+$.

3b was prepared from the corresponding methylester (0.75 g, 2.30 mmol) using general procedure **C** for synthesis of **3**. White solid (0.70 g, yield 98 %).

mp 85-88°C,

$[\alpha]^{20}_D$ = -35.52 (Na, *c* = 1.28 in $CHCl_3$).

^{1}H NMR ($CDCl_3$, 400 MHz): δ 10 (1H, s), 7.24-7.19 (3H, m), 6.97 (2H, dd, *J* = 7.2, 1.6 Hz), 6.94 (1H, s), 6.78 (2H, s), 6.01 (1H, d, *J* = 7.6 Hz), 4.87-4.83 (1H, m), 3.52 (1H, d, *J* = 16.4 Hz), 3.48 (1H, d, *J* = 16.4 Hz), 3.16 (1H, dd, *J* = 14.0, 5.6 Hz), 3.06 (1H, dd, *J* = 14.0, 5.6 Hz), 2.3 (6H, s).

^{13}C NMR ($CDCl_3$, 100.6 MHz): δ 174.36, 172.18, 138.63 (2C), 135.44, 133.68, 129.67, 129.24 (2C), 128.54 (2C), 127.26 (2C), 127.08, 53.17, 43.20, 36.99, 21.23 (2C).

HR-EIMS Anal. Calcd for $[C_{19}H_{21}NO_3]^+$ 311.1521; Found 311.1522.

(*S*)-2-[2-(3,5-bis(trifluoromethyl)phenyl)acetamido]-3-phenylpropanoic acid - (**3c**)

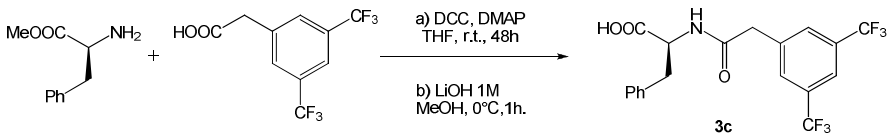

The methylester of acid **3c** was prepared using L-Phenylalaninemethylester hydrochloride (0.72 g, 3.34 mmol) and 3,5-Bis(trifluoromethyl) phenylacetic acid (0.91 g, 3.34 mmol) using general procedure **C** for synthesis of **3**. The crude mixture was purified by flash chromatography (Hex:AcOEt 2:1) to afford the methylester as white solid (0.90 g, yield 63 %).

^{1}H NMR ($CDCl_3$, 400 MHz): δ 7.82 (1H, s), 7.72 (2H, s), 7.27-7.23 (3H, m), 7.01-6.98 (2H, m), 5.97 (1H, d, *J* = 7.2 Hz), 4.93-4.88 (1H, m), 3.79 (3H, s), 3.66 (1H, d, *J* = 15.6 Hz), 3.61 (1H, d, *J* = 15.6 Hz), 3.17 (1H, dd, *J* = 13.6, 5.6 Hz), 3.09 (1H, dd, *J* = 13.6, 5.4 Hz).

EIMS 433 $[M]^+$.

3c was prepared from the corresponding methylester (0.63 g, 1.46 mmol) using general procedure **C** for synthesis of **3**. White solid (0.61 g, yield 99 %).

mp 138-140 °C

$[\alpha]^{20}_D$ = +10.17 (Na, *c* = 1.28 in MeOH).

^{1}H NMR (DMSO-d_6, 400 MHz): δ 8.52 (1H, d, *J* = 8.2 Hz), 7.96 (1H, s), 7.88 (2H, s), 7.22-7.13 (5H, m), 4.49-4.43 (1H, m), 3.65 (1H, d, *J* = 15.3 Hz), 3.57 (1H, d, *J* = 15.3 Hz), 3.09 (1H, dd, *J* = 13.8, 4.6 Hz), 2.86 (1H, dd, *J* = 13.8, 9.8 Hz).

^{13}C NMR (DMSO-d_6, 100.6 MHz): δ 173.88, 169.96, 140.73, 138.55, 131.12 (2C, q, *J* = 32.8 Hz), 130.94 (2C), 130.11 (2C), 129.10 (2C), 127.44, 124.50 (2C, q, *J* = 272.6 Hz), 121.25, 54.60, 42.17, 37.90.

HR-EIMS Anal. Calcd for $[C_{19}H_{15}F_6NO_3]^+$ 419.0956; Found 491.0952.

(*R*)-2-[2-(3,5-bis(trifluoromethyl)phenyl)acetamido]-3-phenylpropanoic acid - (**3d**)

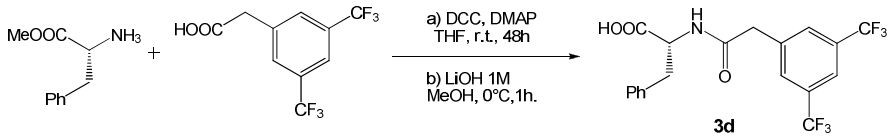

The methylester of acid **3d** was prepared using D-Phenylalaninemethylester hydrochloride (0.600 g, 2.78 mmol) and 3,5-Bis(trifluoromethyl)phenylacetic acid (0.760 g, 2.78 mmol) using general procedure **C** for synthesis of **3**. The crude mixture was purified by flash chromatography (Hex:AcOEt 2:1) to afford the methylester as white solid (0.75 g, yield 62 %).

^{1}H NMR ($CDCl_3$, 400 MHz): δ 7.82 (1H, s), 7.72 (2H, s), 7.27-7.23 (3H, m), 7.01-6.98 (2H, m), 5.97 (1H, d, *J* = 7.2 Hz), 4.93-4.88 (1H, m), 3.79 (3H, s), 3.66 (1H, d, *J* = 15.6 Hz), 3.61 (1H, d, *J* = 15.6 Hz), 3.17 (1H, dd, *J* = 13.6, 5.6 Hz), 3.09 (1H, dd, *J* = 13.6, 5.4 Hz).

EIMS 433 $[M]^+$.

3d was prepared from the corresponding methylester (0.26 g, 0.60 mmol) using general procedure **C** for synthesis of **3**. White solid (0.25 g, yield 99 %).

mp 138-140 °C

$[\alpha]^{20}_D$ = -10.52 (Na, *c* = 0.21 in MeOH).

^{1}H NMR (DMSO-d_6, 400 MHz): δ 8.52 (1H, d, *J* = 8.2 Hz), 7.96 (1H, s), 7.88 (2H, s), 7.22-7.13 (5H, m), 4.49-4.43 (1H, m), 3.65 (1H, d, *J* = 15.3 Hz), 3.57 (1H, d, *J* = 15.3 Hz), 3.09 (1H, dd, *J* = 13.8, 4.6 Hz), 2.86 (1H, dd, *J* = 13.8, 9.8 Hz).

^{13}C NMR (DMSO-d_6, 100.6 MHz): δ 173.88, 169.96, 140.73, 138.55, 131.12 (2C, q, *J* = 32.8 Hz), 130.94 (2C), 130.11 (2C), 129.10 (2C), 127.44, 124.50 (2C, q, *J* = 272.6 Hz), 121.25, 54.60, 42.17, 37.90.

HR-EIMS Anal. Calcd for $[C_{19}H_{15}F_6NO_3]^+$ 419.0956; Found 491.0955.

(*S*)-2-[2-(3,5-difluorophenyl)acetamido]-3-phenylpropanoic acid - (**3e**)

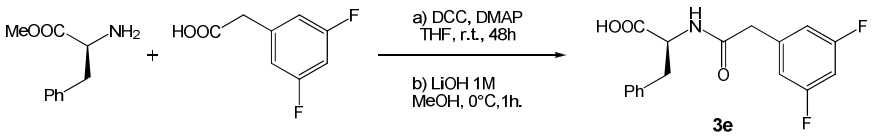

3e

The methylester of acid **3e** was prepared using L-Phenylalaninemethylester hydrochloride (0.80 g, 3.71 mmol) and 3,5-Difluorophenylacetic acid (0.64 g, 3.71 mmol) using general procedure **C** for synthesis of **3**. The crude mixture was purified by flash chromatography (Hex:AcOEt 2:1) to afford the methylester as white solid (0.93 g, yield 75 %).

^{1}H NMR ($CDCl_3$, 300 MHz): δ 7.25-7.23 (3H, m), 6.96-6.92 (2H, m), 6.74-6.70 (3H, m), 5.83 (1H, d, *J* = 6.8 Hz), 4.88-4.82 (1H, m), 3.73 (3H, s), 3.50 (1H, d, *J* = 14.2 Hz), 3.47 (1H, d, *J* = 14.2 Hz), 3.12 (1H, dd, *J* = 13.8, 5.6 Hz), 3.02 (1H, dd, *J* = 13.8, 5.9 Hz).

EIMS 333 $[M]^+$.

3e was prepared from the corresponding methylester (0.73 g, 2.19 mmol) using general procedure **C** for synthesis of **3**. White solid (0.63 g, yield 91 %).

mp 182-184 °C.

$[\alpha]^{20}_D$ = +33.63 (Na, *c* = 0.96 in MeOH:$CHCl_3$ 1:1).

^{1}H NMR (DMSO-d_6, 400 MHz): δ 8.48 (1H, d, *J* = 8.2 Hz), 7.26-7.18 (5H, m), 7.09-7.03 (1H, m), 6.87-6.83 (2H, m), 4.48-4.42 (1H, m), 3.49 (1H, d, *J* = 14.2 Hz), 3.43 (1H, d, *J* = 14.2 Hz), 3.09 (1H, dd, *J* = 13.8, 4.7 Hz), 2.86 (1H, dd *J* = 13.8, 9.8 Hz).

^{13}C NMR (DMSO-d_6, 100.6 MHz): δ 173.38, 169.44, 162.53 (2C, dd, *J* = 245.5, 14.1 Hz), 140.99 (t, *J* = 10.0 Hz), 137.91, 129.55 (2C), 128.55 (2C), 126.89, 112.57 (2C, d, *J* = 25.2 Hz), 102.29 (2C, t, J = 25.2 Hz), 53.91, 41.81, 37.14.

HR-EIMS Anal. Calcd for $[C_{17}H_{15}F_2NO_3]^+$ 319.1020; Found 319.1019.

2-[2-(3,5-dimethylphenyl)acetamido]acetic acid - (**3f**)

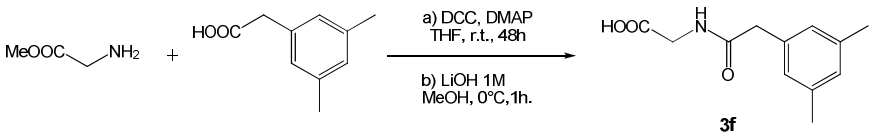

3f

The methylester of acid **3f** was prepared using Glycinemethylester hydrochloride (0.80 g, 6.37 mmol) and 3,5-Dimethylphenylacetic acid (1.05 g, 6.37 mmol) using general procedure **C** for synthesis of **3**. The crude mixture was purified by flash chromatography (Hex:AcOEt 2:3) to afford the methylester as white solid (0.78 g, yield 52 %).

^{1}H NMR ($CDCl_3$, 300 MHz): δ 6.92 (1H, s), 6.88 (2H, s), 5.92 (1H, d, *J* = 5.1 Hz), 3.99 (2H, d, *J* = 5.1 Hz), 3.72 (3H, s), 3.54 (2H, s), 2.30 (6H, s).

EIMS 235 $[M]^+$.

3f was prepared from the corresponding methylester (0.74 g, 3.145 mmol) using general procedure **C** for synthesis of **3**. White solid (0.66 g, yield 95 %).

mp 129-131 °C.

^{1}H NMR (DMSO-d_6, 400 MHz): δ 8.30 (1H, t, *J* = 5.7 Hz), 6.88, (2H, s), 6.85 (1H, s), 3.75 (2H, d, *J* = 5.7 Hz), 3.39 (2H, s), 2.23 (6H, s).

^{13}C NMR (DMSO-d_6, 100.6 MHz): δ 171.79, 171.05, 137.47 (2C), 136.37, 128.19, 127.30 (2C), 42.35, 41.21, 21.34 (2C).

HR-EIMS Anal. Calcd for $[C_{12}H_{15}NO_3]^+$ 221.1052; Found 221.1054.

(*S*)-2-[2-(3,5-dimethylphenyl)acetamido]-3-(4-hydroxyphenyl)propanoic acid - (**3g**)

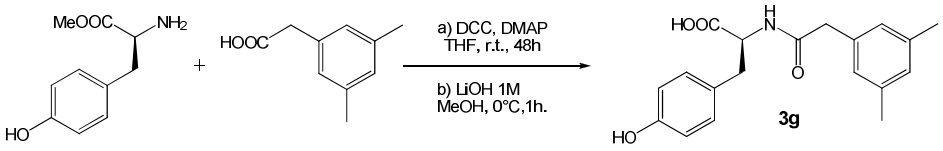

The methylester of acid **3g** was prepared using L-Tyrosine methyl ester hydrochloride (0.47 g, 2.32 mmol) and 3,5-Dimethylphenylacetic acid (0.45 g, 2.32 mmol) using general procedure **C** for synthesis of **3**. The crude mixture was purified by flash chromatography (Hex:AcOEt 2:3) to afford the methylester as white solid (0.34 g, yield 43 %).

^{1}H NMR ($CDCl_3$, 400 MHz): δ 7.12-7.05 (3H, m), 6.80-6.78 (2H, m), 6.69 (2H, d, *J* = 9.0 Hz), 5.71 (1H, d, *J* = 7.6 Hz), 4.85-4.79 (1H, m), 3.53 (3H, s), 3.41 (1H, d, *J* = 15.7 Hz), 3.34 (1H, d, *J* = 15.7 Hz), 2.98 (1H, dd, *J* = 13.8, 5.8 Hz), 2.96 (1H, dd, *J* = 13.8, 5.8 Hz), 2.07 (6H, s).

EIMS 341 $[M]^+$.

3g was prepared from the corresponding methylester (0.22 g, 0.65 mmol) using general procedure **C** for synthesis of **3**. White solid (0.21 g, yield 97 %).

mp 145-148 °C.

$[\alpha]^{20}_D$ = +22.12 (Na, *c* = 1.35 in MeOH).

^{1}H NMR ($CDCl_3$, 400 MHz): δ 7.12-7.07 (3H, m), 6.91 (2H, dd, *J* = 7.1, 1.7 Hz), 6.68 (2H, d, *J* = 9.01 Hz), 5.86 (1H, d, *J* = 7.6 Hz), 4.91-4.85 (1H, m), 3.59 (1H, d, *J* = 16.4 Hz), 3.51 (1H, d, *J* = 16.4 Hz), 3.23 (1H, dd, *J* = 14.0, 5.6 Hz), 3.06 (1H, dd, *J* = 14.0, 5.6 Hz), 2.3 (6H, s).

^{13}C NMR ($CDCl_3$, 100.6 MHz): δ 174.28, 172.18, 155.62, 138.63 (2C), 133.68, 130.27, 129.67, 129.36 (2C), 127.26 (2C), 115.75 (2C), 53.17, 43.20, 36.99, 21.23 (2C).

EIMS 327 $[M]^+$.

(*S*)-2-[(3,5-Difluorophenyl)acetamido]propanoic acid - (**3h**)

3h

The methylester of acid **3h** was prepared using L-alanine methyl ester hydrochloride and 3,5-difluorophenylacetic acid using general procedure **D** for synthesis of **3**. The crude mixture was purified by flash chromatography (Hex:AcOEt 1:1) to afford the methyl ester as white solid (yield 85 %).

^{1}H NMR ($CDCl_3$, 400 MHz) δ: 6.83 (2H, tt, *J* = 6.6, 2.4 Hz), 6.73 (1H, tt, *J* = 11.2, 2.4 Hz), 6.26 (1H, d, *J* = 5.2 Hz), 4.58 (1H, qd, *J* = 7.2, 5.2 Hz), 3.74 (3H, s), 3.55 (2H, s), 1.39 (3H, d, *J* = 7.2 Hz).

3h was prepared from the corresponding methyl ester using general procedure **D** for synthesis of **3**. Amorphous solid (yield 72 %).

$[\alpha]^{20}_D$ = +28.15 (Na, *c* = 0.64 in $CHCl_3$).

^{1}H NMR ($CDCl_3$, 300 MHz) δ: 6.82 (2H, tt, *J* = 6.6, 2.1 Hz), 6.75 (1H, tt, *J* = 9.3, 2.1 Hz), 6.03 (1H, d, *J* = 6.0 Hz), 4.60 (1H, qd, *J* = 7.2 Hz), 3.57 (2H, s), 1.45 (3H, d, *J* = 7.2 Hz).

^{13}C NMR (100.6 MHz, CD_3OD) δ: 175.95, 172.44, 163.69 (2C, dd, *J* = 247.9, 16.8 Hz), 141.07 (t, *J* = 40.0 Hz), 113.22 (2C, d, *J* = 28.0 Hz), 102.95 (t, *J* = 102.0 Hz, CH_{Ar}), 48.26, 42.71, 17.50.

EIMS 243 $[M]^+$

(*R*)-2-[(3,5-difluorophenyl)acetamido]propanoic acid - (**3i**)

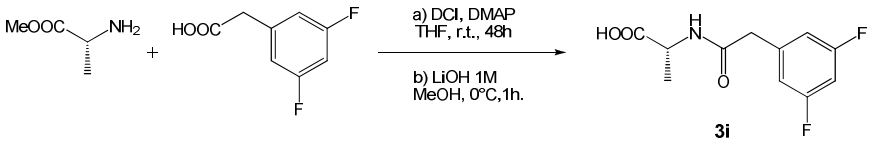

3i

The methylester of acid **3i** was prepared using L-alanine methyl ester hydrochloride and 3,5-difluorophenylacetic acid using general procedure **D** for synthesis of **3**. The crude mixture was purified by flash chromatography (Hex:AcOEt 1:1) to afford the methyl ester as white solid (yield 82 %).

^{1}H NMR ($CDCl_3$, 400 MHz) δ: 6.83 (2H, tt, *J* = 6.6, 2.4 Hz), 6.73 (1H, tt, *J* = 11.2, 2.4 Hz), 6.26 (1H, d, *J* = 5.2 Hz), 4.58 (1H, qd, *J* = 7.2, 5.2 Hz), 3.74 (3H, s), 3.55 (2H, s), 1.39 (3H, d, *J* = 7.2 Hz).

3i was prepared from the corresponding methyl ester using general procedure **D** for synthesis of **3**. Amorphous solid (yield 68 %).

$[\alpha]^{20}_{D}$ = -27.89 (Na, *c* = 0.75 in $CHCl_3$).

^{1}H NMR ($CDCl_3$, 300 MHz) δ: 6.82 (2H, tt, *J* = 6.6, 2.1 Hz), 6.75 (1H, tt, *J* = 9.3, 2.1 Hz), 6.03 (1H, d, *J* = 6.0 Hz), 4.60 (1H, qd, *J* = 7.2 Hz), 3.57 (2H, s), 1.45 (3H, d, *J* = 7.2 Hz).

^{13}C NMR (100.6 MHz, CD_3OD) δ: 175.95, 172.44, 163.69 (2C, dd, *J* = 247.9, 16.8 Hz), 141.07 (t, *J* = 40.0 Hz), 113.22 (2C, d, *J* = 28.0 Hz), 102.95 (t, *J* = 102.0 Hz, CH_{Ar}), 48.26, 42.71, 17.50.

EIMS 243 $[M]^{+}$

2-Amino-4,5,6,7-tetrahydrobenzothiazole - (**4c**)

Bioorg. Med. Chem. Lett. **2005**, *15*, 1561-1564.

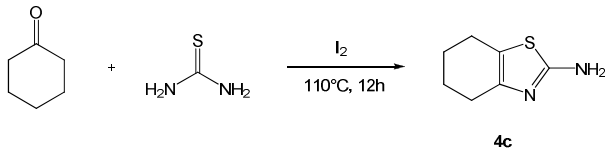

4c

A mixture of cycloexanone (3.00 g, 30.6 mmol), thiourea (4.65 g, 61.1 mmol) and iodine (7.76 g, 30.6 mmol) was stirred at 110°C for 12 h. The reaction mixture was cooled to room temperature. Hot water was then added to solubilize the crude material, and the resulting solution was stirred for 30 min. The aqueous solution was washed with diethyl ether and then neutralized by the addition of solid $NaHCO_3$. The pale yellow crystals were collected by filtration. The hydroiodide salt was dissolved in a hot saturated aqueous solution of Na_2CO_3. After cooling, the aqueous solution was extracted with CH_2Cl_2. The organic layer was dried over anhydrous Na_2SO_4, filtered, and concentrated under reduced pressure. The compound **4c** was obtained without any further purification as pale yellow solid (3.39 g, yield 72 %).

^{1}H NMR (DMSO-d_6 300 MHz) δ 6.61 (2H, s), 2.52-2.48 (2H, m), 2.38-2.35 (2H, m), 1.72-1.68 (4H, m).

EIMS 154 $[M]^+$.

General Procedure **E** for Synthesis of (**5**)

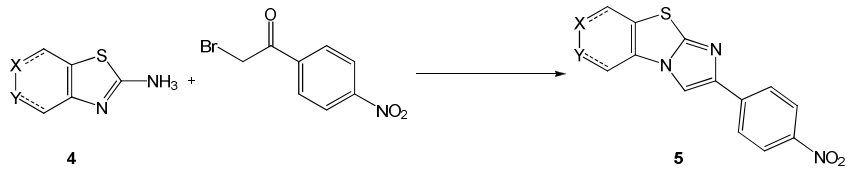

A mixture of **4** (1 mmol) and 2-Bromo-4'-nitroacetophenone (1.1 mmol) was reflux in ethanol or iso-propanol for 50-90 min, then the mixture was cooled to 0 °C. The solid was collected by filtration and washed with ethanol to afford **5** without any further purification.

7-Benzyl-2-(4-nitrophenyl)-5,6,7,8-tetrahydroimidazo[2',1':2,3]thiazolo[5,4-*c*]pyridine - (**5a**)

ARKIVOC **2010**, *3*, 145-151.

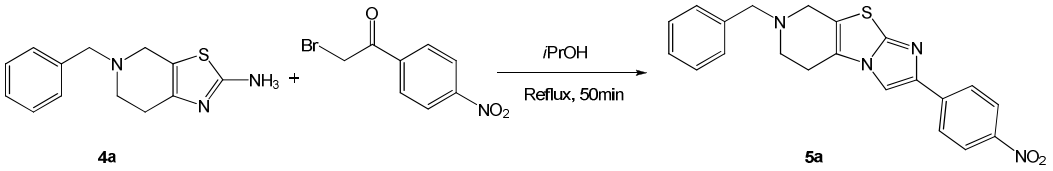

2-amino-5-benzyl-4,5,6,7-tetrahydrothiazolo[5,4-c]pyridine **4a** (1.0 g, 4.08 mmol) and 2-bromo-4'-nitroacetophenone (1.09 g, 4.49 mmol) were dissolved in *i*-PrOH (6 ml). **5a** was obtained following procedure **E** (1.67 g, yield 41 %).

^{1}H NMR ($CDCl_3$, 400 MHz): δ 8.22 (2H, d, *J* = 8.8 Hz), 7.94 (2H, d, *J* = 8.8 Hz), 7.70 (1H, s), 7.27-7.37 (5H, m), 3.78 (2H, s), 3.61 (2H, s), 3.01 (2H, t, *J* = 6.0 Hz), 2.81 (2H, t, *J* = 6.0 Hz).

EIMS 390 $[M]^+$.

6-Benzyl-2-(4-nitrophenyl)-5,6,7,8-tetrahydroimidazo[2',1':2,3]thiazolo[4,5-*c*]pyridine - (**5b**)

ARKIVOC **2010**, *3*, 145-151.

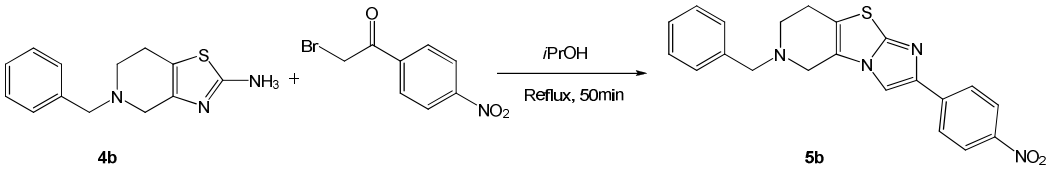

4b **5b**

2-amino-5-benzyl-4,5,6,7-tetrahydrothiazolo[4,5-*c*]pyridine (**4b**, 3.9 g, 16.1 mmol) and 2-bromo-4'-nitroacetophenone (4.7 g, 19.4 mmol) were dissolved in *i*-PrOH (80 ml). **5b** (2.28 g, yield 45 %) was directly submitted to the next step without further purification

2-(4-Nitrophenyl)imidazo[2,1-*b*]-5,6,7,8-tetrahydrobenzothiazole - (**5c**)

Bioorg. Med. Chem. Lett. **2005**, *15*, 1561-1564.

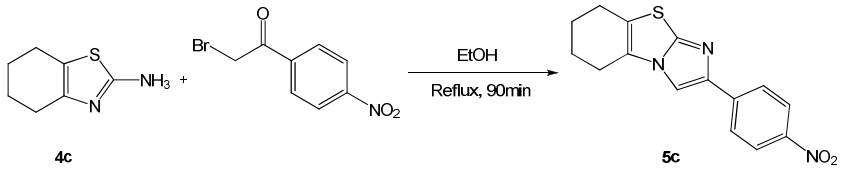

4c **5c**

5c was prepared from 2-amino-5,6,7,8-tetrahydrobenzothiazole **4c** (3.00 g, 19.5 mmol) and 2-Bromo-4'-nitroacetophenone (5.24 g, 21.4 mmol) using general procedure **E** for synthesis of **5**. Yellow solid (2.31 g, yield 40 %).

^{1}H NMR (DMSO-d_6, 300 MHz): δ 8.52 (1H, s), 8.27 (2H, d, *J* = 8.8 Hz), 8.09 (2H, d, *J* = 8.8 Hz), 2.73-2.69 (4H, m), 1.92-1.88 (4H, m).

EIMS 299 $[M]^+$.

2-(4-nitrophenyl)imidazo[2,1-*b*]benzothiazole - (**5d**)

J. Med. Chem. ***1986****, 29,* 386-394.

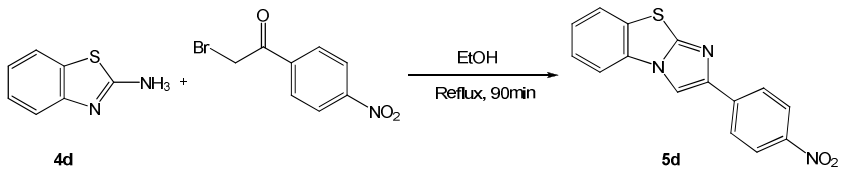

5d was prepared from 2-aminobenzothiazole (1.00 g, 6.46 mmol) and 2-Bromo-4'-nitroacetophenone (1.83 g, 7.10 mmol) using general procedure **E** for synthesis of **5.** Yellow solid (0.495 g, yield 26 %).

^{1}H NMR (DMSO-d_6, 300 MHz): δ 9.10 (1H, s), 8.34 (2H, d, *J* = 9.0 Hz), 8.12 (2H, d, *J* = 9.0 Hz), 8.07 (1H, d, *J* = 8.0 Hz), 8.02 (1H, d, *J* = 8.0 Hz), 7.64 (1H, t, *J* = 8.0 Hz), 7.49 (1H, t, *J* = 8.0 Hz).

EIMS 295 $[M]^+$.

*General Procedures for Synthesis of **9-12***

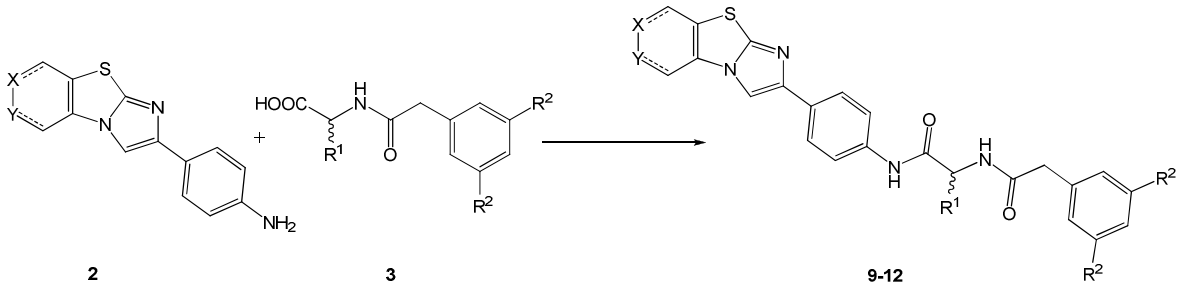

2 **3** **9-12**

Procedure **F**:

Compound **3** (1.1 mmol) was dissolved in anhydrous CH_2Cl_2 that was activated with the addition of HOBt (1.1 mmol), BOP-Cl (1.1 mmol) and DIPEA (4.0 mmol) in the presence of activated MS 4ºA and stirred for 10 min at r.t. under argon. A solution of amine **2** (1.0 mmol) in a small amount of CH_2Cl_2 was transferred to the mixture. The reaction was further stirred at r.t. for 48 h and quenched with a saturated solution of $NaHCO_3$ and the product was extracted with AcOEt, washed with water, brine and dried on $MgSO_4$. The solvent was removed under reduced pressure and the crude was purified by flash chromatography to afford **9-12**.

Procedure **G**:

Compound **3** (1.1 mmol) was dissolved in anhydrous THF under nitrogen and was added in order: HATU (1.1 mmol) and DIPEA (2 mmol) and stirred for 15 min at r.t. The mixture was added **2** (1 mmol) and stirred at room temperature overnight. The solvent was removed under reduced pressure and the crude was purified by flash chromatography to afford **9-12**.

(*S*)-*N*-[4-(7-Benzyl-5,6,7,8-tetrahydroimidazo[2',1':2,3]thiazolo[5,4-*c*]pyridin-2-yl)phenyl]-2-[2-(3,5-dimethylphenyl)acetamido]-3-phenylpropanamide - (**9a**)

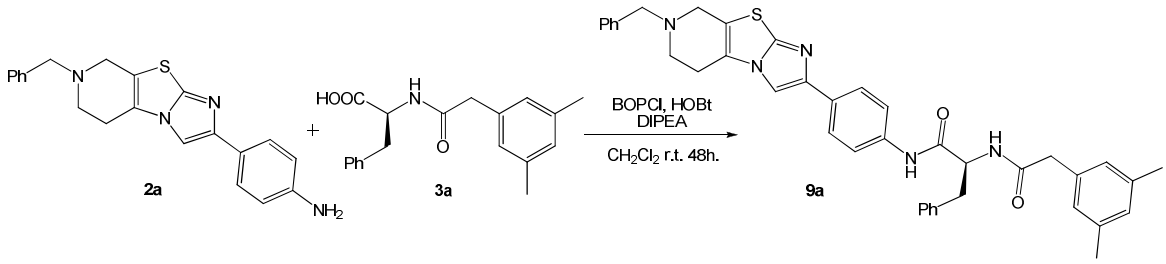

9a was prepared from **2a** (0.12 g, 0.35 mmol) and **3a** (0.11 g, 0.35 mmol) using general procedure **F**. The crude mixture was purified by Byotage chromatography (MeOH:CH_2Cl_2 1:99) to afford **9a** as a white solid (0.12 g, yield 55 %).

$[\alpha]^{20}_D$ = +3.61 (Na, *c* = 0.23 in MeOH).

^{1}H NMR ($CDCl_3$ with drops of CD_3OD, 400 MHz): δ 9.37 (1H , brs), 7.69 (2H, d, *J* = 8.8 Hz), 7.56 (1H, s), 7.47 (2H, d, *J* = 8.4 Hz), 7.38 (1H, s), 7.37 (1H, d, *J* = 1.6 Hz), 7.32-7.47 (3H, m), 7.20-7.24 (3H, m), 7.10 (2H, dd, *J* = 7.2, 2.4 Hz), 6.91 (1H, s), 6.82 (1H, d, *J* = 8.0 Hz), 6.78 (2H, s), 4.75 (1H, dt, *J* = 14.8, 7.2 Hz), 3.79 (2H, 2H), 3.62 (2H, s), 3.46 (2H, s), 3.09 (1H, dd, *J* = 14.0, 6.8 Hz), 3.02 (2H, t, *J* = 5.6 Hz), 2.98 (1H, dd, *J* = 14.0, 6.8 Hz), 2.80 (2H, t, *J* = 5.6 Hz), 2.28 (6H, s).

^{13}C NMR ($CDCl_3$ with drops of CD_3OD, 100.6 MHz): δ 172.01, 169.29, 148.34, 145.89, 138.21, 136.84, 136.83, 136.66, 135.95, 133.89, 129.91, 129.04, 128.98, 128.75, 128.37, 128.24, 127.50, 126.82, 126.67, 125.34, 124.53, 120.23, 120.14, 118.88, 105.56, 61.01, 54.72, 50.02, 48.48, 42.95, 38.02, 22.53, 20.90.

HR-MS Anal. Calcd for $[C_{40}H_{39}N_5O_2S+H]^+$ 654.2902; Found 654.2898.

(*R*)-*N*-[4-(7-Benzyl-5,6,7,8-tetrahydroimidazo[2',1':2,3]thiazolo[5,4-*c*]pyridin-2-yl)phenyl]-2-[2-(3,5-dimethylphenyl)acetamido]-3-phenylpropanamide - (**9b**)

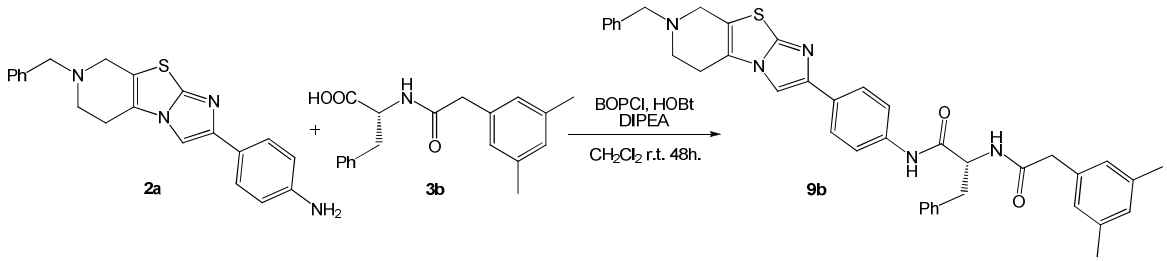

9b was prepared from **2a** (0.15 g, 0.42 mmol) and **3b** (0.13 g, 0.42 mmol) using general procedure **F**. The crude mixture was purified by Byotage chromatography (MeOH:CH_2Cl_2 1:99) to afford **9b** as a white solid (0.12 g, Yield 45 %).

$[\alpha]^{20}_D$ = -3.40 (Na, *c* = 0.20 in MeOH).

^{1}H NMR ($CDCl_3$ with drops of CD_3OD, 400 MHz): δ 9.37 (1H , brs), 7.69 (2H, d, *J* = 8.8 Hz), 7.56 (1H, s), 7.47 (2H, d, *J* = 8.4 Hz), 7.38 (1H, s), 7.37 (1H, d, *J* = 1.6 Hz), 7.32-7.47 (3H, m), 7.20-7.24 (3H, m), 7.10 (2H, dd, *J* = 7.2, 2.4 Hz), 6.91 (1H, s), 6.82 (1H, d, *J* = 8.0 Hz), 6.78 (2H, s), 4.75 (1H, dt, *J* = 14.8, 7.2 Hz), 3.79 (2H, 2H), 3.62 (2H, s), 3.46 (2H, s), 3.09 (1H, dd, *J* = 14.0, 6.8 Hz), 3.02 (2H, t, *J* = 5.6 Hz), 2.98 (1H, dd, *J* = 14.0, 6.8 Hz), 2.80 (2H, t, *J* = 5.6 Hz), 2.28 (6H, s).

^{13}C NMR ($CDCl_3$ with drops of CD_3OD, 100.6 MHz): δ 172.01, 169.29, 148.34, 145.89, 138.21, 136.84, 136.83, 136.66, 135.95, 133.89, 129.91, 129.04, 128.98, 128.75, 128.37, 128.24, 127.50, 126.82, 126.67, 125.34, 124.53, 120.23, 120.14, 118.88, 105.56, 61.01, 54.72, 50.02, 48.48, 42.95, 38.02, 22.53, 20.90.

HR-MS Anal. Calcd for $[C_{40}H_{39}N_5O_2S+H]^+$ 654.2902; Found 654.2908.

(*S*)-N-[4-(6-Benzyl-5,6,7,8-tetrahydroimidazo[2',1':2,3]thiazolo[4,5-*c*]pyridin-2-yl)phenyl]-2-[2-(3,5-difluorophenyl)acetamido]propanamide - (**10a**)

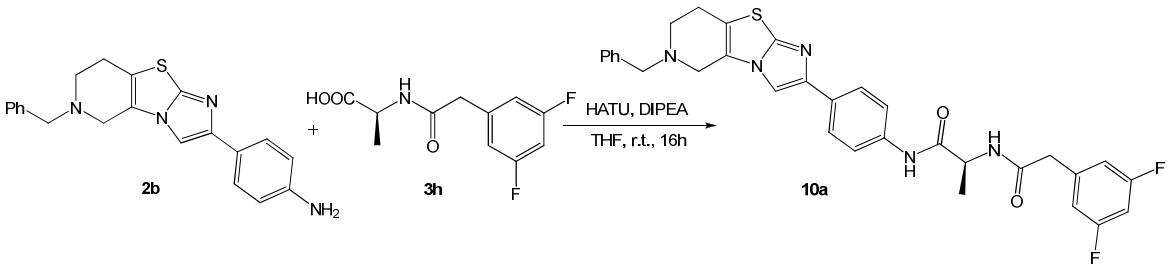

From **2b** and **3h** using procedure **G**. Flash chromatography (DCM:MeOH 99:1) to give **10a** (yield 48 %).

$[\alpha]^{20}_{D}$ = +4.18 (Na, *c* = 0.23 in MeOH);

^{1}H NMR ($CDCl_3$ with drops of CD_3OD, 400 MHz) δ: 9.54 (1H, brs), 7.67 (1H, dt, *J* = 8.8, 1.6 Hz), 7.63 (1H, d, *J* = 7.6 Hz), 7.52 (1H, dt, *J* = 8.8, 1.6 Hz), 7.32-7.42 (6H, m), 6.84 (2H, tt, *J* = 6.4, 2.4 Hz), 6.70 (1H, tt, *J* = 11.2, 2.4 Hz), 4.57 (1H, q, J = 7.2 Hz), 3.81 (2H, s), 3.58 (2H, s), 3.54 (2H, s), 2.95 (2H, t, *J* = 5.6 Hz), 2.82 (2H, t, *J* = 5.6 Hz), 1.41 (3H, d, *J* = 6.8 Hz).

^{13}C NMR ($CDCl_3$ with drops of CD_3OD, 100.6 MHz) δ: 170.80, 170.24, 163.05 (d, *J* = 132.8 Hz), 148.67, 145.84, 137.30 (t, *J* = 93.1 Hz), 136.97, 129.90, 128.87, 128.42, 127.51, 125.38, 124.09, 120.14, 120.05, 119.89, 112.07 (d, *J* = 69.4 Hz), 105.32, 102.40 (t, *J* = 253 Hz), 61.53, 50.02, 49.46, 48.93, 42.25, 24.45, 17.95.

HR-MS Anal. Calcd for $[C_{32}H_{29}F_2N_5O_2S+H]^+$ 586.2088; Found: 586.2075.

(*R*)-*N*-[4-(6-Benzyl-5,6,7,8-tetrahydroimidazo[2',1':2,3]thiazolo[4,5-*c*]pyridin-2-yl)phenyl]-2-[2-(3,5-difluorophenyl)acetamido]propanamide - (**10b**)

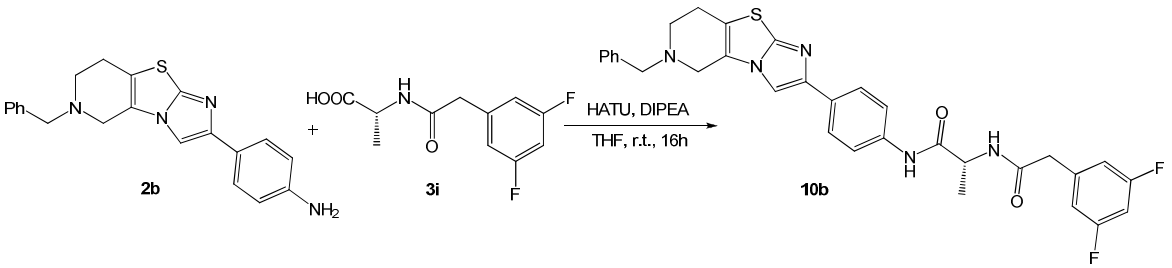

From **2b** and **3i** using procedure **G**. Flash chromatography (DCM:MeOH 99:1) to give **10b** (yield 53 %).

$[\alpha]^{20}_{D}$ = -4.02 (Na, *c* = 0.25 in MeOH);

^{1}H NMR ($CDCl_3$ with drops of CD_3OD, 400 MHz): δ 9.54 (1H, brs), 7.67 (1H, dt, *J* = 8.8, 1.6 Hz), 7.63 (1H, d, *J* = 7.6 Hz), 7.52 (1H, dt, *J* = 8.8, 1.6 Hz), 7.32-7.42 (6H, m), 6.84 (2H, tt, *J* = 6.4, 2.4 Hz), 6.70 (1H, tt, *J* = 11.2, 2.4 Hz), 4.57 (1H, q, J = 7.2 Hz), 3.81 (2H, s), 3.58 (2H, s), 3.54 (2H, s), 2.95 (2H, t, *J* = 5.6 Hz), 2.82 (2H, t, *J* = 5.6 Hz), 1.41 (3H, d, *J* = 6.8 Hz).

^{13}C NMR ($CDCl_3$ with drops of CD_3OD, 100.6 MHz): δ 170.80, 170.24, 163.05 (d, *J* = 132.8 Hz), 148.67, 145.84, 137.30 (t, *J* = 93.1 Hz), 136.97, 129.90, 128.87, 128.42, 127.51, 125.38, 124.09, 120.14, 120.05, 119.89, 112.07 (d, *J* = 69.4 Hz), 105.32, 102.40 (t, *J* = 253 Hz), 61.53, 50.02, 49.46, 48.93, 42.25, 24.45, 17.95.

HR-MS Anal. Calcd. for $[C_{32}H_{29}F_2N_5O_2S+H]^+$ 586.2088; Found 586.2094.

(*S*)-*N*-[4-(5,6,7,8-Tetrahydroimidazo[2,1-*b*]benzothiazol-2-yl)phenyl]-2-[2-(3,5-dimethylphenyl)acetamido]-3-phenylpropanamide - (**11** - CF054)

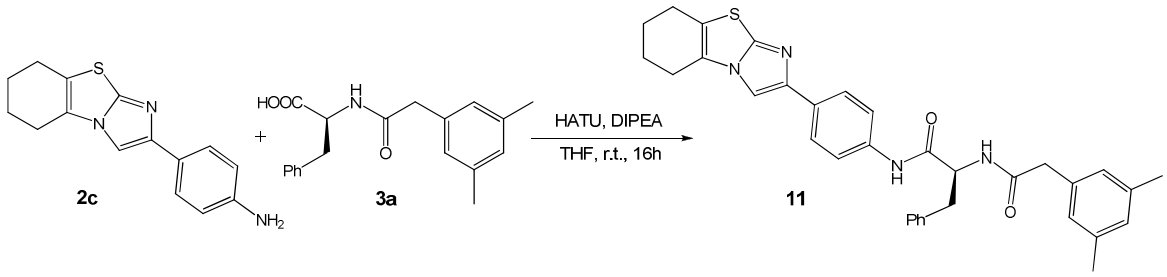

11 was prepared from **2c** (0.08 g, 0.30 mmol) and **3a** (0.10 g, 0.33 mmol) using general procedure **G**. The crude mixture was purified by flash chromatography (EtOH:CH_2Cl_2 1:30) to afford **11** as a white solid (0.15 g, Yield 91 %).

mp 225-228 °C.

$[\alpha]^{20}_D$ = +5.79 (Na, *c* = 0.96 in $CHCl_3$).

^{1}H NMR (DMSO-d_6, 400 MHz): δ 10.14 (1H, s), 8.44 (1H, d, *J* = 8.2 Hz), 8.10 (1H, s), 7.77 (2H, d, *J* = 8.6 Hz), 7.60 (2H, d, *J* = 8.6 Hz), 7.31-7.19 (5H, m), 6.81 (1H, s), 6.75 (2H, s), 4.70-4.67 (1H, m), 3.39 (1H, d, *J* = 14.1 Hz), 3.32 (1H, d, *J* = 14.1 Hz), 3.07 (1H, dd, *J* = 14.2, 4.9 Hz), 2.90 (1H, dd, *J* = 14.2, 9.6 Hz), 2.72-2.68 (4H, m), 2.20 (6H, bs), 1.89-1.85 (4H, m).

^{13}C NMR (DMSO-d_6, 100.6 MHz): δ 171.31, 171.13, 148.12, 146.22, 138.74, 138.63, 138.05, 137.11 (2C), 131.12, 131.97, 130.32 (2C), 129.15 (2C), 128.78, 127.88 (2C), 127.45, 126.03 (2C), 121.57, 120.69 (2C), 107.97, 55.97, 43.09, 38.90, 24.91, 23.83, 23.28, 22.30 , 21.97(2C).

HR-EIMS Anal. Calcd for $[C_{34}H_{34}N_4O_2S]^+$ 562.2402; Found 562.2408.

(*S*)-*N*-[4-(Imidazo[2,1-*b*]benzothiazol-2-yl)phenyl]-2-[2-(3,5-dimethylphenyl)acetamido]-3-phenylpropanamide - (**12a** - CF022)

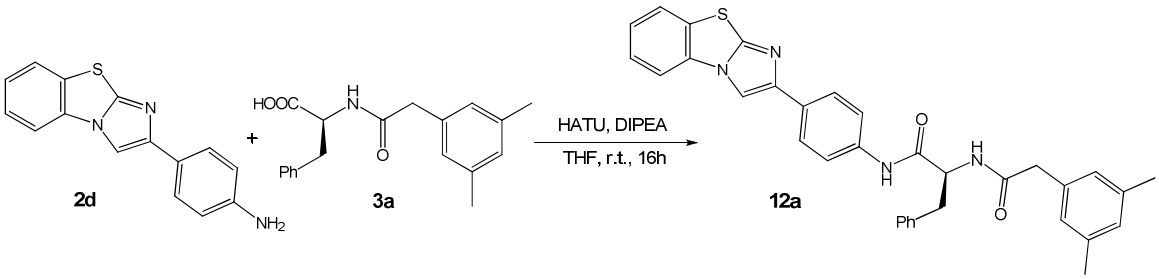

12a was prepared from **2d** (0.54 g, 2.05 mmol) and **3a** (0.70 g, 2.25 mmol) using general procedure **G**. The crude mixture was purified by flash chromatography (EtOH:CH_2Cl_2 1:30) and crystallization with $CHCl_3$ to afford **12a** as white solid (0.86 g, yield 75 %).

mp 224-226 °C

$[\alpha]^{20}_D$ = +4.42 (Na, *c* = 1.28 in $CHCl_3$).

^{1}H NMR ($CDCl_3$, 400 MHz): δ 8.60 (1H, s), 7.92 (1H, s), 7.79 (2H, d, *J* = 8.4 Hz), 7.70 (1H, d, *J* = 7.8 Hz), 7.61 (1H, d, *J* = 7.8 Hz), 7.48-7.44 (3H, m), 7.37 (1H, t, *J* = 7.8 Hz), 7.29-7.21 (3H, m), 7.12-7.10 (2H, m), 6.95 (1H, s), 6.78 (2H, s), 6.29 (1H, d, *J* = 7.6 Hz), 4.92-4.86 (1H, m), 3.51-3.47 (2H, m), 3.14 (1H, dd, *J* = 14.0, 6.4 Hz), 3.05 (1H, dd, *J* = 14.0, 7.8 Hz), 2.30 (6H, s).

^{13}C NMR ($CDCl_3$, 100.6 MHz): δ 172.60, 170.02, 148.34, 146.43, 139.19, 138.16, 137.08, 134.73 (2C), 132.56, 131.01, 130.79, 129.91 (2C), 129.76, 129.22 (2C), 127.78 (2C), 127.56, 127.16, 126.44 (2C), 125.91, 124.80, 121.00 (2C), 113.68, 107.62, 55.99, 44.11, 38.48, 21.84 (2C).

HR-EIMS Anal. Calcd for $[C_{34}H_{30}N_4O_2S]^+$ 558,2089; Found 558,2086.

(*S*)-*N*-[4-(Imidazo[2,1-*b*]benzothiazol-2-yl)phenyl]-2-[2-(3,5-dimethylphenyl)acetamido]-3-phenylpropanamide - (**12b** - CF056)

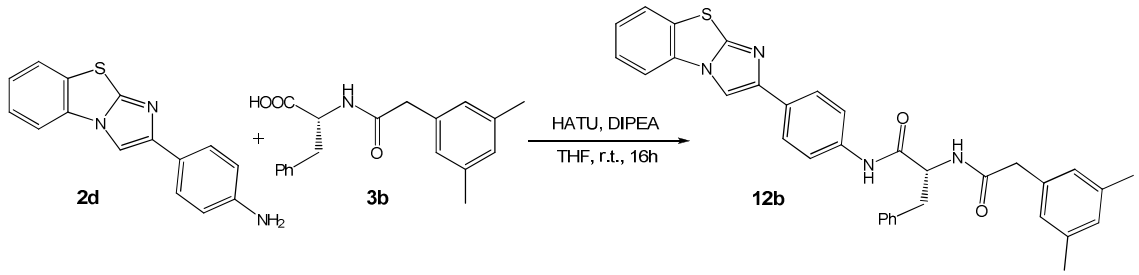

12b was prepared from **2d** (0.54 g, 2.05 mmol) and **3b** (0.70 g, 2.25 mmol) using general procedure **G**. The crude mixture was purified by flash chromatography (EtOH:CH_2Cl_2 1:30) and crystallization with $CHCl_3$ to afford **12b** as white solid (0.89 g, yield 78 %).

mp 224-226 °C

$[\alpha]^{20}_D$ = -4.28 (Na, *c* = 0.83 in $CHCl_3$).

^{1}H NMR ($CDCl_3$, 400 MHz): δ 8.60 (1H, s), 7.92 (1H, s), 7.79 (2H, d, *J* = 8.4 Hz), 7.70 (1H, d, *J* = 7.8 Hz), 7.61 (1H, d, *J* = 7.8 Hz), 7.48-7.44 (3H, m), 7.37 (1H, t, *J* = 7.8 Hz), 7.29-7.21 (3H, m), 7.12-7.10 (2H, m), 6.95 (1H, s), 6.78 (2H, s), 6.29 (1H, d, *J* = 7.6 Hz), 4.92-4.86 (1H, m), 3.51-3.47 (2H, m), 3.14 (1H, dd, *J* = 14.0, 6.4 Hz), 3.05 (1H, dd, *J* = 14.0, 7.8 Hz), 2.30 (6H, s).

^{13}C NMR ($CDCl_3$, 100.6 MHz): δ 172.60, 170.02, 148.34, 146.43, 139.19, 138.16, 137.08, 134.73 (2C), 132.56, 131.01, 130.79, 129.91 (2C), 129.76, 129.22 (2C), 127.78 (2C), 127.56, 127.16, 126.44 (2C), 125.91, 124.80, 121.00 (2C), 113.68, 107.62, 55.99, 44.11, 38.48, 21.84 (2C).

HR-EIMS Anal. Calcd for $[C_{34}H_{30}N_4O_2S]^+$ 558,2089; Found 558,2085.

(*S*)-*N*-[4-(Imidazo[2,1-*b*]benzothiazol-2-yl)phenyl]-2-[2-(3,5-bis(trifluoromethyl)phenyl) acetamido]-3-phenylpropanamide - (**12c** - CF052)

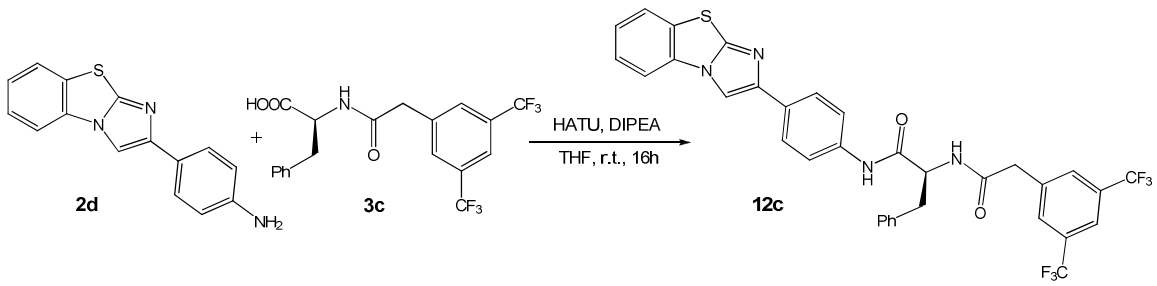

12c was prepared from **2d** (0.77 g, 2.91 mmol) and **3c** (1.34 g, 3.20 mmol) using general procedure **G**. The crude mixture was purified by flash chromatography (Hex:AcOEt 1:1) and crystallization with CH_2Cl_2 to afford **12c** as white solid (1.40 g, yield 72 %).

mp 243-245 °C

$[\alpha]^{20}_D$ = +1.54 (Na, *c* = 0.31 in DMSO).

^{1}H NMR (DMSO-d_6, 400 MHz): δ 10.25 (1H, s), 8.71-8.69 (2H, m), 8.04 (1H, d, *J* = 8.0 Hz), 7.98 (1H, d, *J* = 8.0 Hz), 7.96 (1H, s), 7.90 (2H, s), 7.82 (2H, d, *J* = 8.6 Hz), 7.66 (2H, d, *J* = 8.6 Hz), 7.58 (1H, t, *J* = 8.0 Hz), 7.44 (1H, t, *J* = 8.0 Hz), 7.29-7.13 (5H, m), 4.75-4.70 (1H, m), 3.74 (1H, d, *J* = 15.1 Hz), 3.70 (1H, d, *J* = 15.1 Hz), 3.10 (1H, dd, *J* = 13.8, 4.8 Hz), 2.89 (1H, dd, *J* = 13.8, 9.7 Hz).

^{13}C NMR (DMSO-d_6, 100.6 MHz): δ 172.13, 169.45, 146.82, 145.91, 141.12, 139.44, 138.87, 133.21, 131.98 (2C, q, *J* = 33.2 Hz) 131.80, 131.01 (2C), 130.51, 130.23 (2C), 129.03 (2C), 127.79, 127.41, 126.23 (2C), 126.18, 126.10, 123.42 (2C, q, *J* = 271.0 Hz), 121.79, 120.84 (2C), 114.37, 109.56, 56.04, 42.60, 38.65.

HR-EIMS Anal. Calcd for $[C_{34}H_{24}F_6N_4O_2S]^+$ 666.1524; Found 666.1527.

(*R*)-*N*-[4-(Imidazo[2,1-*b*]benzothiazol-2-yl)phenyl]-2-[2-(3,5-bis(trifluoromethyl)phenyl) acetamido]-3-phenylpropanamide - (**12d** - CF081)

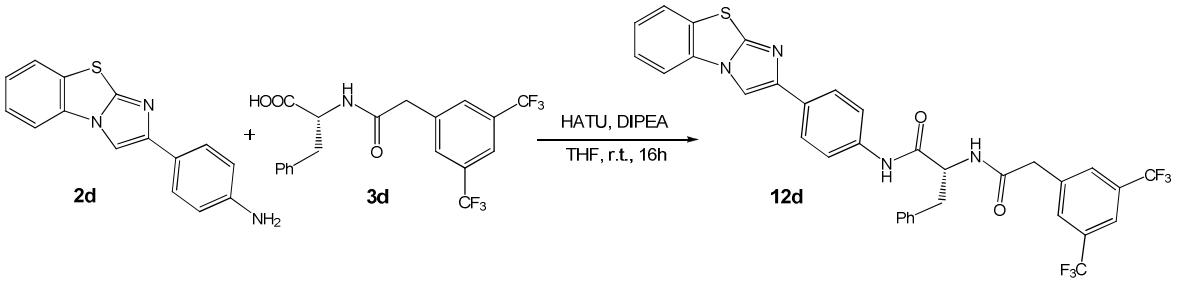

12d was prepared from **2d** (0.10 g, 0.38 mmol) and **3d** (0.17 g, 0.42 mmol) using general procedure **G**. The crude mixture was purified by flash chromatography (Hex:AcOEt 1:1) and crystallization with CH_2Cl_2 to afford **12d** as white solid (0.18 g, yield 74 %).

mp 243-245 °C

$[\alpha]^{20}_D$ = -1.46 (Na, *c* = 0.34 in DMSO).

^{1}H NMR (DMSO-d_6, 400 MHz): δ 10.25 (1H, s), 8.71-8.69 (2H, m), 8.04 (1H, d, *J* = 8.0 Hz), 7.98 (1H, d, *J* = 8.0 Hz), 7.96 (1H, s), 7.90 (2H, s), 7.82 (2H, d, *J* = 8.6 Hz), 7.66 (2H, d, *J* = 8.6 Hz), 7.58 (1H, t, *J* = 8.0 Hz), 7.44 (1H, t, *J* = 8.0 Hz), 7.29-7.13 (5H, m), 4.75-4.70 (1H, m), 3.74 (1H, d, *J* = 15.1 Hz), 3.70 (1H, d, *J* = 15.1 Hz), 3.10 (1H, dd, *J* = 13.8, 4.8 Hz), 2.89 (1H, dd, *J* = 13.8, 9.7 Hz).

^{13}C NMR (DMSO-d_6, 100.6 MHz): δ 172.13, 169.45, 146.82, 145.91, 141.12, 139.44, 138.87, 133.21, 131.98 (2C, q, *J* = 33.2 Hz) 131.80, 131.01 (2C), 130.51, 130.23 (2C), 129.03 (2C), 127.79, 127.41, 126.23 (2C), 126.18, 126.10, 123.42 (2C, q, *J* = 271.0 Hz), 121.79, 120.84 (2C), 114.37, 109.56, 56.04, 42.60, 38.65.

HR-EIMS Anal. Calcd for $[C_{34}H_{24}F_6N_4O_2S]^+$ 666.1524; Found 666.1529.

(*S*)-N-[4-(Imidazo[2,1-*b*]benzothiazol-2-yl)phenyl]-2-[2-(3,5-difluorophenyl)acetamido]-3-phenylpropanamide - (**12e** - CF082)

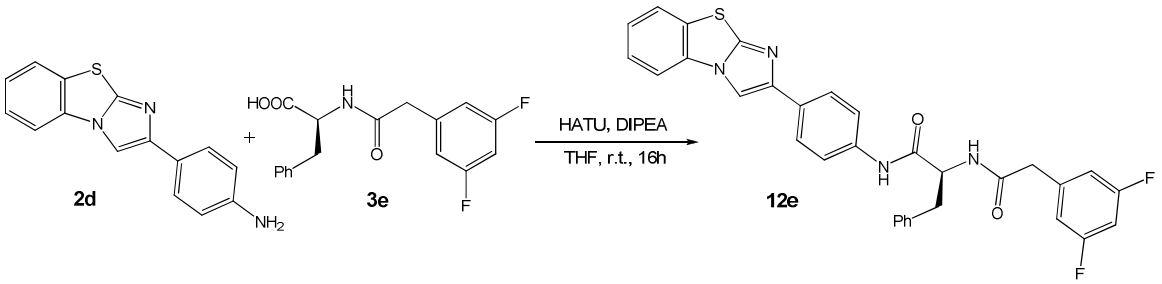

12e was prepared from **2d** (0.10 g, 0.38 mmol) and **3e** (0.13 g, 0.42 mmol) using general procedure **G**. The crude mixture was purified by flash chromatography (Hex:AcOEt 1:1) and crystallization with isopropanol to afford **12e** as white solid (0.13 g, yield 62 %).

mp 242-243 °C

$[\alpha]^{20}_{D}$ = -4.34 (Na, *c* = 0.27 in CH_3OH:$CHCl_3$ 1:1).

^{1}H NMR (DMSO-d_6, 400 MHz): δ 10.29 (1H, s), 8.73 (1H, s), 8.62 (1H, d, *J* = 8.3 Hz), 8.05 (1H, d, *J* = 7.9 Hz), 7.99 (1H, d, *J* = 7.9 Hz), 7.83 (2H, d, *J* = 8.6 Hz), 7.67 (2H, d, *J* = 8.6 Hz), 7.59 (1H, t, *J* = 8.0 Hz), 7.45 (1H, t, *J* = 8.0 Hz), 7.32-7.20 (5H, m), 7.05 (1H, tt, *J* = 9.5, 2.3 Hz), 6.86 (2H, dd, *J* = 8.4, 2.3 Hz), 4.75-4.70 (1H, m), 3.53 (1H, d, *J* = 14.1 Hz), 3.49 (1H, d, *J* = 14.1 Hz), 3.11 (1H, dd, *J* = 13.7, 4.8 Hz) 2.90 (1H, dd, *J* = 13.7, 9.8 Hz).

^{13}C NMR (DMSO-d_6, 100.6 MHz): δ 170.56, 169.51, 162.53 (2C, dd, *J* = 244.5, 14.1 Hz), 147.29, 146.32, 141.07 (t, *J* = 10.1 Hz), 138.46, 137.94, 132.27, 129.67 (2C), 129.40, 129.32, 128.48 (2C), 127.21, 126.87, 125.61 (2C), 125.57, 125.52, 120.10 (2C), 113.80, 112.62 (2C, d, *J* = 24.1 Hz), 109.01, 102.28 (t, *J* = 26.2 Hz), 55.39, 41.90, 38.31.

HR-EIMS Anal. Calcd for $[C_{32}H_{24}F_2N_4O_2S]^+$ 566,1588; Found 566,1584.

N-[4-(Imidazo[2,1-*b*]benzothiazol-2-yl)phenyl]-2-[2-(3,5-dimethylphenyl)acetamido] acetamide - (**12f** - CF083)

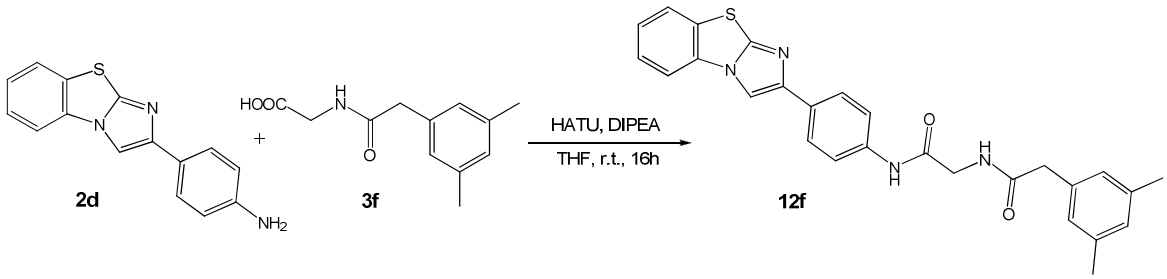

12f was prepared from **2d** (0.10 g, 0.38 mmol) and **3f** (0.09 g, 0.42 mmol) using general procedure **G**. The crude mixture was purified by flash chromatography ($MeOH/CH_2Cl_2$ 1:30) and crystallization with CH_3CN to afford **12f** as white solid (0.13 g, yield 72 %).

mp 250-252 °C.

^{1}H NMR (DMSO-d_6, 400 MHz): δ 10.04 (1H, s), 8.71 (1H, s), 8.37-8.33 (1H, m), 8.05 (1H, d, *J* = 7.9 Hz), 7.98 (1H, d, *J* = 7.9 Hz), 7.82 (2H, d, *J* = 8.6 Hz), 7.66 (2H, d, *J* = 8.6 Hz), 7.59 (1H, t, *J* = 7.9 Hz), 7.44 (1H, t, *J* = 7.9 Hz), 6.92 (2H, s), 6.87 (1H, s), 3.92 (2H, d, *J* = 5.6 Hz), 3.34 (2H, s), 2.26 (6H, s).

^{13}C NMR (DMSO-d_6, 100.6 MHz): δ 171.83, 168.80, 147.93, 147.42, 139.14, 138.16 (2C), 137.09, 132.99, 130.29, 130.21, 128.88, 128.02 (2C), 127.78, 126.29 (2C), 126.17, 126.08, 120.53 (2C), 114.36, 109.48, 44.10, 43.19, 21.99 (2C).

EIMS 468 $[M]^+$.

(*S*)-*N*-[4-(Imidazo[2,1-*b*]benzothiazol-2-yl)phenyl]-2-[2-(3,5-dimethylphenyl)acetamido]-3-(4-hydroxyphenyl)propanamide - (**12g** - CF023)

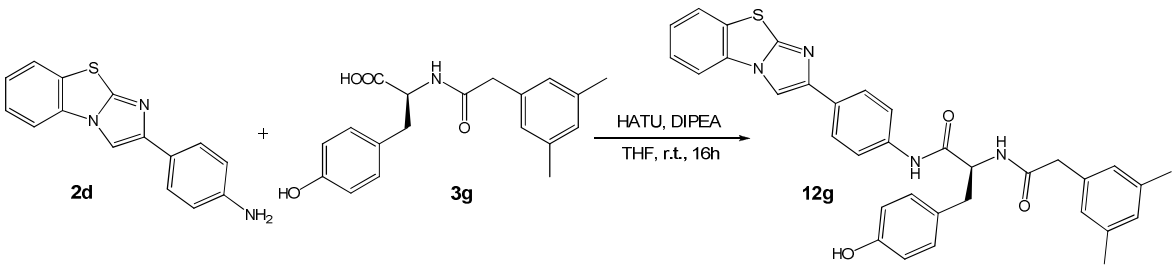

12g was prepared from **2d** (0.07 g ,0.28 mmol) and **3g** (0.10 g, 0.31 mmol) using general procedure **G**. The crude mixture was purified by flash chromatography (IPA/CH_2Cl_2 95:5) to afford **12g** as pale yellow (0.08 g, yield 52 %).

mp 265-268 °C

$[\alpha]^{20}_D$ = +2.76 (Na, *c* = 0.5 in DMSO).

^{1}H NMR (DMSO-d_6, 400 MHz): δ 10.25 (1H, s), 8.73 (1H, s), 8.39 (1H, d, *J* = 7.8 Hz), 8.08 (1H, d, *J* = 8.1 Hz), 7.98 (1H, d, *J* = 8.1 Hz), 7.81 (2H, d, *J* = 8.6 Hz), 7.67 (2H, d, *J* = 8.6 Hz), 7.58 (1H, t, *J* = 8.1 Hz), 7.43 (1H, t, *J* = 8.1 Hz), 7.11 (2H, d, *J* = 7.5 Hz), 6.84 (1H, s), 6.78 (2H, s), 6.67 (2H, d, *J* = 7.5 Hz),5.89 (1H, s), 4.65-4.54 (1H, m), 3.48-3.30 (2H, m), 2.98 (1H, dd, *J* = 14.2, 4.5 Hz), 2.81 (1H, dd, *J* = 14.2, 9.3 Hz), 2.53 (6H, s).

^{13}C NMR (DMSO-d_6, 100.6 MHz): δ 171.64, 169.12, 154.75, 147.78, 146.05, 138.85, 138.06, 134.65 (2C), 132.84 (2C), 132.24, 130.77, 130.61, 130.19, 129.12, 127.13 (2C), 116.78 (2C), 127.02, 126.08 (2C), 125.34, 124.63, 120.53 (2C), 112.89, 107.41, 54.11, 44.01, 35.21, 21.81 (2C).

EIMS 574 $[M]^+$.

2-(4-cyanophenyl)imidazo[2,1-*b*]benzothiazole - (**13**)

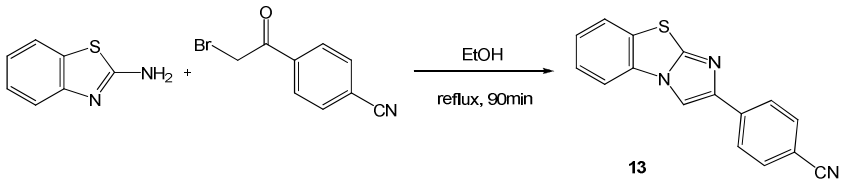

To a solution of 2-aminobenzothiazole (0.930 g, 6.00 mmol) in ethanol (92 ml), 2-Br-4'-cyanoacetophenone (1.50 g, 6.60 mmol) was added and the solution was refluxed for 90 min. After the completion of the reaction, the solution was cooled to 0 °C. The resulting precipitate was filtered and washed with ethanol to provide **13** as foam (0.578 g, yield 35 %).

^{1}H NMR ($CDCl_3$ 400 MHz): δ 8.09 (1H, s), 7.98 (2H, d, *J* = 8.2 Hz), 7.75 (1H, d, *J* = 8.0 Hz), 7.70 (2H, d, *J* = 8.2 Hz), 7.66 (1H, d, *J* = 8.0 Hz), 7.51 (1H, t, *J* = 8.0 Hz), 7.41 (1H, t, *J* = 8.0 Hz).

^{13}C NMR ($CDCl_3$, 100.6 MHz): δ 149.75, 146.43, 138.91, 133.29 (2C), 132.65, 131.17, 127.13, 126.29 (2C), 126.16, 125.26, 119.68, 113.53, 111.31, 109.18.

EIMS 275 $[M]^+$.

2-(4-benzylamine)imidazo[2,1-*b*]benzothiazole - (**14**)

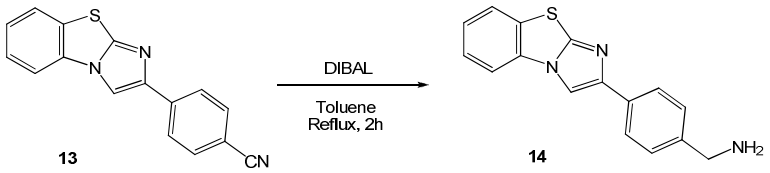

To a cooled at 0 °C mixture of 2-(4-cyanophenyl)imidazo[2,1-*b*]benzothiazole **13** (0.250 g, 0.900 mmol) in dry toluene (5 ml) was added 1M diisobutylaluminum hydride solution in Hexane (4.5 ml, 4.50 mmol) and the solution was refluxed for 2 h. Then, the solution was poured into ice-water (50 ml), an aqueous NaOH 1N solution (15 ml) was added and the organic layer was extracted with Et_2O. The combined organic layers were washed with brine, dried with Na_2SO_4 and evaporated in vacuum to dryness to provide **14** as yellow solid (0.224 g, yield 90 %).

^{1}H NMR (DMSO-d_6, 400 MHz): δ 8.75 (1H, s), 8.03 (1H, d, *J* = 8.0 Hz), 7.98 (1H, d, *J* = 8.0 Hz), 7.83 (2H, d, *J* = 8.1 Hz), 7.57 (1H, t, *J* = 8.0 Hz), 7.43 (1H, t, *J* = 8.0 Hz), 7.41 (2H, d, *J* = 8.1 Hz), 3.78 (2H, s).

^{13}C NMR (DMSO-d_6, 100.6 MHz): δ 147.95, 147.68, 143.12, 133.43, 133.08, 130.30, 128.72 (2C), 127.86, 126.26, 126.11, 126.03 (2C), 114.41, 109.98, 46.18.

EIMS 279 $[M]^+$.

(*S*)-*N*-[4-(Imidazo[2,1-*b*]benzothiazol-2-yl)benzyl]-2-[2-(3,5-bis(trifluoromethyl)phenyl) acetamido]-3-phenylpropanamide - (**15**)

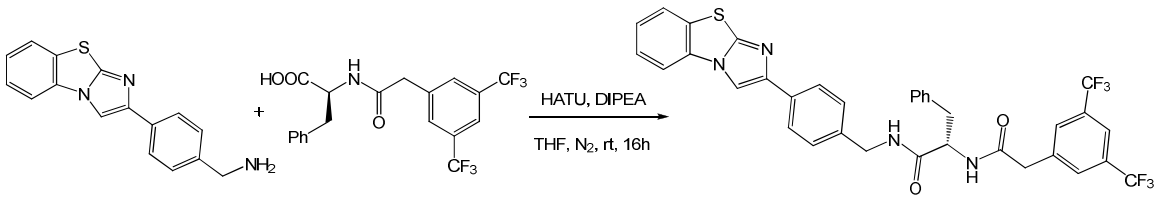

14 **3c** **15**

Compound **3c** (0.058 g, 0.138 mmol) was dissolved in anhydrous THF (10 ml) under nitrogen and was added in order: HATU (0.053 g, 0.138 mmol) and DIPEA (44 µl, 0.250 mmol) and stirred for 15 min. at r.t. The mixture was added **14** (0.035 g, 0.125 mmol) and stirred at room temperature overnight. The solvent was removed under reduced pressure and the crude was purified by flash chromatography (Hex:AcOEt 3:7) to afford **15**. White solid (0.026 g, yield 31 %).

$[\alpha]^{20}_{D}$ = +4.09 (Na, *c* = 0.30 in DMSO)

^{1}H NMR (DMSO-d_6, 400 MHz): δ 8.76 (1H, s), 8.63 (1H, t, *J* = 5.9 Hz), 8.58 (1H, d, *J* = 8.5 Hz), 8.05 (1H, d, *J* = 7.7 Hz), 7.99 (1H, d, *J* = 7.7 Hz), 7.96 (1H, s), 7.87 (2H, s), 7.80 (2H, d, *J* = 8.2 Hz), 7.59 (1H, t, *J* = 7.7 Hz), 7.44 (1H, d, *J* = 7.7 Hz), 7.23 (2H, d, *J* = 8.2 Hz), 7.21-7.15 (5H, m), 4.63-4.57 (1H, m), 4.35 (1H, dd, *J* = 15.3, 5.9 Hz), 4.30 (1H, dd, *J* = 15.3, 5.9 Hz), 3.72 (1H, d, *J* = 14.4 Hz), 3.67 (1H, d, *J* = 14.4 Hz), 3.05 (1H, dd, *J* = 13.6, 5.2 Hz), 2.82 (1H, dd, *J* = 13.6, 9.5 Hz).

^{13}C NMR (DMSO-d_6, 100.6 MHz): δ 171.37, 169.20, 147.34, 146.70, 140.15, 138.59, 138.09, 132.98, 132.30, 130.55 (2C, q, *J* = 36 Hz), 130.37 (2C), 129.94, 129.58 (2C), 128.33 (2C), 128.05 (2C), 127.16, 126.65, 125.61, 125.49, 125.05 (2C), 123.75 (2C, q, 268 Hz), 120.64, 113.77, 109.36,54.65, 42.44, 41.61, 38.46.

EIMS 680 $[M]^{+}$.

3-[2-(3,5-difluorophenyl)acetamido]propanoic acid - (**17**)

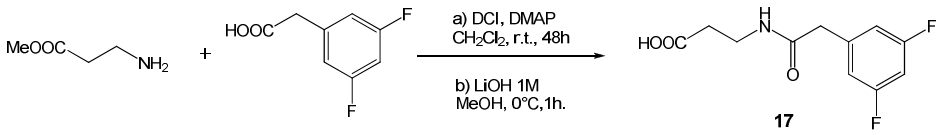

The methylester of acid **17** was prepared using β-alanine methyl ester hydrochloride (1.00 g, 7.16 mmol) and 3,5-difluorophenylacetic acid (1.17 g, 6.823 mmol) using general procedure **D** for synthesis of **3** (page XX). The crude mixture was purified by flash chromatography (Hex:AcOEt 2:3) to afford the methyl ester as white solid (1.32 g, yield 75 %).

^{1}H NMR ($CDCl_3$, 400 MHz): δ 6.73 (2H, tt, *J* = 6.8, 2.4 Hz), 6.73 (1H, tt, *J* = 11.2, 2.4 Hz), 6.22 (1H, brs), 3.67 (3H, s), 3.50 (2H, t, *J* = 6.0 Hz), 2.53 (2H, t, *J* = 6.0 Hz).

HR-FABMS Anal. Calcd 258.0941 $[M+H]^+$; Found 258.0946.

17 was prepared from the corresponding methyl ester using general procedure **D** for synthesis of **3**. White solid (0.96 g, yield 81 %).

^{1}H NMR ($CDCl_3$, 400 MHz): δ 7.02 (1H, brs), 6.74 (2H, tt, *J* = 6.6, 2.4 Hz), 6.63 (1H, tt, *J* = 11.2, 2.4 Hz), 3.40 (3H, s), 3.73 (2H, t, *J* = 6.0 Hz), 2.42 (2H, t, *J* = 6.0 Hz).

^{13}C NMR ($CDCl_3$, 100.6 MHz): δ 172.48, 170.41, 162.09 (2C, d, *J* = 241,3 Hz), 138.43 (t, *J* = 11.2 Hz), 112.06 (2C, d, *J* = 25.4 Hz), 102.37 (t, *J* = 27.2 Hz), 37.28, 35.05, 33.40.

HR-MS Anal. Calcd for $[C_{11}H_{11}F_2NO_3+H]^+$ 244.0780; Found 244.0785.

(*S*)-*N*-[4-(7-Benzyl-5,6,7,8-tetrahydroimidazo[2',1':2,3]thiazolo[5,4-*c*]pyridin-2-yl)phenyl]-2-[2-(3,5-difluorophenyl)acetamido]acetamide - (**18**)

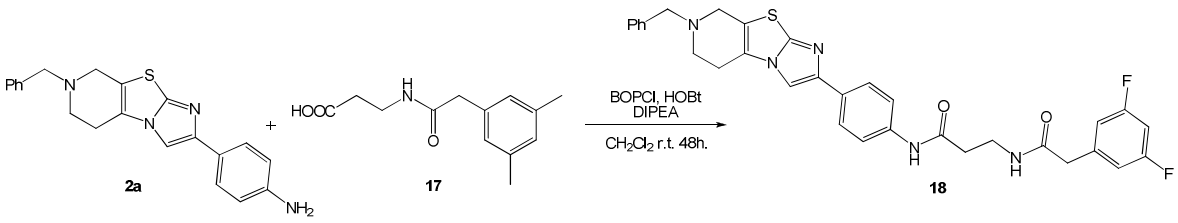

18 was prepared from **2a** (0.15 g, 0.42 mmol) and **17** (0.11 g, 0.44 mmol) using general procedure **F**. The crude mixture was purified by flash chromatography (DCM:MeOH 99:1) to afford **18** as a white solid (0.17 g, Yield 70 %).

^{1}H NMR ($CDCl_3$ with drops of CD_3OD, 400 MHz): δ 9.48 (1H brs), 7.72 (2H, dt, *J* = 9.2, 1.6 Hz), 7.58 (1H, s), 7.55 (1H, dt, *J* = 9.2, 1.6 Hz), 7.30-7.38 (5H, m), 6.82 (1H, tt, *J* = 6.4, 2.4 Hz), 6.69 (1H, tt, *J* = 11.2, 2.4 Hz), 3.80 (2H, s), 3.64 (2H, s), 3.52 (2H, dd, *J* = 12.0; 6.4 Hz), 3.48 (2H, s), 3.03 (2H, t, *J* = 5.6 Hz), 2.83 (2H, t, *J* = 5.6 Hz), 2.57 (2H, t, *J* = 6.4 Hz).

^{13}C NMR ($CDCl_3$ with drops of CD_3OD, 100.6 MHz): δ 172.96, 170.27, 163.97 (d, *J* = 123.7 Hz), 161.52 (d, *J* = 132.8 Hz), 148.32, 145.90, 138.48 (t, *J* = 92.6 Hz), 137.13, 136.84, 129.61, 128.94, 128.32, 127.45, 124.58, 119.93, 118.92, 111.90 (d, *J* = 70.4 Hz), 111.72 (d, *J* = 69.4 Hz), 105.56, 102.21 (t, *J* = 253.0 Hz), 61.00, 50.06, 48.46, 42.41, 35.96, 33.74, 22.51.

HR-MS Anal. Calcd for $[C_{32}H_{29}F_2N_5O_2S+H]^+$ 586.2088; Found 586.2077.

(*S*)-*N*-[4-(6-Benzyl-5,6,7,8-tetrahydroimidazo[2',1':2,3]thiazolo[4,5-*c*]pyridin-2-yl)phenyl]-2-[2-(3,5-difluorophenyl)acetamido]acetamide - (**19**)

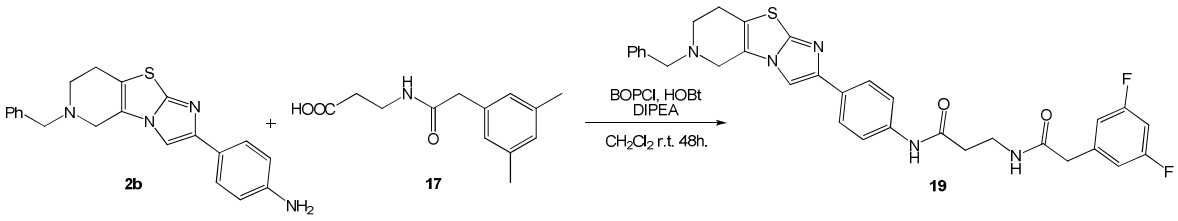

From **2b** and **17** using procedure **F** (pag. 111). Flash chromatography (DCM:MeOH 99:1) to give **19** (65 %).

^{1}H-NMR ($CDCl_3$ with drops of CD_3OD, 400 MHz): δ 9.40 (1H, s), 7.67 (1H, dt, *J* = 8.8, 1.6 Hz), 7.52 (1H, dt, *J* = 8.8, 1.6), 7.47 (1H, t, *J* = 5.6 Hz), 7.43 (1H, s), 7.30-7.41 (6H, m), 6.80 (2H, tt, *J* = 6.4, 2.4 Hz), 6.67 (1H, tt, *J* = 11.2, 2.4 Hz), 3.81 (2H, s), 3.59 (2H, s), 3.51 (2H, dt, *J* = 12.4, 6.4 Hz), 3.47 (2H, s), 2.96 (2H, t, *J* = 5.2 Hz), 2.83 (2H, t, *J* = 5.2 Hz), 2.55 (2H, t, *J* = 6.0 Hz).

^{13}C-NMR ($CDCl_3$ with drops of CD_3OD, 100.6 MHz): δ 170.84, 170.27, 164.05 (2C, d, *J* = 241.7 Hz), 148.68, 145.92, 138.47 (t, *J* = 11.2 Hz), 137.11, 136.98, 129.69, 128.89 (2C), 128.44, 127.52, 125.36, 124.11; 119.95 (2C), 119.89, 112.01 (2C, d, *J* = 24.3 Hz), 105.28, 102.35 (t, *J* = 25.6 Hz), 61.55, 50.04, 48.94, 42.61, 36.06, 35.92, 24.47.

HR-MS Anal. calcd for $[C_{32}H_{29}F_2N_5O_2S+H]^+$ 586.2088; Found 586.2075.

(*S*)-*N*-[4-(7-bromoimidazo[2,1-*b*]benzothiazol-2-yl)phenyl]-2-[2-(3,5-bis(trifluoromethyl) phenyl)acetamido]-3-phenylpropanamide - (**20** – CF203)

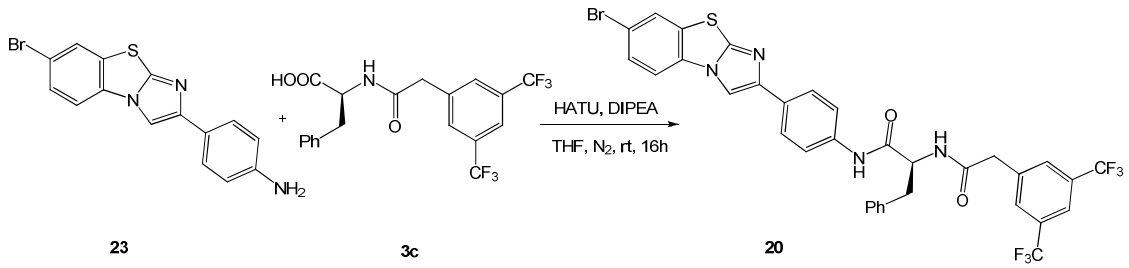

23 3c 20

Compound **3c** (0.201 g, 0.479 mmol) was dissolved in anhydrous THF (15 ml) under nitrogen and was added in order: HATU (0.199 g, 0.523 mmol) and DIPEA (152 µl, 0.872 mmol) and stirred for 15 min. at r.t. The mixture was added **23** (0.150 g, 0.436 mmol) and stirred at room temperature overnight. The solvent was removed under reduced pressure and the crude was purified by flash chromatography (Hex:AcOEt 1:1) and it was crystallized by CH_3CN (40 ml) to afford **20**. White solid (0.155 g, yield 48 %).

$[\alpha]^{20}_D$ = 2.95 (Na, *c* = 0.28 in DMSO)

^{1}H NMR (DMSO-d_6, 400 MHz): δ 10.26 (1H, s), 8.71 (1H, d, *J* = 8.7 Hz), 8.70 (1H, s), 8.34 (1H, d, *J* = 1.8 Hz), 7.95 (1H, s), 7.93 (1H, d, *J* = 8.5 Hz), 7.89 (2H, s), 7.81 (2H, d, *J* = 8.7 Hz), 7.75 (1H, dd, *J* = 8.5, 1.8 Hz), 7.66 (2H, d, *J* = 8.7 Hz), 7.27-7.13 (5H, m), 4.75-4.69 (1H, m), 3.75 (1H, d, *J* = 16.4 Hz), 3.70 (1H, d, *J* = 16.4 Hz), 3.10 (1H, dd, *J* = 13.8, 4.8 Hz), 2.89 (1H, dd, *J* = 13.8, 9.8 Hz).

^{13}C NMR (DMSO-d_6, 100.6 MHz): δ 170.48, 169.49, 147.42, 146.85, 140.10, 138.44, 137.86, 131.82, 131.59, 130.58 (2C, q, *J* = 37 Hz), 130.37 (2C), 129.99, 129.59, 129.50, 128.40 (2C), 127.86, 126.80 (2C), 125.60 (2C), 123.85 (2C, q, *J* = 272 Hz), 120.68, 120.11, 117.12, 115.29, 109.14, 55.42, 41.48, 38.30.

HR-EIMS Anal. Calcd for $[C_{34}H_{23}BrF_6N_4O_2S]^+$ 744.0629; Found 744.06134.

Synthesis of 6-Bromo-2-benzothiazolamines - (**21**)

Pharmaceutical Chemistry Journal Vol. 42, No. 4, 2008

21

A solution of 4-bromoaniline (0.500 g, 2.91 mmol) and potassium thiocyanate (1.13 g, 11.6 mmol) in AcOH (10 ml) was stirred at 20 °C for 10 min. Bromine (150 µl, 2.91 mmol) was added over 20 min. to the above solution. The reaction mixture was stirred further at room temperature for 90 min. On completion of reaction following a TLC examination, the reaction mixture was poured into a solution of NH_3 5M and extracted with AcOEt. The organic phase was dried over anhydrous Na_2SO_4 and the solvent was evaporated under vacuo. The crude product obtained was purified by flash chromatography (Hex:AcOEt 1:1) to afford **21** as white solid (2.67 g, yield 79 %).

^{1}H NMR (DMSO-d_6, 400 MHz): δ 7.91 (1H, d, *J* = 2.5 Hz), 7.63 (2H, s), 7.35 (1H, dd, *J* = 11.6, 2.5 Hz), 7.26 (1H, d, *J* = 11.6 Hz).

EIMS 228 $[M]^+$.

2-(4-Nitrophenyl)imidazo[2,1-*b*]-7-bromobenzothiazole - (**22**)

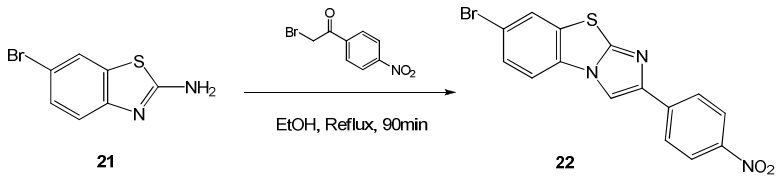

A mixture of **21** (1.20 g, 5.24 mmol) and 2-Bromo-4'-nitroacetophenone (1.41 g, 5.76 mmol) was reflux in ethanol for 90 min, the mixture was cooled to 0 °C. The solid was collected by filtration and washed with ethanol to afford **22** without any further purification. Yellow solid (0.665 g, yield 34 %).

^{1}H NMR (DMSO-d_6, 400 MHz) 80 °C: δ 8.92 (1H, s), 8.32 (1H, d, *J* = 1.9 Hz), 8.28 (2H, d, *J* = 8.8 Hz), 8.12 (2H, d. *J* = 8.8 Hz), 7.96 (1H, d, *J* = 8.6 Hz), 7.76 (1H, dd, *J* = 8.6, 1.9 Hz).

^{13}C NMR (DMSO-d_6 100.6 MHz) 80 °C: δ 155.67, 146.92, 145.02, 140.78, 132.15, 131.47, 130.15, 127.93, 125.93 (2C), 124.62 (2C), 117.76, 115.53, 112.47

EIMS 373 $[M]^{+}$.

2-(4-Aminophenyl)-7-bromoimidazo[2,1-*b*]benzothiazole - (**23**)

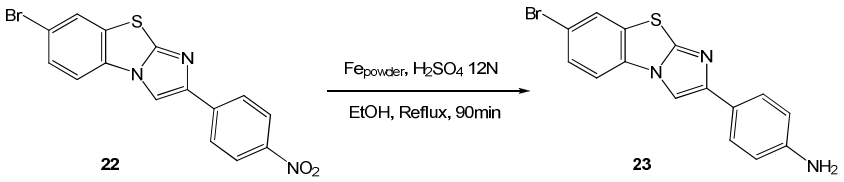

22 **23**

A mixture of **22** (0.225 mg, 0.602 mmol) in ethanol (25 ml), were added in the order: iron powder (0.671 g, 12.03 mmol), H_2SO_4 12N (5 ml). The mixture was refluxed for 30 min. and then it was extracted by satured solution of $NaHCO_3$ and AcOEt. The organic phase was dried with Na_2SO_4 anhydrous. The solvent was removed in vacuo. Compound **23** was obtained without any further purification. Light brown solid (0.191 g, yield 92 %).

^{1}H NMR (DMSO-d_6, 400 MHz): δ 8.46 (1H, s), 8.31 (1H, d, *J* = 1.9 Hz), 7.89 (1H, d, *J* = 8.6 Hz), 7.73 (1H, dd, *J* = 8.6, 1.9 Hz), 7.53 (2H, d, *J* = 8.5 Hz), 6.62 (2H, d, *J* = 8.5 Hz), 5.21 (2H, s).

^{13}C NMR (DMSO-d_6, 100.6 MHz): δ 149.41, 149.07, 147.41, 132.39, 132.35, 130.52, 128.41, 126.94 (2C), 122.78, 117.31, 115.67, 115.08 (2C), 107.58.

HR-EIMS Anal. Calcd for $[C_{15}H_{10}BrN_3S]^+$ 342.9779; Found 342.9784.

N-[1-(1-(4-(Imidazo[2,1-*b*]benzothiazol-2-yl)phenyl)-1*H*-1,2,3-triazol-4-yl)-2-phenylethyl]-2-[3,5-bis(trifluoromethyl)phenyl]acetamide - (**30** - CF120)

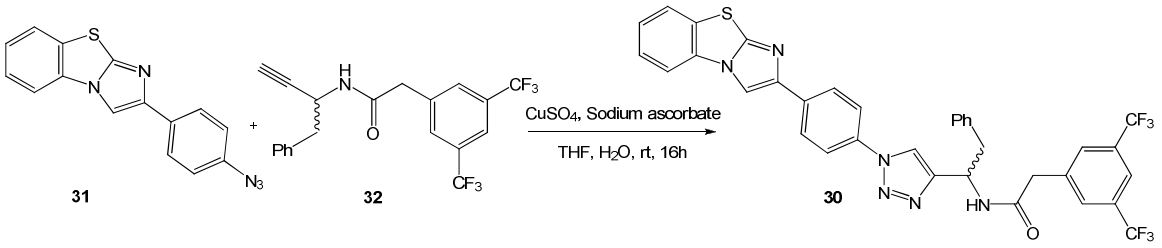

A solution of **31** (0.054 g, 0.188 mmol) and **32** (0.075 g, 0.188 mmol) in THF (6 ml) was added a solution of $CuSO_4 \cdot 5H_2O$ (0.001 g, 0.004 mmol) in H_2O (1.5 ml) and then a solution of sodium ascorbate (0.004 g, 0.019 mmol). The reaction was stirred at r.t. for 6 h and then the mixture was extracted with brine and AcOEt. The organic phase was dried over anhydrous Na_2SO_4 and the solvent was removed in vacuo. The crude was purified by flash chromatography (Hex:AcOEt 1:1) to afford **30** as white solid (0.090 g, yield 68 %)

^{1}H NMR (DMSO-d_6, 400 MHz): δ 8.92 (1H, s), 8.82 (1H, d, *J* = 8.6 Hz), 8.72 (1H, s), 8.08 (2H, d, *J* = 8.7 Hz), 8.04 (1H, d, *J* = 7.7 Hz), 8.00 (1H, d, *J* = 7.7 Hz), 7.97 (2H, d, *J* = 8.7 Hz), 7.96 (1, s), 7.87 (2H, s), 7.60 (1H, t, *J* = 8.4 Hz), 7.46 (1H, t, *J* = 8.4 Hz), 7.23-7.12 (5H, m), 5.33-5.27 (1H, m), 3.69 (2H, s), 3.29 (1H, dd, *J* = 13.7, 6.0 Hz), 3.13 (1H, dd, *J* = 13.7, 9.2 Hz).

^{13}C NMR (DMSO-d_6, 100.6 MHz): δ 169.38, 150.12, 146.26, 140.73, 139.10, 136.54, 135.26, 132.87, 131.41 (2C, q, *J* = 36 Hz), 131.03 (2C), 130.41, 130.24 (2C), 129.04 (2C), 127.90, 127.27, 127.01 (2C), 126.47, 126.19, 124.43 (2C, q, *J* = 274 Hz), 121.53, 121.39 (2C), 121.38, 114.52, 110.98, 47.98, 42.36, 41.38.

HR-EIMS Anal. Calcd for $[C_{35}H_{24}F_6N_6OS]^+$ 690.1637; Found 690.1629.

2-(4-azido)imidazo[2,1-*b*]benzothiazole - (**31**)

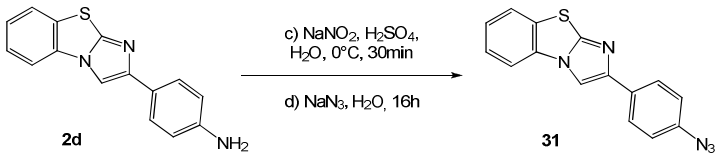

A solution of **2d** (0.300 g, 1.13 mmol) in H_2O (10 ml) and $H_2SO_{4conc.}$ (1.8 ml) was cooled to 0 °C with ice bath. A solution of $NaNO_2$ (0.117 g, 1.17 mmol) in H_2O (5 ml) was added dropwise in 5 min. The mixture was stirred to 0 °C for 30 min. and then a solution of NaN_3 (0.147 g, 2.26 mmol) in H_2O (5 ml) was added dropwise in 10 min. constantly at 0 °C. The mixture was warmed to rt and was stirred overnight. After complete conversion the pH was increased to pH 10 using a satured solution of $NaHCO_3$ and then TEA (2 ml). The crude material was extracted with CH_2Cl_2 and the organic phase was dried over anhydrous Na_2SO_4. The solvent was removed in vacuo and the crude mixture was purified by flash chromatography (Hex:AcOEt 3:1) to afford **31** as brown-orange solid (0.258 mg, yield 78 %).

^{1}H NMR (DMSO-d_6, 400 MHz): δ 8.75 (1H, s), 8.02 (1H, d, *J* = 8.0 Hz), 7.95 (1H, d, *J* = 8.0 Hz), 7.89 (2H, d, *J* = 8.6 Hz), 7.56 (1H, t, *J* = 7.5 Hz), 7.42 (1H, t, *J* = 7.5 Hz), 7.17 (2H, d, *J* = 8.6 Hz).

^{13}C NMR (DMSO-d_6 100.6 MHz): δ 148.10, 146.68, 139.09, 132.88, 132.11, 130.32, 127.78, 127.31 (2C), 126.26, 126.10, 120.60 (2C), 114.40, 110.10.

HR-EIMS Anal. Calcd for $[C_{15}H_9N_5S]^+$ 291.0579; Found 291.0573.

N-(1-phenylbut-3-yn-2-yl)-2-[3,5-bis(trifluoromethyl)phenyl]acetamide - (**32**)

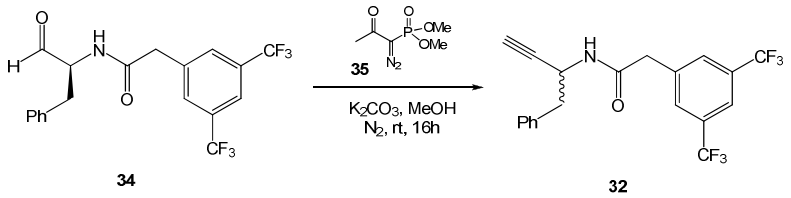

A solution of **34** (0.190 g, 0.471 mmol) in anhydrous MeOH (20 ml) was cooled to 0 °C and then were added in the order: K_2CO_3 (0.130 g, 0.942 mmol) and Bestmann Ohira Reagent **35** (0.109 g, 0.566 mmol). The reaction mixture was stirred at rt for 16 h, then the solvent was removed under reduced pressure and the crude solid was extracted by AcOEt and satured solution of $NaHCO_3$. The organic phase was washed with H_2O, it was dried over anhydrous Na_2SO_4 and the solvent was removed in vacuo. The solid was purified by flash chromatography (Hex:AcOEt 3:1) to afford **32** as white solid (0.159 mg, yield 84 %).

^{1}H NMR ($CDCl_3$, 400 MHz): δ 7.81 (1H, s), 7.72 (1H, s), 7.31-7.26 (3H, m), 7.20-7.18 (2H, m), 5.71 (1H, d, *J* = 8.0 Hz), 5.09-5.03 (1H, m), 3.63 (1H, d, *J* = 15.4 Hz), 3.57 (1H, d, *J* = 15.4 Hz), 3.01-2.99 (2H, m), 2.34 (1H, s).

^{13}C NMR (CDCl3, 100.6 MHz): δ 168.33, 137.47, 136.28, 132.67 (2C, q, *J* = 33 Hz), 130.27 (2C), 130.13 (2C), 129.02 (2C), 127.85, 123.83 (2C, q, *J* = 271 Hz), 121.99, 82.67, 73.34, 43.25, 43.11, 41.50.

EIMS 399 $[M]^+$.

(*S*)-*N*-(1-hydroxy-3-phenylpropan-2-yl)-2-[3,5-bis(trifluoromethyl)phenyl]acetamide - (**33**)

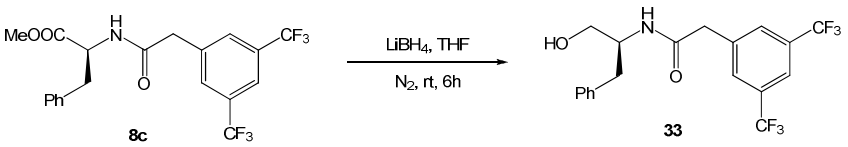

A solution of **8c** (0.800 mg, 1.85 mmol) in anhydrous THF (15 ml) was cooled to 0 °C under nitrogen and a second solution of $LiBH_4$ 2M in THF (288 µL, 0.577 mmol) was added dropwise in 15 min. The solution was stirred for 6 h at r.t. After the complete conversion of the ester into the alcohol the mixture was quenched in HCl 0.1M solution, extracted with AcOEt, and the organic phase was dried over anhydrous Na_2SO_4. The solvent was removed in vacuo and the crude mixture was purified by flash chromatography (CH_2Cl_2:MeOH 30:1) to afford **33** as white solid (0.692 mg, yield 92 %).

$[\alpha]^{20}_D$ = -21.02 (Na, *c* = 1.04 in MeOH)

^{1}H NMR (DMSO-d_6, 400 MHz): δ 8.09 NH (1H, d, *J* = 8.6 Hz), 7.95 (1H, s), 7.86 (2H, s), 7.18-7.09 (5H, m), 4.85 OH (1H, t, *J* = 5.5 Hz), 3.94-3.88 (1H, m), 3.64 (1H, d, *J* = 14.4 Hz), 3.60 (1H, d, *J* = 14.4 Hz), 3.43-3.32 (2H, m), 2.85 (1H, dd, *J* = 13.7, 5.2 Hz), 2.61 (1H, dd, *J* = 13.7, 8.9 Hz).

^{13}C NMR (DMSO-d_6 100.6 MHz): δ 168.89, 140.36, 139.41, 130.36 (2C, q, *J* = 33 Hz), 130.30 (2C), 129.46 (2C), 128.32 (2C), 126.27 (2C), 123.87 (2C, q, *J* = 271 Hz), 120.58, 63.20, 52.99, 41.88, 37.09.

HR-EIMS Anal. Calcd for $[C_{19}H_{17}F_6NO_2]^+$ 405.1163; Found 405.1156.

(*S*)-*N*-(1-oxo-3-phenylpropan-2-yl)-2-[3,5-bis(trifluoromethyl)phenyl]acetamide - (**34**)

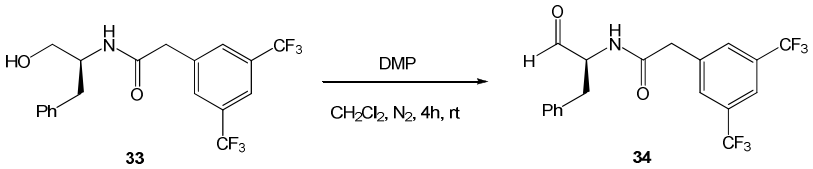

The alcohol **33** (0.400 g, 0.987 mmol) was dissolved in anhydrous CH_2Cl_2 (50 ml) under nitrogen. Solid DMP (0.502 mg, 1.18 mmol) was added to the solution and the mixture was stirred at r.t. After 4 h the reaction mixture was filtered over celite and the solution of CH_2Cl_2 was washed with a satured solution of $NaHCO_3$. The organic phase was dried over anhydrous Na_2SO_4 and the solvent was removed in vacuo. The crude solid was purified by flash chromatography (AcOEt:Hex 2:3) to afford **34** as white solid (0.315 g, yield 78 %).

$[\alpha]^{20}_D$ = +38.18 (Na, *c* = 0.57 in $CHCl_3$)

^{1}H NMR ($CDCl_3$, 400 MHz): δ 9.68 (1H, s), 7.84 (1H, s), 7.74 (2H, s), 7.29-7.24 (3H, m), 7.06-7.03 (2H, m), 6.05 (1H, s), 4.83-4.78 (1H, m), 3.71 (1H, d, *J* = 15.4 Hz), 3.66 (1H, d, *J* = 15.4 Hz), 3.23-3.15 (2H, m).

^{13}C NMR (CDCl3, 100.6 MHz): δ 198.02, 169.83, 136.71, 134.88, 131.87 (2C, q, *J* = 36 Hz), 129.53 (2C), 129.14 (2C), 128.83 (2C), 127.40 (2C), 123.48 (2C, q, *J* = 274 Hz), 121.41, 59.90, 42.54, 34.83.

HR-EIMS Anal. Calcd for $[C_{19}H_{15}F_6NO_2]^+$ 403.1007; Found 403.1012.

Dimethyl(1-diazo-2-oxopropyl)phosphonate - (**35**)

Eur. J. Org. Chem. **2003**, 821-832

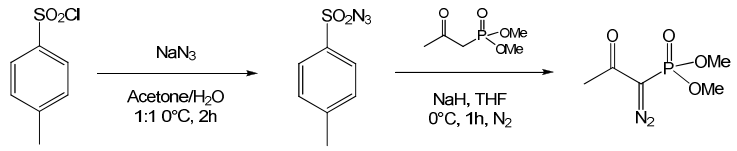

35

A solution of NaN_3 (0.341 g, 5.25 mmol) in acetone (15 ml) and H_2O (15 ml) was added TsCl (1.00 g, 5.25 mmol). The reaction mixture was stirred at 0 °C for 2 h. Acetone was evaporated, the reaction mixture was extracted with diethyl ether, and the organic phase was dried over Na_2SO_4. Evaporation of solvent gave tosyl azide (0.972 g, yield 94 %) as a colourless oil.

^{1}H NMR ($CDCl_3$, 300 MHz): δ 7.75 (2H, d, *J* = 8.1 Hz), 7.33 (2H, d, *J* = 8.1 Hz), 2.39 (3H, s).

A solution of NaH (80 % dispersion in mineral oil and washed with hexane, 0.150 g, 4.93 mmol) in anhydrous THF (20 ml) was cooled to 0 °C under nitrogen. Dimethyl(2-oxopropyl)phosphonate (0.744 g, 4.48 mmol) in anhydrous THF (10 ml) was added dropwise in 20 min. The solution was stirred at 0 °C for 30 min. A solution of Tosyl azide (0.972 g, 4.93 mmol) in anhydrous THF (10 ml) was then added in one portion and the resulting mixture was stirred at 0 °C for 10 min. The reaction mixture was quickly passed through a short column (silica, AcOEt) and the crude mixture was purified by flash chromatography (AcOEt) to give dimethyl(1-diazo-2-oxopropyl)phosphonate **35** (0.781 g, yield 91 %) as a colourless oil.

^{1}H NMR ($CDCl_3$, 300 MHz): δ 3.75 (3H, s), 3.71 (3H, s), 2.15 (3H, s).

^{13}C NMR ($CHCl_3$, 75 MHz): δ 189.7, 115.6, 53.6, 53.5, 27.1.

Chapter IV: Abl inhibitors

4.1 Abl inhibitors: Imatinib

For the treatment of CML is very important to develop molecules that can bind selectively the Bcr-Abl protein. Among them, Imatinib (Gleevec®), a 2-phenylamino pirimidine derivative, seemed to be a promising therapeutic agent. Imatinib mesilate (N-(4-methyl-3-(4-(pyridin-3-yl)-pyrimidin-2-ylamino) phenyl- 4- ((4-methyl-piperazin-1-yl) methyl) benzamide methanesulfonate) is a known inhibitor of tyrosine kinases targeted against platelet derived growth factor receptors (PDGFR), Bcr-Abl and c-Kit.[73] Overexpression of these tyrosine kinases can be detected in many types of cancer such as meningiomas, melanomas, and cancer of the ovary, prostate, pancreas, and breast. In particular our interest was focused to PDGFR for its relationship with angiogenesis, and Bcr-Abl for the treatment of chronic myeloid leukemia (CML)[74] and gastrointestinal stromal tumors (GISTs).[75] Imatinib was developed by Novartis Pharma AG, Basel, Switzerland and approved in November 2001 by FDA for the treatment of affected patients with CML. Imatinib targets in a selective way the inactive conformation of Abelson Tyrosine Kinase. Binding the protein, the drug is sandwiched between the N- and C-lobes of the kinase domain and penetrates through the central region of the kinase, from one side to the other (*Figure 1*).

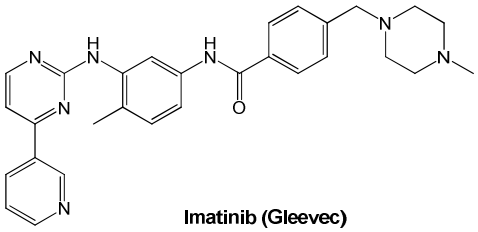

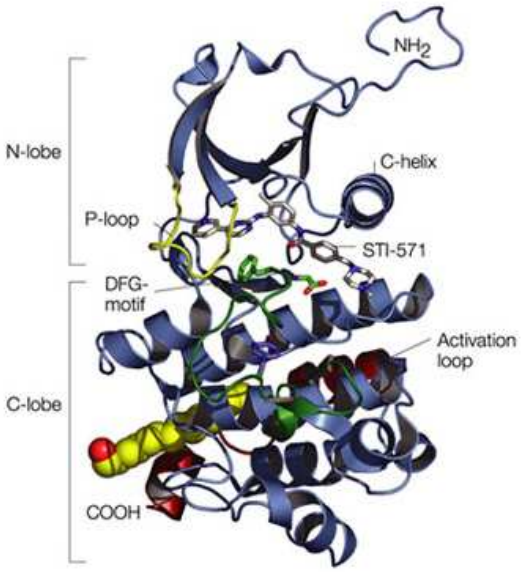

Figure 1: *Binding mode of Imatinib in Abl protein.*

Only the pyridine and pyrimidine rings occlude the region where the adenine ring of ATP normally binds. The rest of the compound penetrates into the hydrophobic core of the

[73] M.T. Weigel, I. Meinhold-Heerlein, D.O. Bauerschlag, C. Schem, M. Bauer, W. Jonat, N. Maass, C. Mundhenke, Combination of imatinib and vinorelbine enhances cell growth inhibition in breast cancer cells via PDGFR β signaling *Cancer Lett.* **2009**, *273*, 70–79.

[74] I.R. Radford, Imatinib Novartis, *Curr. Opin. Invest. Drugs*, **2002**, *3*, 492-499.

[75] R.L. Jones, I.R. Judson, The development and application of Imatinib, *Expert Opin. Drug Saf.*, **2005**, *4*, 183-191.

kinase and wedges itself between the activation loop and the helix αC, freezing the kinase in its inactive conformation and preventing transphosphorilation (*Figure 2*)

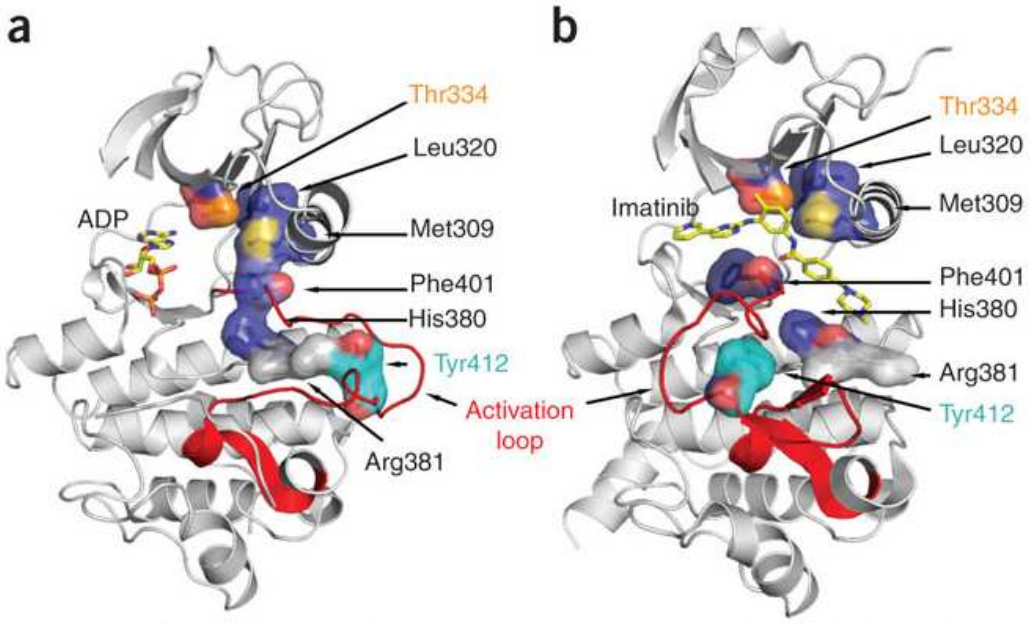

Figure 2: *(**A**) Assembled hydrophobic spine of the active Abl kinase (PDB 2G2I). (**B**) Dismantled hydrophobic spine of the inactive Abl kinase (PDB 1OPJ).*

In total, the compound makes six hydrogen bonds with the protein, and the majority of contacts are mediated by Van der Waals interactions (*Figure 3*).

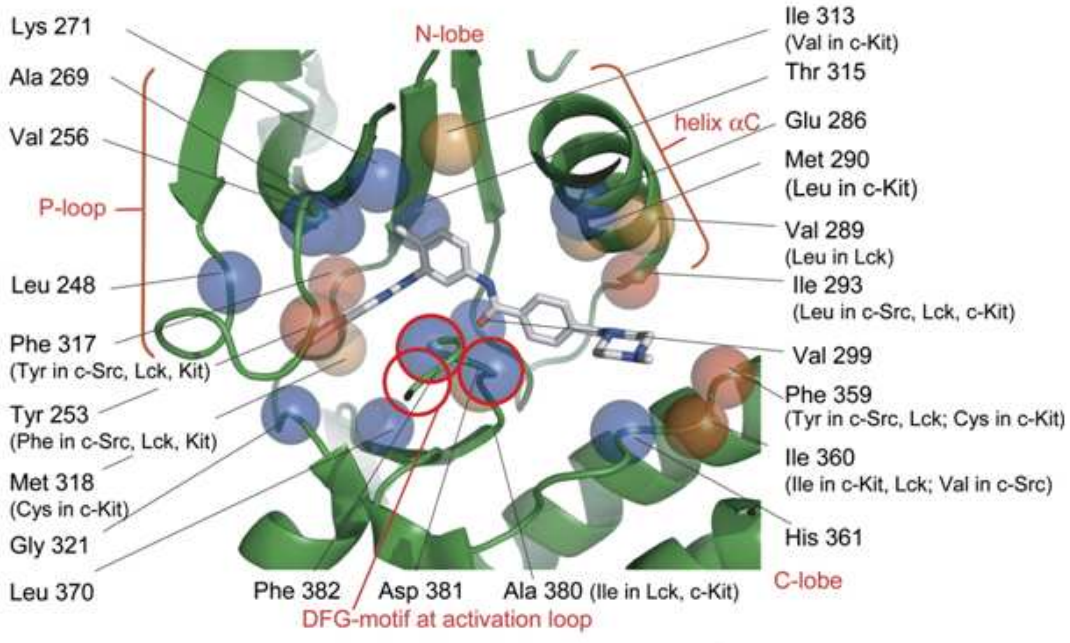

Figure 3: *The interactions between Abl protein and Imatinib.*

The adenine group of ATP normally makes two hydrogen bonds with the backbone atoms of the peptide chain connecting the N- and C-lobes of kinase domains. The extracyclic amino group of ATP donates a hydrogen bond to the carbonyl oxygen of the residue corresponding to Glu-316 in Abl, and nitrogen N1 of the purine ring accepts a hydrogen bond from the amide nitrogen of residue Met-318. Many small molecules which inhibit the protein kinases are anchored to the kinase domain by a pair of hydrogen bonds that mimic those which formed from adenine.

4.2 Synthesis of Imatinib

Imatinib was synthesized for the first time in 1993 by Zimmermann[76] and coworkers, following the synthetic pathway represented in *Scheme 1*. This method involves the use of the toxic cyanamide for the synthesis of phenyl-guanidine derivatives **1**. Furthermore, the enaminone **2** is obtained by a three-step synthesis, in one of which metallic sodium at low temperature is employed.

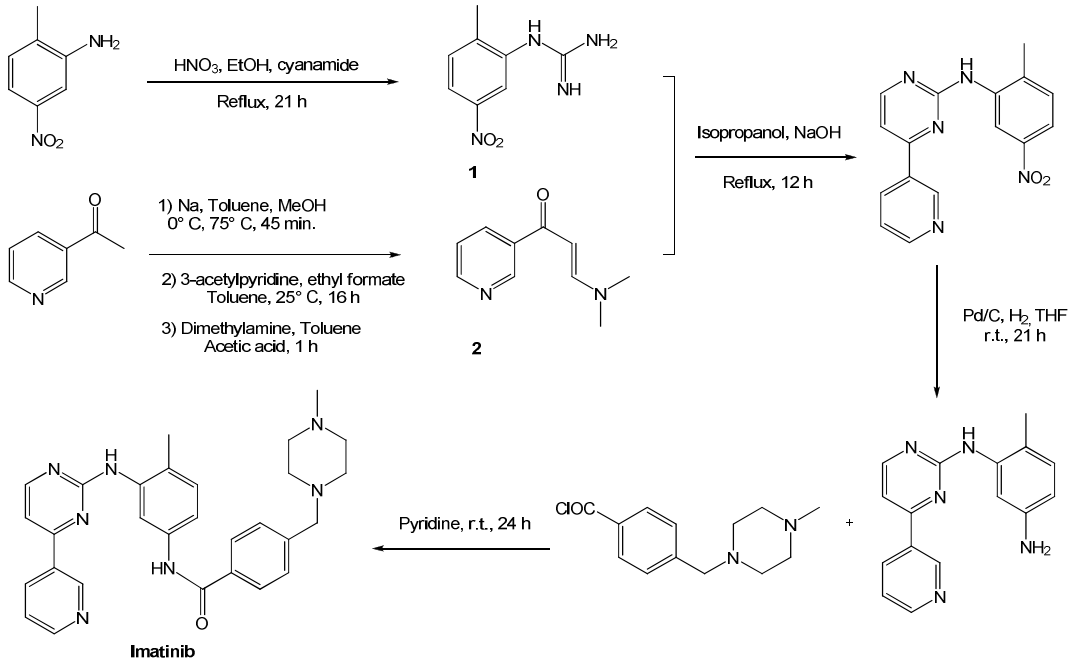

Scheme 1: *Zimmermann's synthesis of imatinib.*

[76] J. Zimmermann, E. Buchdunger, H. Mett, T. Meyer, N.B. Lydon, P. Traxler, Phenylamino-pyrimidine (PAP)-derivatives: a new classo of potent and highly selective PDGF-receptor autophosphorylation inhibitors *Bioorg. Med. Chem. Lett.* **1996**, *11*, 1221-1226.

Loiseleur[77] and coworkers described a process in which Imatinib is prepared by a reductive amination reaction of the methyl 4-formylbenzoate through a Pd/C catalyzed hydrogenation (*Scheme 2*).

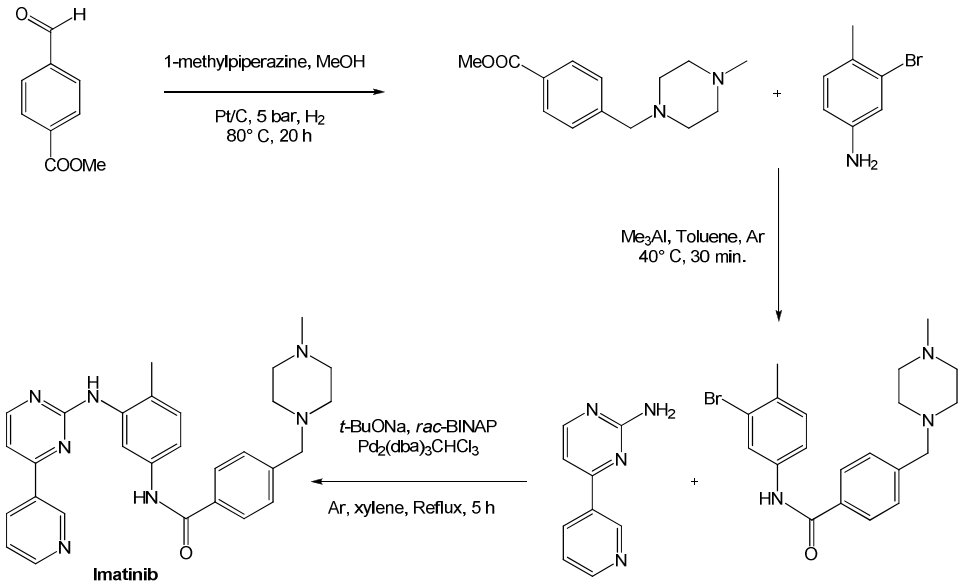

Scheme 2: *Loiseleur's synthesis of imatinib.*

A simplier and large-scale applicable pathway is described in *Scheme 3*[78] and includes the reaction of enaminone **3** with guanidine nitrate, which forms the corresponding pyrimidinyl amine, followed by the coupling reaction with *o*-bromo-*p*-nitro-toluene, using CuI as a catalyst and DMEDA as a ligand. This results in the formation of the key intermediate **5** that is reduced by $N_2H_4 \cdot H_2O/FeCl_3/C$ in an aqueous solvent.

[77] a) O. Loiseleur, D. Kaufmann, S. Abel, H.M. Buerger, M. Meisenbach, B. Schmitz, G. Sedelmeier, N-Phenyl-2-pyrimidine-amine derivatives *W. O. Patent 03/066613*, **2003**. b) Z. Szakacs, S. Beni, Z. Varga, L. Orfi, G. Keri, B. Noszal, Acid-Base profiling of Imatinib (Gleevec) and its fragments, *J. Med. Chem.* **2005**, *48*, 249-255.

[78] Y.F. Liu, Y.J. Bai, N. Han, J.P. Jiao, X.L. Gi, A facile total synthesis of Imatinib and its analogues *Org. Process res. Dev.* **2008**, *12*, 490-495.

Compound **6** is then condensed with 4-(chloromethyl)benzoyl chloride to provide compound **7**. Then, via an amination reaction using N-methyl piperazine, Imatinib is obtained.

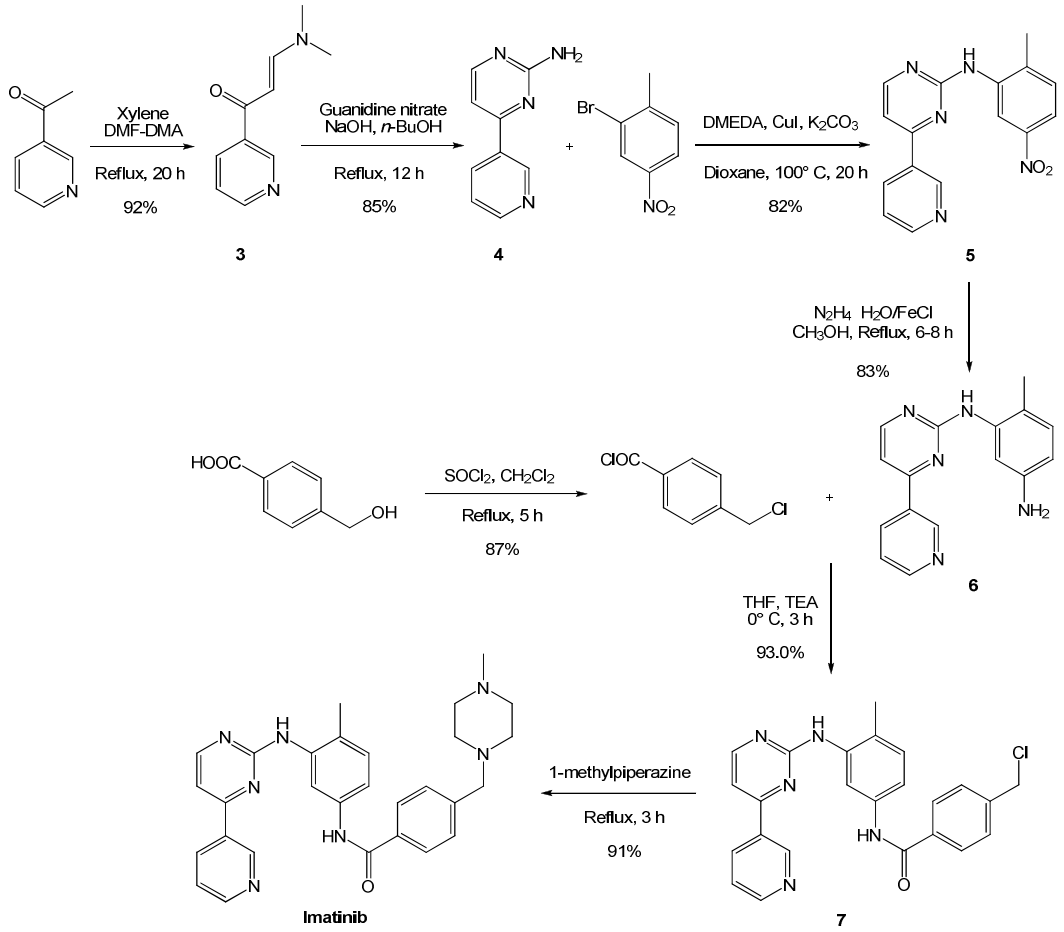

Scheme 3: *Liu synthesis of imatinib.*

N,*N*-Dimethylformamide dimethyl acetal (DMF-DMA) is very useful in organic synthesis as a formylating reagent. DMF-DMA is used in the synthesis of enaminones from active methylene compounds. Enaminones are useful intermediates in the formation and modification of many heterocyclic compounds. In general, enaminone formation is conducted in refluxing aromatic hydrocarbons. In this case, the enamination of acetylpyridine with DMF-DMA is conducted in xylene and provides enaminone **3** in 92.6 % yield. The following reaction with guanidine nitrate is processed in *n*-butanol for 10 h, to give pyrimidinyl amine **4** in 85.5 % yield. In contrast to Zimmermann's route, in this synthetic pathway cyanamide is not involved. In order to obtain formation of the C-N coupling product, in the beginning an Ullmann reaction was used, but with the formation of the desired product **5** only in 5 % of yield. In recent years, the "classic" Ullmann reaction has been transformed into an "Ullmann-type" reaction, in which the use of copper salts, a base, and a ligand allow the coupling reaction to go smoothly in mild

conditions. The optimal reaction conditions are the use of CuI as catalyst, *N,N*-dimethylethylenediamine as ligand, KI as accelerant, and K_2CO_3 as base, and the reaction is processed in dioxane at 100 °C for 20 h. Continuosly, the reduction of the nitro compound **5** can be achieved by several reagents in solution-phase reactions, but classical reactions with metals like Fe, Sn, Zn, or Al are complicated because of the difficult isolation of the product due to emulsions of metallic hydroxides. Fortunately, the reduction with hydrazine hydrate results in the formation of the desired amine **6** in 83% yield producing harmless byproducts such as nitrogen gas and water. The acylating reaction of compound **6** is proceeded in very good yield due to high activity of 4-(chloromethyl)benzoyl chloride. Finally, the mixture of intermediate **7** and 1-methylpiperazine was heated to reflux, maintained for 2 h and produced Imatinib base in 91% yield.

4.3 Synthesis of Imatinib 1,2,3-triazole-based analogues

Because of the enormous success in treatment of CML-affected patients, in the last few years it was observed an increase in the research about Imatinib. On the base of bioisosterism of peptide bond and the triazole ring, as showed before in chapter 3.6 , we performed the synthesis of a 1,2,3-triazole analogue **8** based on Imatinib scaffold (*Figure 4*).

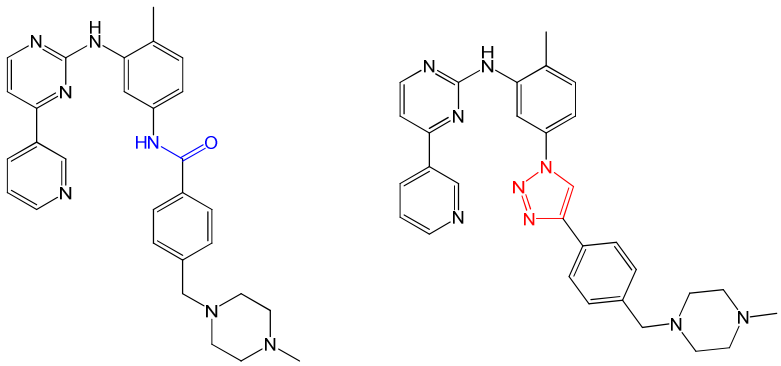

Figure 4: *Imatinib and its 1,2,3-triazole analogue* ***8****.*

The synthetic pathway we decided to follow is presented in *Scheme 4*. The synthesis proceeded with a convergent approach with a final key step based on a cycloaddition in Sharpless conditions (as show in paragraph 3.6.2) between azide **9** and alkyne **12** that lead only to the desired 1,2,3-triazole derivatives 1,4-disubstituited.

The first step is the synthesis of enaminone **3**, obtained from the reaction of 3-acetylpyridine with an excess (4 equivalents) of DMF-DMA in xylene at 140 °C. On the top of the flask, a soxhlet containg 4 Å molecular sieves has been put in order to catch MeOH molecules that are generated.

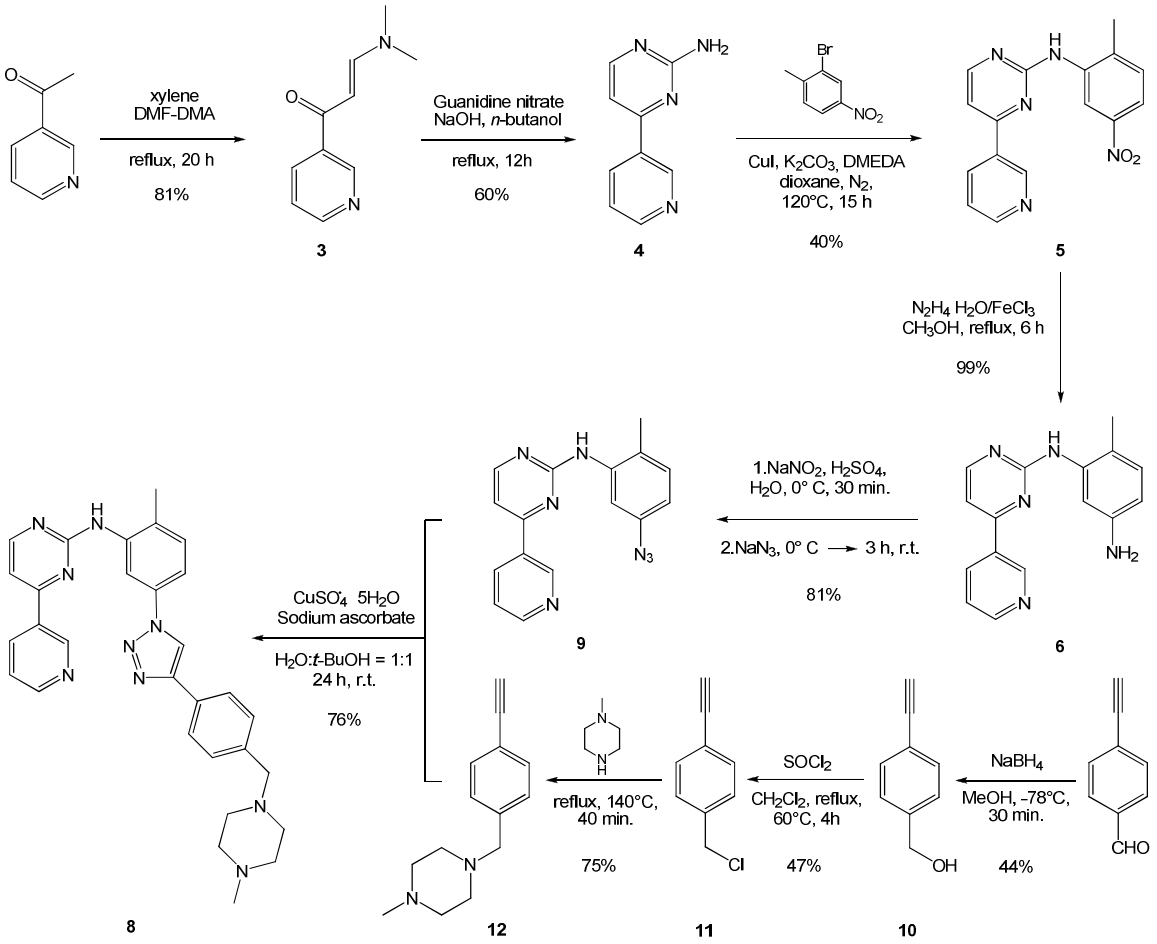

Scheme 4: *Synthesis of 1,2,3-thiazole* ***8****.*

After a simple filtration, enaminone **3** was obtained in 81 % yield. Then compound **3** reacted with guanidine nitrate and sodium hydroxide in *n*-butanol. After 4 hours the product, **4**, was collected by filtration in 60 % yield. The following step consists in an "Ullmann-type" coupling between compound **4** and *o*-bromo-*p*-nitrotoluene. This reaction was performed in N_2 atmosphere using CuI as a catalyst, DMEDA as a ligand and K_2CO_3 as a base in refluxing dioxane. After 15 hours the reaction was quenched with concentrated ammonia solution, then brine was added and extracted with AcOEt. The crude was purified by chromatographic column, and the nitro derivative **5** was obtained in 41 % yield. The reduction of the nitro group to the corresponding amine **6,** achieved via a system of hydrazine-monohydrate/$FeCl_3$/active carbon in MeOH and after 4 hours the

amine **6** was extracted in 95 % yield. Furthermore, amine **6** was converted in the corresponding azide. Firstly, diazonium salt was formed using $NaNO_2$, after 30 min. Then, a solution of NaN_3 in H_2O was added and the reaction mixture was stirred at room temperature for 3 h. The desired product, **9**, was produced in 81 % yield. Differently the synthesis of alkyne **12** proceeded starting from *p*-ethynyl benzaldehyde. This aldehyde was reducted to the corresponding benzyl alcohol **10** using $NaBH_4$ in MeOH at -78 °C in order to avoid the reduction of the alkyne moiety (we observed this collateral reaction doing the reduction at 0 °C). The crude was purified by chromatographic column leading to the desired product **10** in 44 % yield. Alcohol **10** was then converted in the chloride **11** in presence of an excess of $SOCl_2$ and after chromatographic purification **11** was collected in 47 % yield. The reaction of **11** with *N*-methylpiperazine led to alkyne **12** in 75 % yield after chromatographic purification. Finally, azide **9** alkyne **12**, through a cycloaddition reaction in Sharpless conditions lead only to the desired 1,2,3-triazole derivatives 1,4-disubstituited **8**. In order to give evidence that the 1,4 regioisomer was obtained, we recordered the ^{1}H-NMR NOESY spectrum (400 MHz, $CDCl_3$) as showed in *Figure 5*:

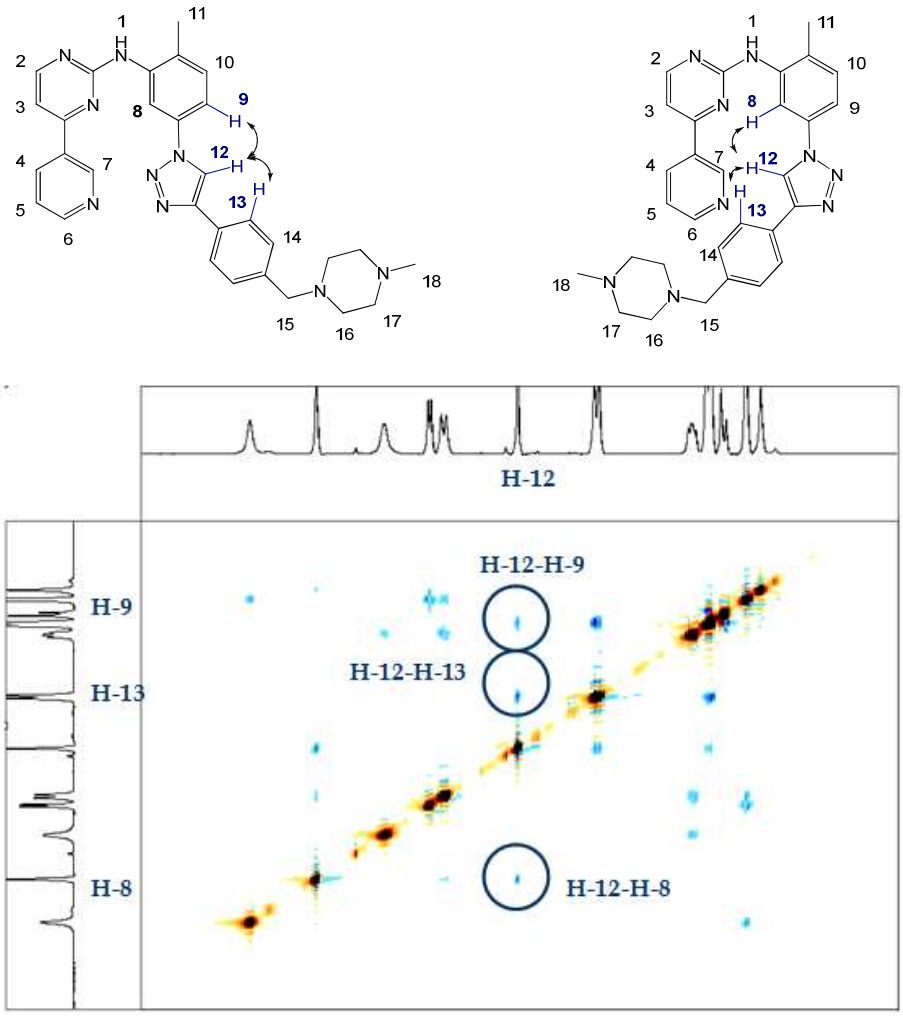

Figure 5: *^{1}H-NMR NOESY spectrum (400 MHz, $CDCl_3$) of compound **8**.*

The *H*-12, that in both the regioisomers shows a coupling with *H*-13, only in the 1,4-disubstituted triazole can show also a coupling with *H*-8 e *H*-9.

*4.4 Docking calculations on analogue **8***

In collaboration with Professor Maurizio Botta of the Università degli Studi di Siena docking calculations were carried out for analogue **8** on the inactive conformation of Abl. From these, it appeared that the binding mode of this analogue perfectly reflects the one of Imatinib and also the interactions are the same, making an exception for the hydrogen bond with E286, which is missing (*Figure 6*). Nevertheless, the interaction energy has a very similar value to that of Imatinib, which could mean also a similar activity.

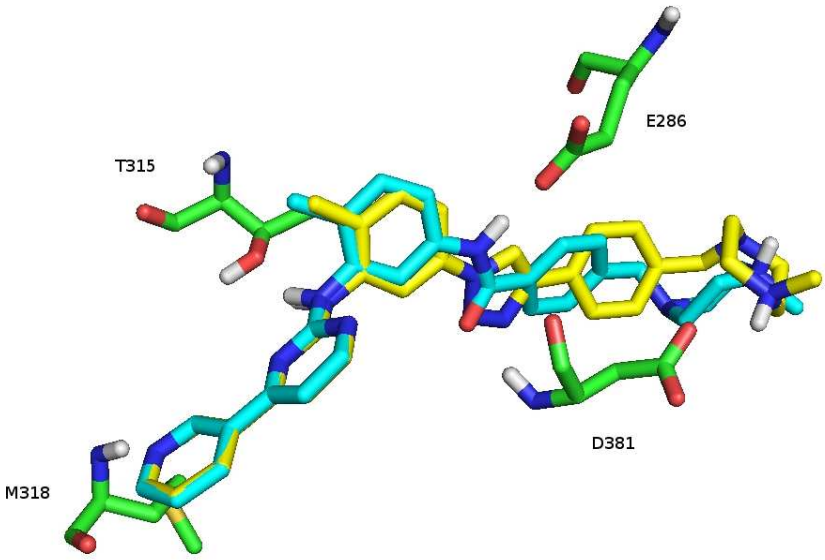

Figure 6: *Doking of Imatinib (light blue) and its 1,2,3-triazole analogue **8** (yellow) in Abl protein.*

*4.5 Synthesis of compound **8** analogues*

The good results of analogue **8** that brought to light, led us to go deeply in the studies of the interactions between these kind of compounds and abl protein. These supplementary modeling studies showed that the core of interactions reside in the central portion of the compound (*Figure 7 in red*). For this reason we studied the synthesis of analogues **13** in which pyridine ring is substituted with a phenyl ring and with the employment of different alkyne portions.

In addition the molecular modeling results showed that the two rings, pyridine end phenyl, are isosteric, but the presence of the nitrogen atom could be important for an optimal interaction with Abl (see *Figure 6*, M318), so this modification is certainly useful in order to make an exhaustive study about Imatinib binding site conformation.

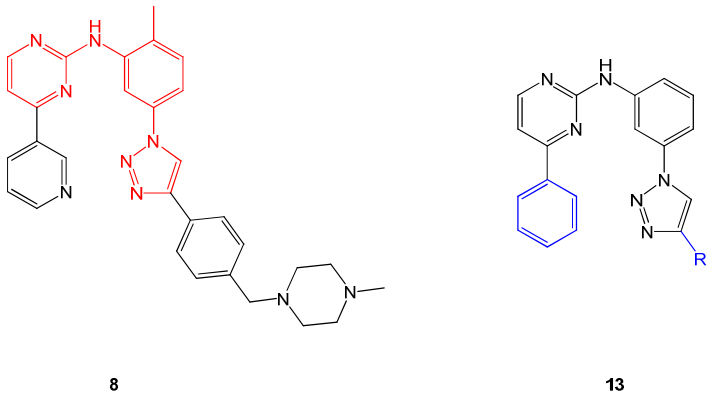

Figure 7: *Compound **8**) in red is highlighted the fundamental portion of the moleculefor the interaction with Abl. General structure **13**) It is the scaffold of new analogues of **8**. In blue are showed the portions replaced.*

All the compounds synthesized were obtained as the product of a cycloaddition reaction, in Sharpless conditions, between azide **18** and different alkynes. The portion of the molecule containing the azide moiety has remained unchanged in all the reactions and was synthesized following the synthetic pathway described in *Scheme 5*.

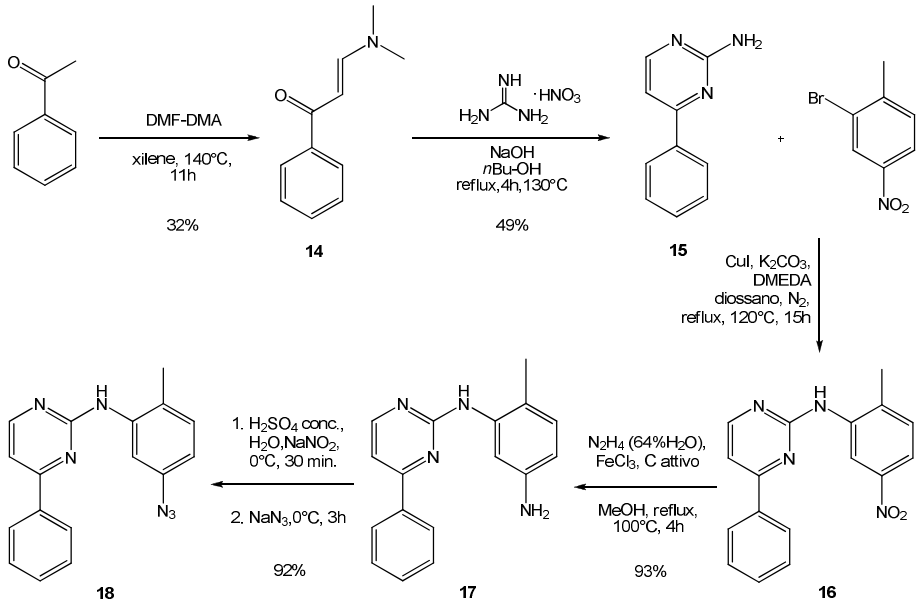

Scheme 5: *Synthesis of key intermediate **18**.*

The synthetic strategy is the same we used to prepare analogue **8** (see *Scheme 4*), except for the fact that, instead of starting from acetyl pyridine, in this case we started from acetophenone. In regard to alkyne moieties we employed five different compounds: three commercially available and two synthesized in our labs. Alkyne **19** was synthesized starting from 2,4-dichloro-benzaldehyde using Bestmann-Ohira reaction (see paragraph 3.6.5 for the discussion about Bestmann-Ohira).

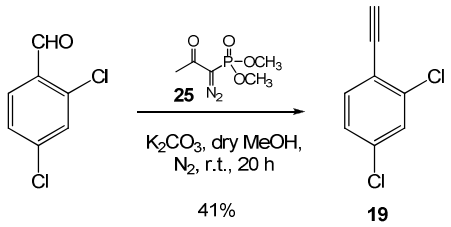

The cycloaddition reaction in Sharpless condition of azide **18** and alkyne **19** led to the isolation, after chromatographic column, of triazole **20** in 44 % yield:

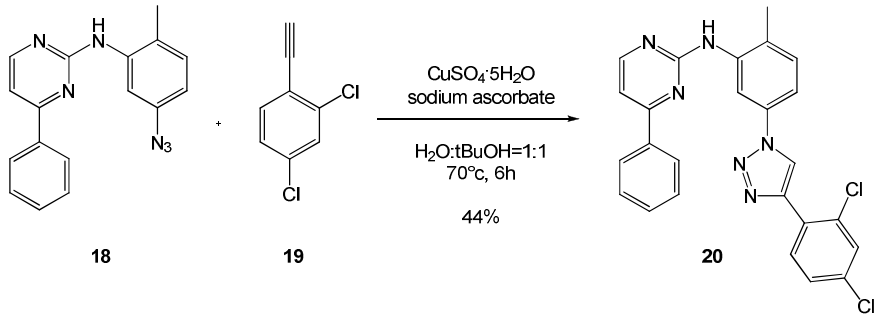

In addition using azide **18** and alkyne **12** we synthesized **21**, the corresponding compound of analogue **8** with the replacement of pyridine with phenyl moieties.

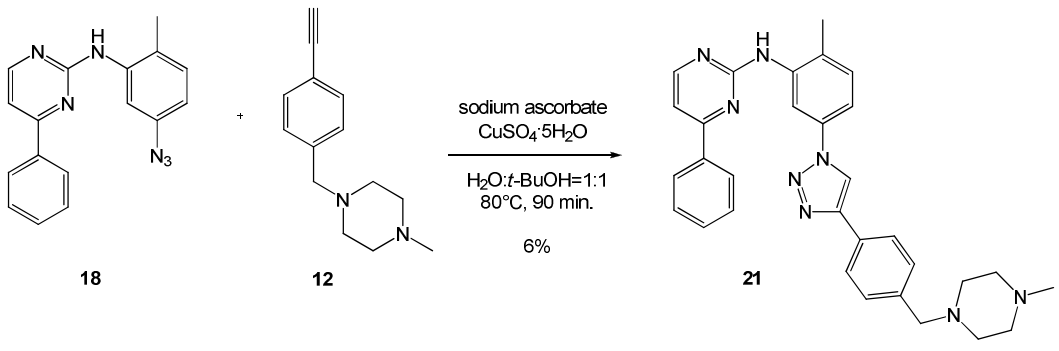

Three other cycloaddition reactions were performed of azide **18** employing three commercially available alkynes:

- *Methyl propiolate*: the reaction mixture was stirred at 50 °C for 5 h, then the crude was purified by chromatographic column and triazole **22** was collected in 41% yield:

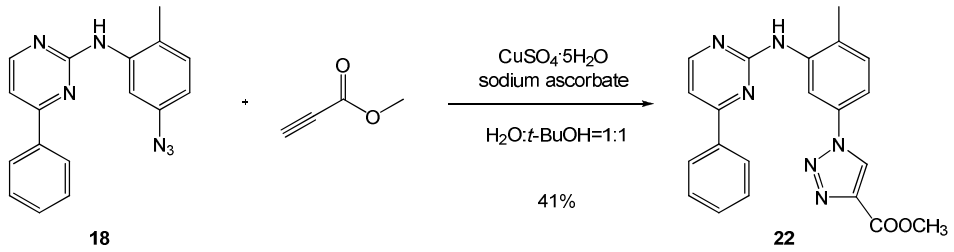

18 **22**

- *Dimethylamino propyne*: the reaction mixture was stirred at room temperature for 30 h. Then, after extraction, triazole **23** was obtained in 16% yield:

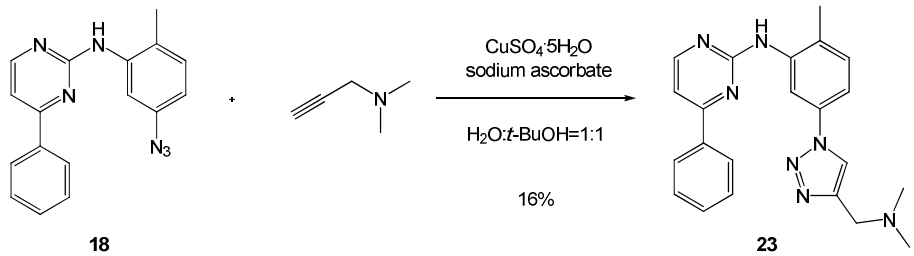

18 **23**

- *Phenyl acetylene*: the reaction was performed using a large excess of alkyne (12 equiv.). The reaction mixture was stirred at room temperature for 28 h and after chromatographic purification compound **24** was obtained in 19 % yield:

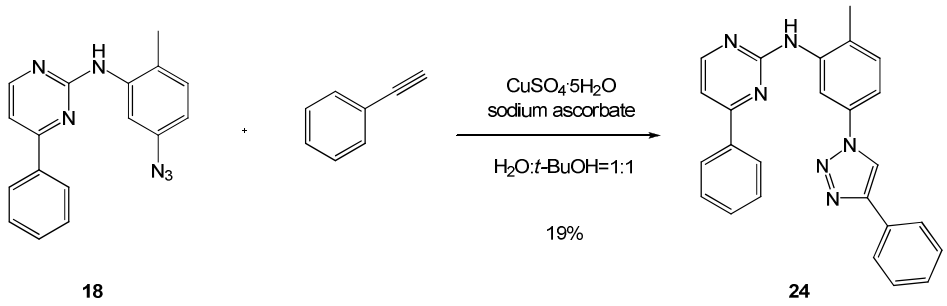

18 **24**

General summarizing scheme for the cycloaddition addition step in Sharpless conditions (in *Table 1* are summarized the conditions for each reaction):

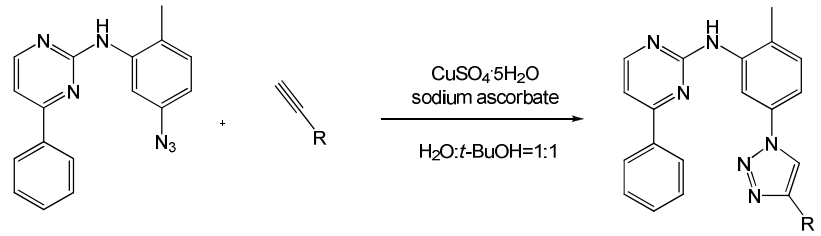

18 **20-24**

Compound	R	Temp. (°C)	Reaction time (h)	Yield %
20	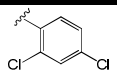	70	6	44
21	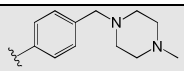	80	1,5	6
22		50	5	41
23		r.t.	30	16
24		r.t.	28	19

Table 1: *Summary of different experimental datas employed in cycloaddition in Sharpless conditions.*

The values of yield are very far from what we could expected for such click reactions. This might be due to the structural complexity of the azide **13** and also to electronic factors depending on the substituents of the alkynes: in fact, it is known that alkynes substituted with electron withdrawing groups are the most reactive in this kind of reactions. Anyway, in the most cases the 1,2,3-triazoles were isolated without the necessity of a chromatographic purification.

4.6 Biological tests

To assess the potency of our compounds, their effects on three Bcr-Abl-positive leukemia cell lines (K-562, MEG-01, KU-812) were evaluated in proliferation assays, in comparison to Imatinib (Gleevec®), which was used as the reference compound.

Inhibition of proliferation

The decrease in the viability of K-562, MEG-01 and KU-812 cells treated with the compounds for 72 hours was assessed using the Resazurin assay. Experiments performed to determine the *in vitro* effects of our compounds displayed a significant antiproliferative activity of compound **8**. In fact, activity data were in the low micromolar range (*Table 2*). No similar good biological activity was found among the other compounds (**20-24**), that were tested only on K-562 cells. For biological profile in terms of activity toward cell lines, compound **8** was selected and submitted to further assays.

Compound	K-562	MEG-01	KU-812
8	0,89 ± 0,003	10,97 ± 0,46	25,42 ± 1,24
20	> 150	ND	ND
21	54,38 ± 2,08	ND	ND
22	> 100	ND	ND
23	24,4 ± 0,28	ND	ND
24	> 100	ND	ND

Table 2: *IC_{50} anti-proliferative values (μM) on K-562, MEG-01, KU-812 cell lines. ND = Not determined. IC_{50} values are means ± SEM of series separate assays, each performed in triplicate.*

Inhibition of Bcr-Abl phosphorylation

With the aim of better understanding the antiproliferative activity of the new compound **8** (FAO30) toward leukemia cells, we decided to check in each cell line a direct link between the antiproliferative effects of **8** and the inhibition of Bcr-Abl activity. As showed in *Figure 8*, after 3 hours we observed a significant reduction in the phosphorylation of all targets in the presence of **8** when compare to control. The dose dependent inhibition of **8** is comparable to Imatinib (Gleevec®) effect.

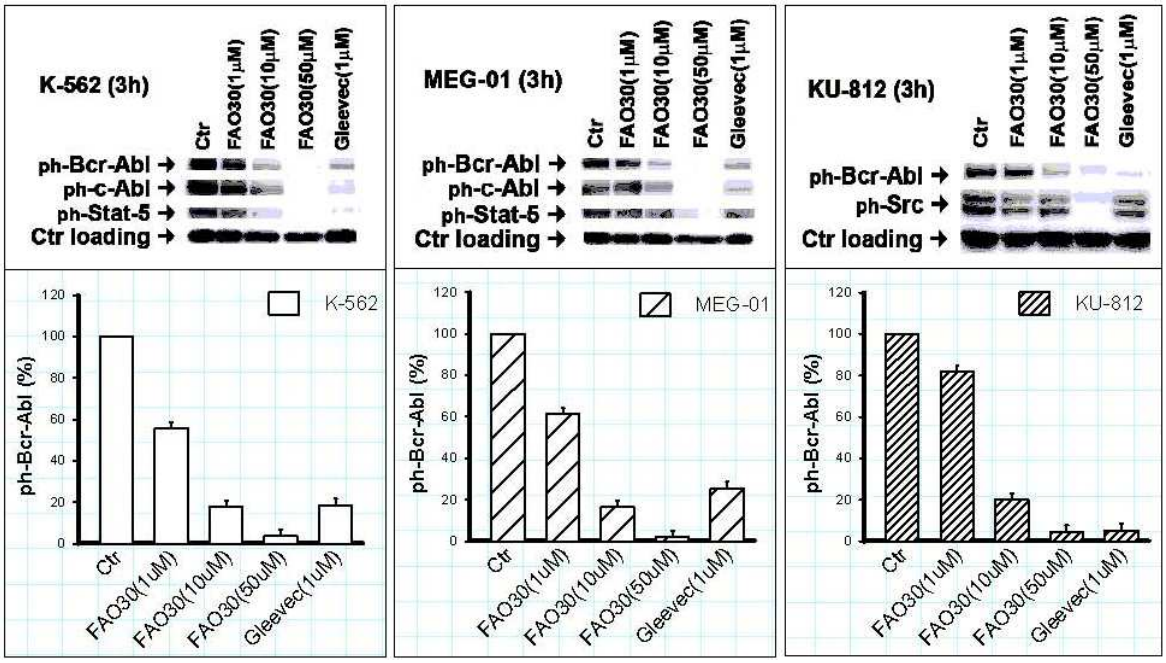

Figure 8: *Compound **8** (FAO30), used at different concentration, reduces phosphorylation of Bcr-Abl in K-562, MEG-01 and in KU-812 incubated for 3 hours, in comparison to Gleevec® used as reference compound. Quantification was achieved by chemiluminescence and results represented as the percent of the phospho protein.*

Inhibition of cdc25A expression

Cell division cycle 25 (cdc25) phosphatases are key regulators of the cell cycle and its checkpoints. They are required to dephosphorylate and thus activate the Cdk-cyclin complexes that trigger progression through the various cell-cycle phases. Cdc25A is required for progression from G1 to the S phase and G2/M in cell cycle and have been showed to be overexpressed in a number of cancer cells.[79] For this reason, we examined the action of compound **8** (FAO30) on cdc25A expression. *Figure 9* shows that **8** significantly inhibited cdc25A mRNA level after 3 hours in K-562 cells and this inhibition was increased after 24 hours exposition in K-562 (*Figure 9 A*). A similar inhibitory effect at 24 hours exposition was also observed in MEG-01 cells (*Figure 9 B*). Of notice, **8** result more active at 24 hours than Imatinib in the inhibitory effect on both cell lines.

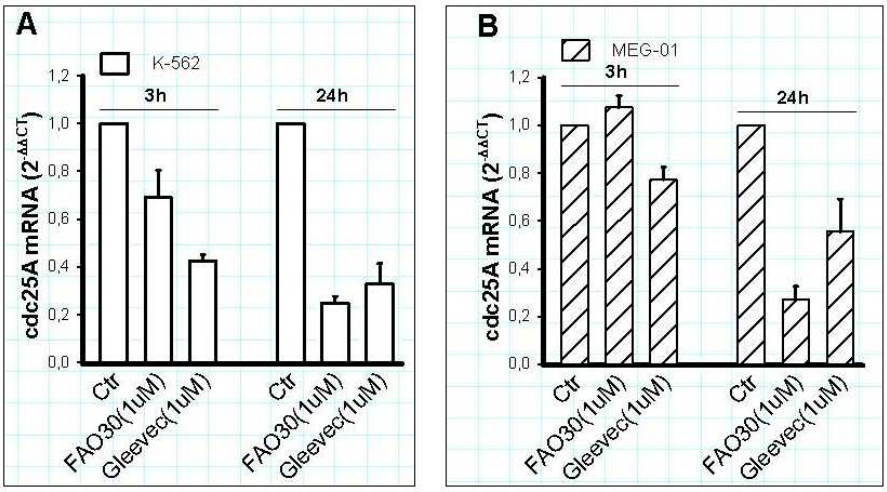

Figure 9: *Compound **8** (FAO30) inhibits cdc25A expression at 3 and 24 hours in K-562 (**A**) and in MEG-01 (**B**), in comparison to Gleevec® (Imatinib) used as reference compound. Both compounds were used at the concentration of 1µM. The results were obtained by qRT-PCR analysis.*

[79] K. Kristjansdottir, J. Rudolph, Cdc25 Phosphatases and cancer, *Chem. Biol.* **2004**, *11*, 1043-1051.

4.7 Conclusion

A convenient and versatile synthesis of a new collection of potential Bcr-Abl TK inhibitors based on a *N*-[2-methyl-5-(triazol-1-yl)phenyl]pyrimidin-2-amine scaffold was realized using Imatinib (Gleevec®) as inspiring compound.

Biological evaluation confirmed the importance of the pyridine ring in the interaction of the compounds with the target. This is due to a hydrogen bond between the molecule and the M318 residue of the protein that is possible only if the pyridine ring is present.

The evaluation demonstrated that compound **8** (FAO30) is able to inhibit the proliferation of three Bcr-Abl-positive leukemia cell lines (IC_{50} = 0.89 µM ± 0.003).

The replacement of pyridine ring with phenyl resulted in the obtainment of unreactive compounds. We retain this information useful to confirm three-dimensional structure of the biological target.

4.8 Experimental details

4.8.1 Biology

Cell culture

Human Chronic Myeloid Leukemia (CML) K-562 cells in blast crisis[80], human CML MEG-01 cell line in megakaryocytic blast crisis[81], and human CML KU-812[82] cell line in myeloid blast crisis were obtained from the American Type Culture Collection and were grown in RPMI 1640 medium (Euroclone, Devon, UK) containing 10% fetal bovine serum (FBS) or 20% FBS for KU-812, and antibiotics (100 U/mL penicillin and 100 µg/mL streptomycin). The cultures were free of mycoplasma. The compounds were dissolved in DMSO and used at the indicated concentrations, same amount of DMSO was used for the control.

Resazurin assay

The Resazurin assay (Acros Organics, Geel, Belgium) was used to determinate cell proliferation[83]. Starved cells ($1x10^4$cells/well) were plated in 96 well plate in RPMI containing FBS, with or without different concentrations (0,05-150 µM) of the studied compounds. Resazurin was dissolved in sterile water and added to the wells, 6 hours before the term of 72 hours incubation, in amounts equal to 5% volume and at a concentration of 320 µM. The resazurin reduction was determined by measuring the fluorescence at 530 nm (excitation) and 590 nm (emission) wavelengths using FLUOstar Optima (BMG Labtech, Offenburg, Germany). Data analysis for IC_{50} calculations was performed with the L5W Data Analysis Package plug-in for Excel (Microsoft). Results are reported as mean ± SEM.

Western blot analysis

The inhibitory effect of compounds toward the phosphorylation of Bcr-Abl (Tyr245) and STAT-5 (Tyr694) was tested using a PathScan Multiplex Western Detection Kit (Cell Signaling Technology, Beverly, MA). This Kit was used to assay the inhibition of multiple proteins on membrane without stripping and reprobing.

---

[80] D. Hudig, M. Djobadze, D. Redelman, J. Mendelsohn, Active tumor cell resistance to human natural killer lymphocyte attack. *Cancer Res*. **1981**, *41*, 2803-2808.

[81] M. Ogura, Y. Morishima, R. Ohno, Y. Kato, N. Hirabayashi, H. Nagura, H. Saito, Establishment of a novel human megakaryoblastic leukemia cell line, MEG-01, with positive Philadelphia chromosome. *Blood* **1985** *66*, 1384-1392.

[82] K. Kishi, A new leukemia cell line with Philadelphia chromosome characterized as basophil precursors, *Leuk. Res*. **1985**, *9*, 381-390.

[83] M.K. McMillian, L. Li, J.B. Parker, L. Patel, Z. Zhong, J.W. Gunnett, W.J. Powers, M.D. Johnson, An improved resazurin-based cytotoxicity assay for hepatic cells. *Cell Biol. Toxicol* **2002**, *18*, 157-173.

The inhibitory effect toward the phosphorilation of Src (Tyr416) was assessed using specific antibody (Cell signaling Technology). Cells were cultured at a concentration of $1x10^6$cells/well and challenged with the compound (FAO30 50µM, 10µM, 1µM and reference compound Gleevec 1µM). After 3 hours, cells were harvested and lysed in an appropriate buffer containing 1% Triton X-100. Filters were additionally reprobed with β-actin (control loading, Cell Signaling Technology). The proapoptic activity of the selected compounds was also tested, using immunoblot analysis with Poly-ADP-Ribose-Polymerase (PARP)-specific antibody that reveals both the uncleaved (113 kDa) and cleaved (89 kDa) forms of PARP (Cell Signaling Technology). Cell lines were cultured at a concentration of $14x10^5$cells/well and challenged with different concentrations of the studied compound or control compound for 72 hours. Proteins were quantitated by BCA method (Pierce, Rockford, IL). Equal amounts of total cellular protein were resolved by SDS-polyacrylamide gel electrophoresis, transferred to PVDF filters, and subjected to immunoblot. Non saturated, immunoreactive bands were detected with a CCD camera gel documentation system (ChemiDocXRS, Bio-Rad Laboratories, Hercules, CA) and than quantitated with Quantity One (Bio-Rad Laboratories).

4.8.2 Chemistry

General

All non-aqueous reactions were performed under inert atmosphere with dry, freshly distilled solvents using standard procedures. Drying of organic extracts during the work-up of reactions was performed over anhydrous Na_2SO_4 or $MgSO_4$. Evaporation of solvents was accomplished with a rotatory evaporator. Thin-layer chromatography (TLC) was performed on Merck precoated 60F254 plates. Reactions were monitored by TLC on silica gel, with detection by UV light (254 nm) or by charring with 1 % permanganate solution. Flash chromatography was performed using Silica gel (240–400 mesh, Merck). NMR spectra were recorded with Brucker 300 and 400 MHz spectrometers using chloroform-d ($CDCl_3$), dimethylsolfoxide-d_6 (DMSO-d_6) and methanol-d_4 (CD_3OD). Chemical shifts are reported in parts per million (δ) downfield from tetramethylsilane (TMS). EI mass spectra were recorded at an ionizing voltage of 6Kev on a VG 70-70 EQ. ESI mass spectra were recorded on FT-ICR APEXII (Bruker Daltonics). All reactions were carried out in dry solvents. Specific rotations were misured by a polarimeter “P-1030 Jasco” with 10 cm of Optical path cells and 1 ml of capacity. The mesures were done between 18 and 22 °C at 589 nm Wavelength (Na lamp). The melting point was determined by “Digital Melting Point IA9100 series - Electrothermal”.

(E)-3-(dimethylamino)-1-(pyridine-3-yl)prop-2-en-1-one - (**3**)

Org. Process Res. Dev. **2008**, *12*, 490-495.

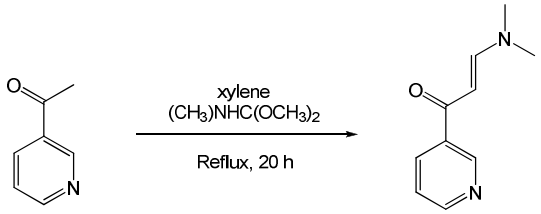

3

A solution of 3-acetyl-pyridine (6.06 g, 50 mmol) and N,N-dimethylformamide dimethylacetal (11.90 g, 100 mmol) in xylene (50 ml) was refluxed at 140 °C for 20 h. The solvent was removed *in vacuo* and hexane (200 ml) was added with consequent formation of yellow crystals. After complete crystallization, the product **3** was collected by filtration in 81 % yield. No further purification was needed.

^{1}H-NMR ($CDCl_3$, 300 MHz): δ 9.02 (1H, s), 8.61 (1H, dd, *J* = 5.3, 2.7 Hz), 8.15 (1H, dd, *J* = 8.0, 2.7 Hz), 7.80 (1H, d, *J* = 12 Hz), 7.31 (1H, dd, *J* = 8.0, 5.3 Hz), 5.67 (1H, d), 3.16 (3H, s), 2.94 (3H, s).

^{13}C-NMR ($CDCl_3$, 300 MHz): δ 186.30, 154.68, 151.38, 148.85, 135.62, 135.03, 123.25, 91.79, 45.18, 37.35.

4-(pyridine-3-yl)pyrimidin-2-amine - (**4**)

Org. Process Res. Dev. **2008**, *12*, 490-495.

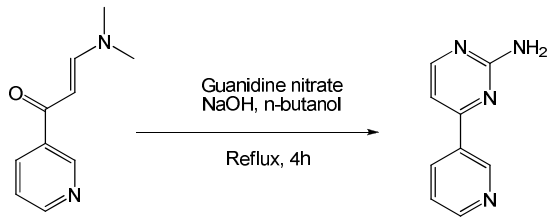

3 **4**

Guanidine nitrate (4.92 g, 40.3 mmol) and sodium hydroxide (1.25 g, 40.3 mmol) were added to a solution of Compound **3** (7.10 g, 40.3 mmol) in *n*-BuOH (45 ml). The reaction mixture was refluxed at 120 °C for 4 h, then cooled to room temperature. The precipitate was collected by filtration and washed with water (70 ml), then dried in the oven at 75-80 °C. No further purification was needed and the desired product **4** was obtained as white crystals in 60 % yield.

^{1}H-NMR ($CDCl_3$, 300 MHz): δ 9.21 (1H, d, *J* = 2.6 Hz), 8.63 (1H, d, *J* = 3.3 Hz), 8.47 (1H, dt, *J* = 8.3, 1.7 Hz), 8.33 (1H, d, *J* = 5.9 Hz), 7.55 (1H, dd, *J* = 8.3, 3.3 Hz), 7.19 (1H, d, *J* = 5.9 Hz), 4.86 (1H, s).

^{13}C-NMR ($CDCl_3$, 300 MHz): δ 160.4, 161.1, 154.4, 147.9, 147.5, 134.0, 133.0, 124.0, 103.3.

N-(2-methyl-5-nitrophenyl)-4-(pyridin-3-yl)pyrimidin-2-amine - (**5**)

Org. Process Res. Dev. **2008**, *12*, 490-495.

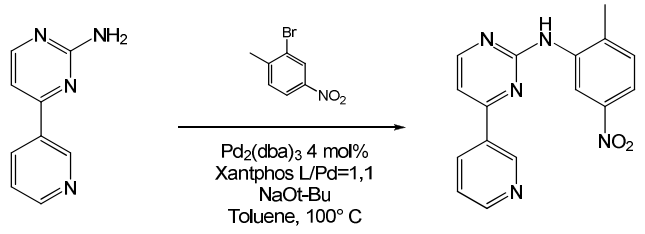

4 **5**

To a solution of Compound **4** (0.19 g, 1.1 mmol) in dry dioxane (5 ml) under nitrogen atmosphere, *o*-bromo-*p*-nitrotoluene (0.22 g, 1.0 mmol), CuI (0.05 g, 0.25 mmol), DMEDA (0.270 ml, 0.25 mmol), and K_2CO_3 (0.28 g, 2.0 mmol) were added and the reaction mixture was refluxed at 120 °C for 15 h, then cooled to room temperature. Concentrated ammonia (4 ml) and brine (20 ml) were added and extracted with ethyl acetate. The organic layers were dried over Na_2SO_4 and concentrated *in vacuo*. The crude was purified by column chromatography on silica gel (MeOH:CH_2Cl_2 1:80) to give the desired product **5** as yellowish powder in 40 % yield.

^{1}H-NMR ($CDCl_3$, 300 MHz): δ 9.47 (1H, d, *J* = 1.8 Hz), 9.28 (1H, bs), 8.76 (1H, d, *J* = 4.3 Hz), 8.59 (1H, d, *J* = 6.5 Hz), 7.87 (1H, dd, *J* = 7.2, 1.8 Hz), 7.54 (1H, dd, *J* = 7.2, 4.3 Hz), 7.38 (1H, s), 7.32 (1H, d, *J* = 6.5 Hz), 7.23 (1H, bs), 2.44 (3H, s).

^{13}C-NMR ($CDCl_3$, 400 MHz): δ 159.32, 158.76, 147.19, 146.94, 144.44, 139.02, 137.65, 134.58, 132.09, 131.03, 125.68, 118.14, 115.48, 109.03, 29.71, 18.42.

6-Methyl-*N*-(4-(pyridine-3-yl)pyrimidin-2-yl)benzene-1,3-diamine - (**6**)

Org. Process Res. Dev. **2008**, *12*, 490-495.

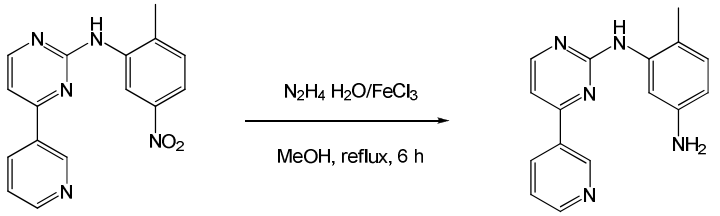

5 **6**

To a solution of compound **5** (0.300 g, 0.98 mmol) in MeOH (10 ml) hydrazine monohydrate (0.223 ml, 3.91 mmol), $FeCl_3$ (0.003 g, 0.02 mmol) and active carbon (0.001 g) were added and the reaction mixture was refluxed at 80 °C for 6 h. The solvent was removed *in vacuo*, water (30 ml) was added and extracted with CH_2Cl_2 (3x10 ml). The organic layers were dried over Na_2SO_4 and concentrated *in vacuo*. No further purification was needed and the desired product **6** was collected as yellow powder in 99% yield.

^{1}H-NMR (DMSO-d_6, 300 MHz): δ 9.22 (1H, s), 8.67 (1H, d, *J* = 4.4 Hz), 8.63 (1H, s), 8.44 (1H, d, *J* = 5.1 Hz), 8.39 (1H, d, *J* = 8.0 Hz), 7.51 (1H, dd, *J* = 7.9, 4.4 Hz), 6.85 (1H, d, *J* = 8.0 Hz), 6.77 (1H, d, *J* = 1.4 Hz), 6.32 (1H, dd, *J* = 8.0, 2.0 Hz), 4.80 (2H, s), 2.04 (3H, s).

^{13}C-NMR (DMSO-d_6, 300 MHz): δ 168.6, 161.1, 154.4, 147.9, 147.8, 147.5, 144.8, 134.0, 133.0, 130.6, 124.0, 119.0, 105.1, 103.3, 102.6, 17.6.

N-(2-methyl-5-(4-(4-((4-methylpiperazin-1-yl)methyl)phenyl)-1*H*-1,2,3-triazol-1-yl)phenyl)-4-(pyridine-3-yl)pyrimidin-2-amine - (**8**)

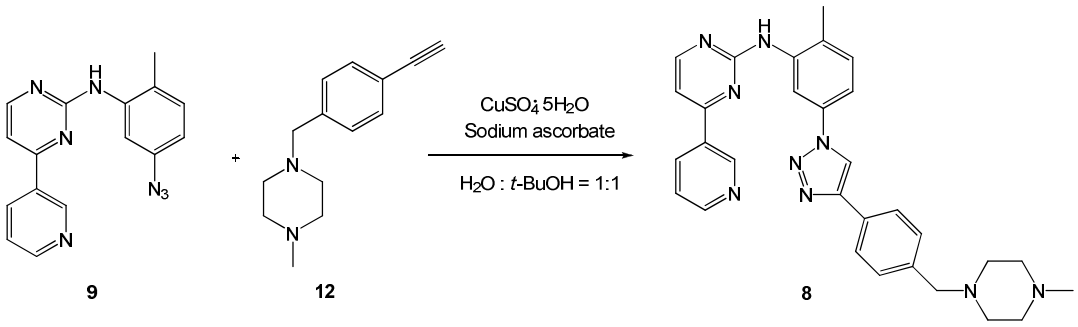

9 **12** **8**

To a solution of compound **9** (0.07 g, 0.23 mmol) and compound **12** (0.05 g, 0.23 mmol) in H_2O:*t*-BuOH 1:1 (5 ml) sodium ascorbate (0.004 g, 0.02 mmol) and copper(II)sulfate pentahydrate (0.001 g) were added and the reaction mixture was stirred at room temperature for 24 h. The reaction mixture was filtered and the solid was washed with water and dried in the oven at 80 °C. The crude was purified by column chromatography on silica gel (MeOH:CH_2Cl_2 1:10) and the desired product **8** was obtained as a yellow solid in 76 % yield.

^{1}H-NMR ($CDCl_3$, 400 MHz): δ 9.32 (1H, s), 9.05 (1H, s), 8.88 (1H, s), 8.58 (1H, d, *J* = 5.0 Hz), 9.39 (1H, d, *J* = 7.9 Hz), 8.22 (1H, s), 7.90 (2H, d, *J* = 7.8 Hz), 7.51 (1H, m), 7.44 (3H, d, *J* = 7.8 Hz), 7.38 (1H, d, *J* = 8.2 Hz), 7.29 (1H, d, *J* = 5.3 Hz), 3.60 (2H, s), 2.63 (8H, s), 2.42 (3H, s), 2.36 (3H, s).

^{13}C-NMR ($CDCl_3$, 400 MHz): δ 163.44, 160.94, 159.84, 152.41, 149.16, 148.80, 139.43, 138.94, 136.48, 135.32, 133.19, 131.94, 130.27 (2C), 130.08, 127.86, 126.49 (2C), 124.48, 118.07, 115.00, 113.14, 109.58, 63.22, 55.61 (2C), 53.22 (2C), 46.25, 18.34.

EIMS 517 $[M]^+$

N-(5-azido-2-methylphenyl)-4-(pyridine-3-yl)pyrimidin-2-amine - (**9**)

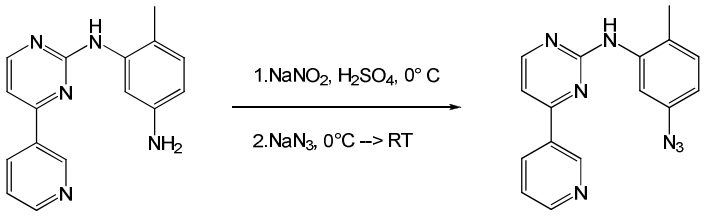

6 **9**

Compound **6** (0.29 g, 1.06 mmol) was suspended in water (15 ml) and was cooled to 0 °C, then concentrated H_2SO_4 was added until compound 19 was completely dissolved. A solution of sodium nitrite (0.11 g, 1.59 mmol) in water (2 ml) was added and the reaction mixture was stirred at 0 °C for 30 min. Then a solution of sodium azide (0.14 g, 2.12 mmol) in water (2 ml) was added at 0 °C and the reaction mixture was stirred at room temperature for 3 h. Potassium carbonate was added until pH 8 and the reaction mixture was extracted with CH_2Cl_2. The organic layers were dried over Na_2SO_4 and concentrated *in vacuo*. No further purification was needed and the desired product **9** were collected as orange crystals in 81 % yield.

^{1}H-NMR ($CDCl_3$, 300 MHz): δ 9.12 (1H, s), 8.79 (1H, d, *J* = 4.5 Hz), 8.62 (1H, d, *J* = 7.8 Hz), 8.54 (1H, d, *J* = 5.0 Hz), 8.06 (1H, s), 7.55-7.67 (2H, m), 7.27 (1H, s), 7.19 (1H, d, *J* = 8.1 Hz), 6.37 (1H, dd, *J* = 8.1, 2.3 Hz), 2.30 (3H, s).

^{13}C-NMR ($CDCl_3$, 400 MHz): δ 163.32, 160.99, 159.71, 152.20, 149.07, 139.38, 139.13, 135.25, 133.23, 132.03, 124.36, 114.29, 111.62, 109.28, 30.32, 18.13.

EIMS 303 $[M]^+$

(4-ethynylphenyl) methanol - (**10**)

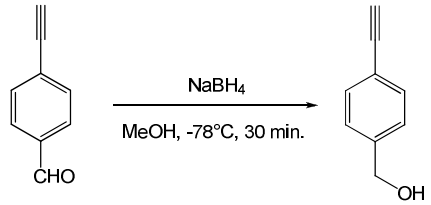

10

A solution of 4-ethynylbenzaldehyde (0.20 g, 1.5 mmol) in MeOH (10 ml) was cooled to -78 °C and sodium borohydride (0.02 g, 0.4 mmol) was added in little amounts. The reaction mixture was stirred at -78°C for 30 min and then warmed to room temperature. Hydrochloric acid 1N was added in order to quench sodium borohydride not reacted and the solvent was removed *in vacuo*. Water (50 ml) was added and extracted with ethyl acetate (3x15 ml). The organic layers were dried over Na_2SO_4 and concentrated *in vacuo*. The crude was purified by column chromatography on silica gel (AcOEt:Hex 3:7) and the desired product **10** were obtained as a white solid in 44 % yield.

^{1}H-NMR ($CDCl_3$, 300 MHz): δ 7.47 (2H, d, *J* = 8,4 Hz), 7.33 (2H, d, *J* = 8.4 Hz), 4.57 (2H, s), 3.09 (1H, s).

EIMS 132 $[M]^+$

1-(chloromethyl)-4-ethynylbenzene - (**11**)

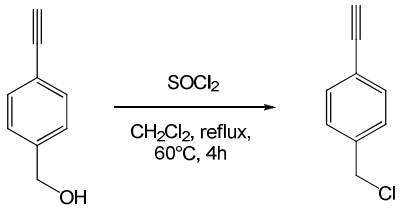

10 **11**

To a solution of compound **10** (0.09 g, 0.7 mmol) in CH_2Cl_2 (2 ml) thionyl chloride (2 ml) was added and the reaction mixture was refluxed at 60 °C for 4 h. Then the volatiles were removed *in vacuo* and the crude was purified by column chromatography on silica gel (Hex). The desired product **11** was obtained as a yellow oil in 47 % yield.

^{1}H-NMR ($CDCl_3$, 300 MHz): δ 7.42 (2H, d, *J* = 8.3 Hz), 7.26 (2H, d, *J* = 8.3Hz), 3.49 (2H, s), 3.04 (1H, s), 2.49 (8H, bs), 2.31 (3H, s).

EIMS 150 $[M]^+$

1-(4-ethynylbenzyl)-4-methylpiperazine - (**12**)

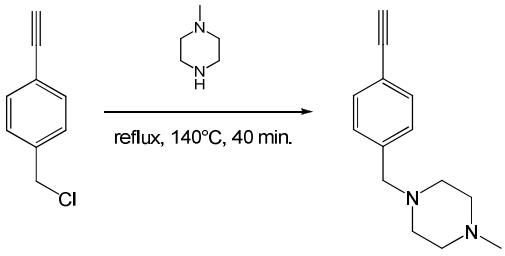

11 **12**

A solution of compound **11** (0.05 g, 0.3 mmol) and N-methylpiperazine was refluxed at 140 °C for 40 min. Water (30 ml) was added and extracted with CH_2Cl_2 (3x10 ml). The organic layers were dried over Na_2SO_4 and concentrated *in vacuo*. The crude was purified by column chromatography on silica gel (CH_2Cl_2:MeOH 20:1) and the desired product **12** was obtained as a colourless oil in 75 % yield.

^{1}H-NMR ($CDCl_3$, 300 MHz): δ 7.42 (2H, d, *J* = 8.3 Hz), 7.26 (2H, d, *J* = 8.3Hz), 3.49 (2H, s), 3.04 (1H, s), 2.49 (8H, bs), 2.31 (3H, s).

EIMS 214 $[M]^+$

(E)-3-(dimethylamino)-1-phenylprop-2-en-1-one - (**14**)

Org. Process Res. Dev. **2008**, *12*, 490-495.

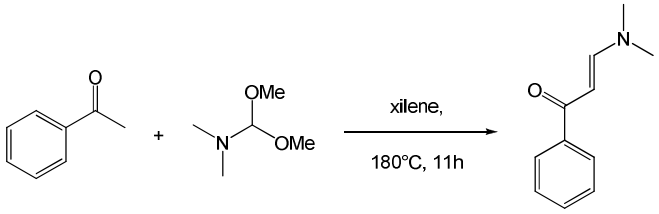

14

A solution of acetophenone (3.00 g, 25 mmol) and N,N-dimethylformamide dimethylacetal (11.90 g, 100 mmol) in xylene (50 ml) was refluxed at 180 °C for 11 h. The solvent was removed *in vacuo* and hexane (200 ml) was added with consequent formation of yellow crystals. After complete crystallization, the product was collected by filtration in 32 % yield. No further purification was needed.

^{1}H-NMR ($CDCl_3$, 300 MHz): δ 7.88 (2H, d, *J* = 6.3 Hz), 7.79 (1H, d, *J* = 12.4 Hz), 7.46-7.36 (3H, m), 3.14 (3H, bs), 2.92 (3H, bs).

4-phenylpyrimidin-2-amine - (**15**)

Org. Process Res. Dev. **2008**, *12*, 490-495.

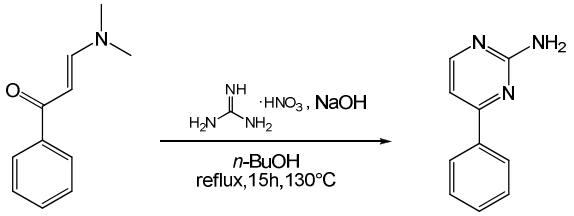

14 **15**

Guanidine nitrate (0.87 g, 7.1 mmol) and sodium hydroxide (0.22 g, 7.1 mmol) were added to a solution of compound **14** (1.26 g, 7.1 mmol) in *n*-BuOH (70 ml). The reaction mixture was refluxed at 130 °C for 15 h, then cooled to room temperature. The precipitate was collected by filtration, washed with water (70 ml) and dried in the oven at 75-80 °C. No further purification was needed and the desired product **15** was obtained as white crystals in 49 % yield.

^{1}H-NMR ($CDCl_3$, 300 MHz): δ 8.30 (1H, d, *J* = 5.6 Hz), 8.00-7.97 (2H, m), 7.48-7.46 (3H, m), 7.04 (1H, d, *J* = 5.6 Hz), 5.27 (2H, bs).

N-(2-methyl-5-nitrophenyl)-4-phenylpyrimidin-2-amine - (**16**)

Org. Process Res. Dev. **2008**, *12*, 490-495.

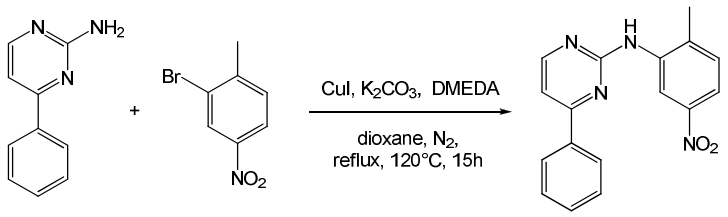

15 **16**

To a solution of compound **15** (0.89 g, 5.2 mmol) in dry dioxane (23 ml) under nitrogen atmosphere, *o*-Bromo-*p*-nitro toluene (1.02 g, 4.7 mmol), CuI (0.25 g, 1.3 mmol), DMEDA (0.14 ml, 1.3 mmol), and K_2CO_3 (1.44 g, 10.5 mmol) were added and the reaction mixture was refluxed at 120 °C for 15 h, then cooled to room temperature. Concentrated ammonia (12 ml) and brine (60 ml) were added and extracted with ethyl acetate. The organic layers were dried over Na_2SO_4 and concentrated *in vacuo*. The crude was purified by column chromatography on silica gel (AcOEt:Hex 1:1) to give the desired product **16** as yellowish powder in 31 % yield.

^{1}H-NMR (DMSO-d_6, 300 MHz): δ 9.16 (1H, s), 8.89 (1H, d, *J* = 2.6 Hz), 8.60 (1H, d, *J* = 5.0 Hz), 8.20-8.17 (2H, m), 7.92-7.89 (1H, m), 7.56-7.51 (5H, m), 4.46 (3H, s).

6-Methyl-*N*-(4-phenylpyrimidin-2-yl)benzene-1,3-diamine - (**17**)

Org. Process Res. Dev. **2008**, *12*, 490-495.

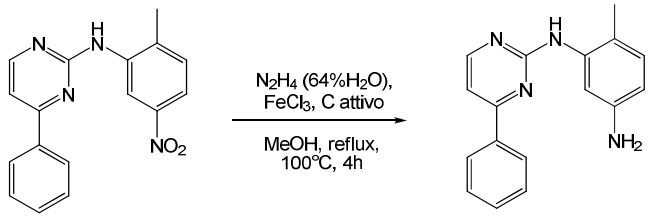

16 **17**

To a solution of compound **16** (0.49 g, 1.6 mmol) in MeOH (20 ml), hydrazine monohydrate (2.00 g, 25.6 mmol), $FeCl_3$ (0.005 g, 0.03 mmol) and active carbon (0.01 g) were added and the reaction mixture was refluxed at 100 °C for 4 h. The solvent was removed *in vacuo*, water (100 ml) was added and extracted with CH_2Cl_2 (3x30 ml). The organic layers were dried over Na_2SO_4 and concentrated *in vacuo*. No further purification was needed and the desired product **17** was collected as yellow powder in 93 % yield.

^{1}H-NMR ($CDCl_3$, 300 MHz): δ 8.41 (1H, d, *J* = 5.0 Hz), 8.06-8.02 (2H, m), 7.65 (1H, d, *J* = 2.3 Hz), 7.52-7.48 (3H, m), 7.41 (1H, bs), 7.14 (1H, d, *J* = 5.8 Hz), 7.00 (1H, d, *J* = 8.0 Hz), 6.46 (1H, dd, *J* = 7.9, 2.1 Hz), 4.0-3.1 (2H, bs), 2.26 (3H, s).

N-(5-azido-2-methylphenyl)-4-phenylpyrimidin-2-amine - (**18**)

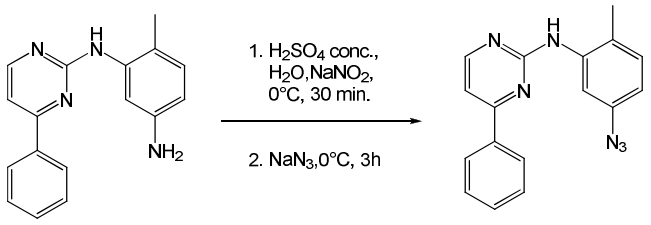

17 **18**

Compound **17** (0.41 g, 1.5 mmol) was suspended in water (70 ml) and cooled to 0 °C, then concentrated H_2SO_4 was added until compound **17** was completely dissolved. A solution of sodium nitrite (0.51 g, 2.2 mmol) in water (9 ml) was added and the reaction mixture was stirred at 0°C for 30 min. Then a solution of sodium azide (0.19 g, 2.9 mmol) in water (9 ml) was added at 0 °C and the reaction mixture was stirred at room temperature for 3 h. Potassium carbonate was added until pH=8 and the reaction mixture was extracted with CH_2Cl_2 (4x30 ml). The organic layers were dried over Na_2SO_4 and concentrated *in vacuo*. No further purification was needed and the desired product **18** was collected as orange crystals in 92 % yield.

^{1}H-NMR ($CDCl_3$, 300 MHz): δ 8.46 (2H, d, *J* = 5.2 Hz), 8.32 (1H, d, *J* = 2.1 Hz), 8.10-8.05 (2H, m), 7.51-7.49 (2H, m), 7.21-7.13 (3H, m), 6.64 (1H, dd, *J* = 7.9 Hz, *J* = 2.7 Hz), 2.33 (3H, s).

EIMS 302 $[M]^+$

2,4-dichloro-ethynylbenzene - (**19**)

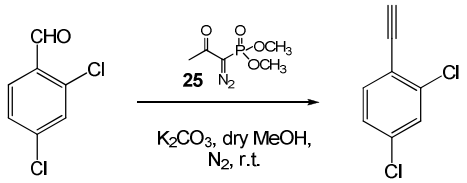

19

A solution of 2,4-dichloro-benzaldehyde (0.10 g, 0.6 mmol) in dry MeOH (20 ml) was cooled to 0°C and then potassium carbonate (0.16 g, 1.2 mmol) and dimethyl-1-diazo-2-oxopropylphosphonate (0.21 g, 0.7 mmol) were added. The reaction mixture was stirred at room temperature for 20 h. The solvent was removed *in vacuo*, saturated $NaHCO_3$ (70 ml) was added and extracted with ethyl acetate (3x20 ml). The organic layers were dried over Na_2SO_4 and the solvent was removed *in vacuo*. The crude was purified by column chromatography on silica gel (AcOEt:Hex 1:1) and the desired product **19** was obtained as a white solid in 41 % yield.

^{1}H-NMR ($CDCl_3$, 300 MHz): δ 7.46-7.42 (2H, m), 7.20 (1H, dd, *J* = 8.6, 1.7 Hz), 3.39 (1H, s).

EIMS 170 $[M]^+$

N-[2-methyl-5-(4-(2,4-dichlorophenyl)-1*H*-1,2,3-triazol-1-yl)phenyl]-4-phenylpyrimidin-2-amine - (**20**)

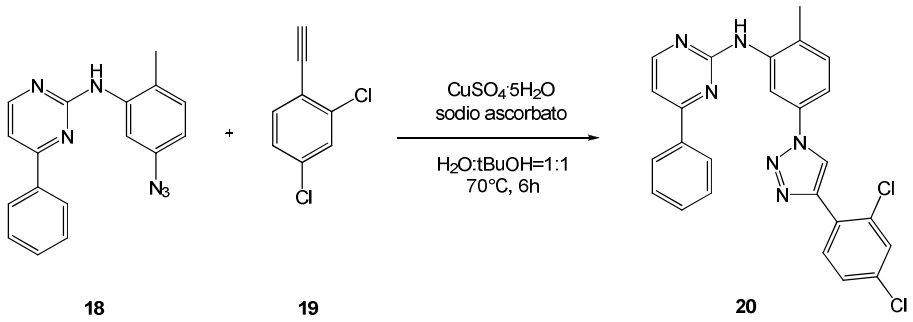

18 **19** **20**

To a solution of compound **18** (0.05 g, 0.16 mmol) and 2,4-dichloro-ethynylbenzene **19** (0.04 mg, 2.4 mmol) in H_2O:tBuOH 1:1 (4 ml) sodium ascorbate (0.003 g, 0.016 mmol) and copper(II)sulfate pentahydrate (0.001 g) were added and the reaction mixture was stirred at 70 °C for 6 h. The solvent was removed *in vacuo*, water (50 ml) was added and extracted with CH_2Cl_2 (4x20 ml). The organic layers were dried over Na_2SO_4 and concentrated *in vacuo*. The crude was purified by column chromatography on silica gel (AcOEt:Hex 2:3) and the desired product **20** was obtained as a yellow solid in 44 % yield.

^{1}H-NMR ($CDCl_3$, 400 MHz): δ 9.07 (1H, d, *J* = 2.1 Hz), 8.62 (1H, s), 8.53 (1H, d, *J* = 5.1 Hz), 8.33 (1H, d, *J* = 8.5 Hz), 8.14-8.16 (2H, m), 7.51-7.85 (4H, m), 7.45 (1H, dd, *J* = 8.1, 2.1 Hz), 7.42 (1H, dd, *J* = 8.5, 2.1 Hz), 7.39 (1H, d, *J* = 8.18 Hz), 7.26-7.28 (2H, m), 2.49 (3H, s).

^{13}C-NMR ($CDCl_3$, 400 MHz): δ 165.36, 159.90, 158.44, 143.56, 138.98, 136.68, 135.62, 134.29, 131.78, 131.31, 131.15, 130.75, 129.98, 129.03 (2C), 127.87, 127.64, 127.21 (2C), 121.23, 114.38, 112.35, 109.13, 29.70, 17.86.

HR-EIMS Anal. Calcd for $[C_{25}H_{18}Cl_2N_6]^+$ 472.0970, Found 472.0972.

N-(2-methyl-5-(4-(4-((4-methylpiperazin-1-yl)methyl)phenyl)-1*H*-1,2,3-triazol-1-yl)phenyl)-4-phenylpyrimidin-2-amine - (**21**)

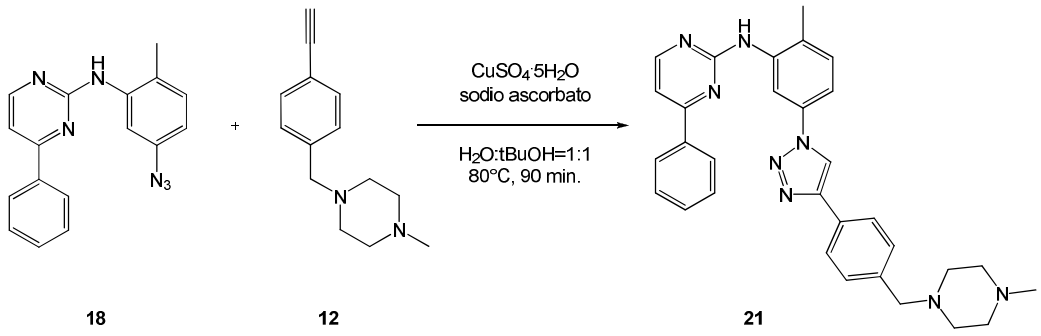

18 **12** **21**

To a solution of compound **18** (0.02 g, 0.07 mmol) and compound **12** (0.014 g, 0.07 mmol) in H_2O:tBuOH 1:1 (2.5 ml) sodium ascorbate (0.002 g, 0.007 mmol) and copper(II)sulfate pentahydrate (0.001 g) were added and the reaction mixture was stirred at 80 °C for 1.5 h. The solvent was removed *in vacuo*, water (10 ml) and brine (10 ml) were added and extracted with DCM (5x5 ml). The organic layers were dried over Na_2SO_4 and concentrated *in vacuo*. The crude was purified by column chromatography on silica gel (AcOEt:Hex 1:2) and the desired product **21** was obtained as a yellow powder in 6 % yield.

^{1}H-NMR ($CDCl_3$, 300 MHz): δ 9.08 (1H, d, *J* = 2.0 Hz), 8.54 (1H, bs), 8.21 (1H, s), 8.12-8.15 (2H, m), 7.85 (2H, d, *J* = 7.8 Hz), 7.51-7.53 (3H, m), 7.34-7.48 (5H, m), 7.16 (1H, bs), 3.63 (2H, s), 2.77 (8H, bs), 2.56 (3H, s), 2.44 (3H, s).

EIMS 516 $[M]^+$

Methyl 1-(4-methyl-3-(4-phenylpyrimidin-2-ylamino)phenyl)-1*H*-1,2,3-triazole-4-carboxylate - (**22**)

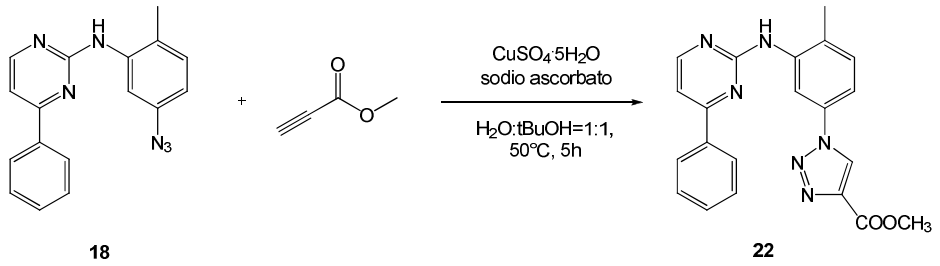

18 **22**

To a solution of compound **18** (0.050 g, 0.16 mmol) and methyl propiolate (0.015 ml, 0.16 mmol) in H_2O:tBuOH 1:1 (3 ml) sodium ascorbate (0.003 g, 0.016 mmol) and copper(II)sulfate pentahydrate (0.001 g) were added and the reaction mixture was stirred at 50 °C for 5 h. The solvent was removed *in vacuo*, water (30 ml) was added and extracted with DCM (4x10 ml). The organic layers were dried over Na_2SO_4 and concentrated *in vacuo*. The crude was purified by column chromatography on silica gel (AcOEt:Hex 1:1) and the desired product **22** was obtained as an orange solid in 41 % yield.

^{1}H-NMR ($CDCl_3$, 400 MHz): δ 9.14 (1H, bs), 8.58 (1H, s), 8.51 (1H, d, *J* = 5.1 Hz), 8.13-8.15 (2H, m), 7.53-7.60 (3H, m), 7.40 (1H, dd, *J* = 8.3, 1.9 Hz), 7.36 (1H, d, *J* = 8.3 Hz), 7.31 (1H, bs), 7.26-7.28 (2H, m), 4.03 (3H, s), 2.46 (3H, s).

^{13}C-NMR ($CDCl_3$, 400 MHz): δ 165.97, 161.83, 160.37, 159.03, 141.00, 139.80, 137.22, 135.68, 132.03, 131.90, 129.73(2C), 127.97, 127.85 (2C), 126.15, 114.71, 112.52, 109.82.

HR-EIMS Anal. Calcd for $[C_{21}H_{18}N_6O_2]^+$ 386.1491, Found 386.1492.

N-[2-methyl-5-(4-((dimethylamino)methyl)-1*H*-1,2,3-triazol-1-yl)phenyl]-4-phenylpyrimidin-2-amine - (**23**)

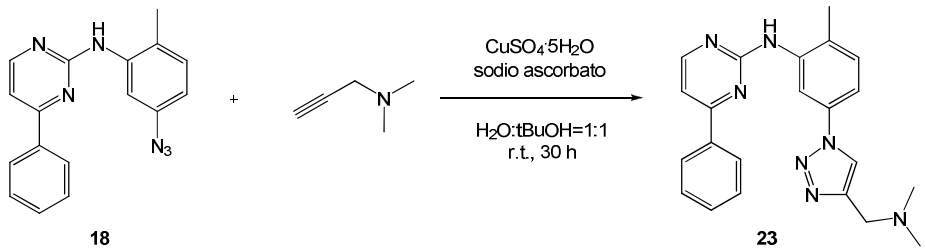

18 23

To a solution of compound **18** (0.050 g, 0.16 mmol) and 3-dimethylamino-1-propyne (0.018 ml, 0.16 mmol) in H_2O:tBuOH 1:1 (3 ml) sodium ascorbate (0.003 g, 0.016 mmol) and copper(II)sulfate pentahydrate (0.001 g) were added and the reaction mixture was stirred at room temperature for 30 h. The solvent was removed *in vacuo*, water (30 ml) was added and extracted with CH_2Cl_2 (4x10 ml). The organic layers were dried over Na_2SO_4 and concentrated *in vacuo*. No further purification was needed and the desired product **23** was obtained as yellow solid in 16 % yield.

^{1}H-NMR ($CDCl_3$, 400 MHz): δ 9.06 (1H, d, *J* = 1.8 Hz), 8.58 (1H, bs), 8.31 (1H, s), 8.13-8.15 (2H, m), 7.52-7.56 (3H, m), 7.40 (1H, dd, *J* = 8.2, 1.8 Hz), 7.34 (1H, d, *J* = 8.2 Hz), 7.18 (1H, bs), 3.99 (2H, bs), 2.55 (6H, bs), 2.45 (3H, s).

HR-EIMS Anal. Calcd for $[C_{22}H_{23}N_7]^+$ 385.2015; Found 385.2005.

N-[2-methyl-5-(4-phenyl-1*H*-1,2,3-triazol-1-yl)phenyl]-4-phenylpyrimidin-2-amine - (**24**)

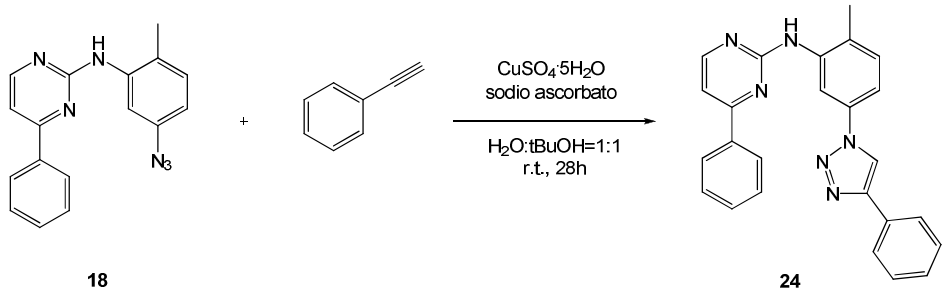

18 **24**

To a solution of compound **19** (0.050 g, 0.16 mmol) and phenylacetylene (0.260 ml, 2,4 mmol) in H_2O:tBuOH 1:1 (3.5 ml) sodium ascorbate (0.003 g, 0.016 mmol) and copper(II)sulfate pentahydrate (0.001 g) were added and the reaction mixture was stirred at room temperature for 28 h. The solvent was removed *in vacuo*, water (60 ml) was added and extracted with CH_2Cl_2 (4x20 ml). The organic layers were dried over Na_2SO_4 and concentrated *in vacuo*. The crude was purified by column chromatography on silica gel (AcOEt:Hex 1:2) and the desired product **24** was obtained as yellow solid in 19 % yield.

^{1}H-NMR ($CDCl_3$, 400 MHz): δ 9.10 (1H, d, *J* = 2.1 Hz), 8.53 (1H, d, *J* = 5.2 Hz), 8.25 (1H, s), 8.14-8.17 (2H, m), 7.92 (2H, dd, *J* = 8.4, 1.3 Hz), 7.53-7.56 (3H, m), 7.46-7.50 (3H, m), 7.36-7.41 (3H, m), 7.26 (1H, d, *J* = 5.2 Hz), 2.47 (3H, s).

^{13}C-NMR ($CDCl_3$, 400 MHz): δ 166.04, 160.44, 158.90, 148.85, 139.52, 137.43, 136.40, 131.96, 11.83, 131.17, 129.70 (2C), 129.51 (2C), 128.94, 127.92 (2C), 127.52, 126.53, 118.25, 114.82, 112.64, 109.68, 18.46.

HR-EIMS Anal. Calcd for $[C_{25}H_{20}N_6]^+$ 404.1749; Found 404.1763.

dimethyl(1-diazo-2-oxopropyl)phosphonate - (**25**)

Eur. J. Org. Chem. **2003**, 821-832

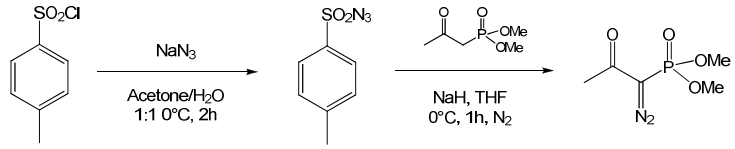

25

A solution of NaN_3 (0.341 g, 5.25 mmol) in acetone (15 ml) and H_2O (15 ml) was added TsCl (1.00 g, 5.25 mmol). The reaction mixture was stirred at 0 °C for 2 h. Acetone was evaporated, the reaction mixture was extracted with diethyl ether, and the organic phase was dried over Na_2SO_4. Evaporation of solvent gave tosyl azide (0.972 g, yield 94 %) as a colourless oil.

^{1}H NMR ($CDCl_3$, 300 MHz): δ 7.75 (2H, d, *J* = 8.1 Hz), 7.33 (2H, d, *J* = 8.1 Hz), 2.39 (3H, s).

A solution of NaH (80 % dispersion in mineral oil and washed with hexane, 0.150 g, 4.93 mmol) in anhydrous THF (20 ml) was cooled to 0 °C under nitrogen. Dimethyl(2-oxopropyl)phosphonate (0.744 g, 4.48 mmol) in anhydrous THF (10 ml) was added dropwise in 20 min. The solution was stirred at 0 °C for 30 min. A solution of Tosyl azide (0.972 g, 4.93 mmol) in anhydrous THF (10 ml) was then added in one portion and the resulting mixture was stirred at 0 °C for 10 min. The reaction mixture was quickly passed through a short column (silica, AcOEt) and the crude mixture was purified by flash chromatography (AcOEt) to give dimethyl(1-diazo-2-oxopropyl)phosphonate **35** (0.781 g, yield 91 %) as a colourless oil.

^{1}H NMR ($CDCl_3$, 300 MHz): δ 3.75 (3H, s), 3.71 (3H, s), 2.15 (3H, s).

^{13}C NMR ($CHCl_3$, 75 MHz): δ 189.7, 115.6, 53.6, 53.5, 27.1.

Acknowledgements

I want to thanks CM 0602 COST Action “Inhibitors of Angiogenesis: design, synthesis and biological exploitation” for the financial support for international collaboration. This project was developed in collaboration with different research groups. For this reason I’m grateful to:

Prof. Joan Bosch and Mercedes Amat of Universitat de Barcelona and their research group, in particular Andrea Kover, for the chemical collaboration regarding Met project;

Dr. Flavio Maina and Rosanna Dono of IBDML of Marseille and their group, in particular Alessandro Furlan and for the biological studies carried out on Met inhibitors;

Prof. Maurizio Botta of Università degli Studi di Siena and his coworkers Cristina and Lucilla for all the modelling studies on Met and Abl projects;

Prof. Fabio Carraro of the Università degli Studi di Siena and his research group for the biological studies on Abl project;

Prof. Giovanni Maga and his coworkers of the Università degli Studi di Pavia for the biological studies on Abl project;

Dr. Sergio Crippa and Teresa Recca for the NMR studies concerning both projests.